University of London

Imperial College of Science and Technology
Blackett Laboratory
Optics Section

Theoretical analysis of an all-optical directional coupler

by

Diane Joan Love

Thesis submitted in partial fulfillment of the requirements for the PhD degree of the University of London, and the Diploma of Imperial College of Science and Technology.

1988

ABSTRACT

This thesis reports a mainly theoretical study of an all-optical directional coupler - a signal processing device which could be capable of high data rates because it has no electronic components.

The one-dimensional theory of the all-optical directional coupler due to Jensen (1980, 1982) was used for comparison with our methods. This theory takes no account of transverse information about the refractive index distribution in the waveguide and hence gives no information about the beam profiles.

A computational split-step Fourier transform algorithm, the Beam Propagation Method (BPM) of Feit and Fleck (1978) was developed and adapted to the device under consideration. The BPM was tested using an Epstein-profile waveguide (Adams 1981) which has an analytical solution for certain initial conditions, and was then used to obtain transverse information and power level predictions for nonlinear operation.

An alternative computational method requiring no Fourier transforms was adapted from its first application in pulse dispersion. The trade-off between speed and accuracy was studied and compared with the BPM.

Experiments were conducted using a $LiNbO_3$ device fabricated at Barr and Stroud and mode-locked pulses and diagnostics in the Photonics group at Imperial College. Sadly no nonlinear behaviour of the switch was observed at power levels below the optical damage threshold.

DEDICATION

To my parents,

to Manju and DP,

and to Pallab.

CONTENTS

List of figures 6

List of tables 9

Acknowledgements 10

Chapter 1 Introduction and review 11
1.1 Introduction 12
1.2 Communicating with light 12
1.3 Integrated optics 17
1.4 All-optical devices 31
1.5 Preview of chapters 2-7 43

Chapter 2 One-dimensional theory of the all-optical directional coupler 44
2.1 Introduction 45
2.2 Discussion of units and values of n_2 49
2.3 Empirical derivations of switching power 51
2.4 Derivation of coupled mode equations 52
2.5 Results of coupled mode equations 55
2.6 Predictions for switching power 58

Chapter 3 Beam Propagation Method 60
3.1 Introduction 61
3.2 Derivation of the BPM 63
3.3 Limitations of the BPM 67
3.4 Setting up the BPM 69
3.5 Testing the BPM 71

Chapter 4 Results of the BPM 82
4.1 Introduction 83
4.2 Modification to model a directional coupler 83
4.3 Modification to model nonlinearity 86
4.4 Runs and results 87
4.5 Conclusions 106

Chapter 5 The Gire Tournois Interferometer transform 107
5.1 Introduction 108
5.2 Overview of the GTI 108
5.3 Derivation of the GTI transform for the dispersive case 110
5.4 Conversion to the diffractive case 112
5.5 Programming details 113
5.6 Results 114
5.7 Conclusions 119

Chapter 6 Experiments with a $LiNbO_3$ directional coupler 120
6.1 Introduction 121
6.2 Fabrication of the directional coupler 123
6.3 The experiments 132
6.4 Conclusions 135

Chapter 7 Ideas for further work and conclusions 136
7.1 Computational work 137
7.2 Experimental work 138
7.3 Materials 138
7.4 Conclusions 138

Appendix A Programming details 140
A.1 Introduction 141
A.2 Hardware 142
A.3 Choice of language 142
A.4 BPM program variables 144
A.5 BPM program modules 146
A.6 Program function 148
A.7 Graphics 148

References 149

Publication

D J Love, G H C New and M A Lauder,
Optics Communications 59 3 177-182 (1986).

Program code for BPM and GTI programs.

LIST OF FIGURES

1.1 The integrated optics radio-frequency spectrum analyser. 17
1.2 End view of dual channel directional coupler. 19
1.3 Plan view of dual channel directional coupler. 19
1.4 Symmetric and anti-symmetric modes of dual channel directional coupler. 21
1.5 Solutions of coupled mode equations for directional coupler. 23
1.6 Solution of coupled mode equations with $\Delta\beta \neq 0$. 25
1.7 Y-junction made from multiple channel directional coupler. 26
1.8 Mach-Zehnder switch. 27
1.9 X-switch. 29
1.10 Output of X-switch. 30
1.11 An optically bistable etalon. 32
1.12 The two constraints on the output of the etalon. 35
1.13 Transmission of etalon versus input intensity. 36
1.14 Output versus input intensity of etalon, showing optical hysteresis. 36
1.15 Various devices made from optically bistable elements. 37
1.16 The all-optical gate. 38
1.17 All-optical directional coupler. 41

2.1 The all-optical directional coupler. 45
2.2 Power remaining in input guide of AODC versus distance. 55
2.3 Input-output curves for four AODCs. 57

3.1 Field distribution before and after propagation through 1mm of free space. 72
3.2 Spatial Fourier transform of figure 3.1. 73
3.3 The field is multiplied by this function each step. 73

3.4 Refractive index distribution for the Epstein layer profile. 77
3.5 Modal field distribution for the Epstein layer profile. 77
3.6 Intensity distribution during the Epstein layer profile test. 78
3.7 Log intensity throughout the propagation. 78
3.8 As figure 3.6, but with width parameter of waveguide 20μm and for field 5μm. 79
3.9 Log intensity of figure 3.8. 79
3.10 As figure 3.6 with width parameter of field 20μm and waveguide 5μm. 80
3.11 Log intensity of figure 3.10. 80
3.12 As figure 3.6 for N=1 mode with a=5λ. 81
3.13 Log intensity of figure 3.12. 81

4.1a Refractive index profile for offset 10. 84
4.1b Refractive index profile for offset 12. 85
4.1c Refractive index profile for offset 15. 85
4.2 Estimation of the power left in the input guide. 89
4.3 BPM results for offset 10.
4.3a I_{MAX} 1 GW/cm^2, propagation distance 10.8mm. 92
4.3b I_{MAX} 20 GW/cm^2, propagation distance 10.8mm. 93
4.4 BPM results for offset 12.
4.4a I_{MAX} 1 GW/cm^2, propagation distance 10.8mm. 94
4.4b I_{MAX} 5 GW/cm^2, propagation distance 10.8mm. 95
4.4c I_{MAX} 7.5 GW/cm^2, propagation distance 10.8mm. 96
4.4d I_{MAX} 10 GW/cm^2, propagation distance 10.8mm. 97
4.4e Power-distance plots for figures 4.4a-d. 98
4.5 BPM results for offset 15.
4.5a I_{MAX} 1 GW/cm^2, propagation distance 28.8mm. 99
4.5b I_{MAX} 3 GW/cm^2, propagation distance 28.8mm. 100
4.5c I_{MAX} 4 GW/cm^2, propagation distance 28.8mm. 101
4.5d I_{MAX} 5 GW/cm^2, propagation distance 28.8mm. 102
4.5e I_{MAX} 7 GW/cm^2, propagation distance 28.8mm. 103
4.5f I_{MAX} 10 GW/cm^2, propagation distance 28.8mm. 104
4.5g Power-distance plots for figures 4.5a-f. 105

5.1a BPM propagation test over 1.2mm. 116
5.1b Paraxial BPM propagation test over 1.2mm. 116
5.2a GTI propagation test, z step 10 μm. 117
5.2b GTI propagation test, z step 5 μm. 117
5.2c GTI propagation test, z step 2.5 μm. 118

6.1a-e Steps in making photolithographic mask. 124
6.2a-f Steps in exposure of $LiNbO_3$ substrate. 126
6.3 Schematic of the $LiNbO_3$ directional coupler. 128
6.4a Input region of $LiNbO_3$ directional coupler. 129
6.4b Interaction region of directional coupler. 130
6.4c Output region of directional coupler. 131
6.5 Experimental set-up. 132
6.6a-d Far-field diffraction "rising sun" patterns. 134
6.7 Device input and two outputs at 200mW. 135

5.0a Plot of ϕ against θ for various values of r. 110a

5.0b Plot of normalised group time delay against θ for various values of r. 111a

LIST OF TABLES

2.1 Properties of some classes of nonlinear materials. 47

2.2 Values of n_2 for different materials. 50

4.1 Parameters for figures 4.3 - 4.6. 88

4.2 Dependence of nonlinearity on waveguide separation. 106

5.1 Summary of GTI test results. 114

ACKNOWLEDGEMENTS

I would like to acknowledge the help and friendship of the staff and students of the Laser Theory Group. My supervisor, Prof Geoffrey New, provided many hours of good-humoured discussions and suggestions. My friends, in particular Hercules Avramopoulos, Steve Barnett, John Catherall, Robert Ettinger, Mark Lauder,Charles Penman and Luis Zenteno variously helped me to learn programming languages and operating systems, consulted with me on the GTI work, and provided word-processing advice, as well as being steadfast companions.

I would like to thank the CASE collaborating company, Barr and Stroud, for their financial help during my studentship. I also received experimental help and research ideas from Neil McFadyen, Walter Johnstone and Ivan Andonovic.

I was aided in my experiments at Imperial by Anderson Gomes and Roy Taylor of the Laser Group, and also by the technicians who made part of the rig which held the directional coupler.

My past and present employers, respectively Kings College Electrical Engineering Department and Logica plc, have provided help in the production of this thesis in the form of time and computer resources.

I would like to thank Pallab for many things; however in this context I should mention that he sub-edited some of the chapters of this thesis.

Finally, I must acknowledge the financial support of SERC during the years of my studentship.

CHAPTER 1

INTRODUCTION AND REVIEW

1.1 Introduction 12

1.2 Communicating with light 12

1.3 Integrated optics 17
- 1.3.1 Dual channel directional coupler 18
- 1.3.2 Mach-Zehnder switch 27
- 1.3.3 X-switch 28

1.4 All-optical devices 31
- 1.4.1 Optical bistability 31
- 1.4.2 The all-optical gate 38
- 1.4.3 The all-optical directional coupler 40

1.5 Preview of chapters 2-7 43

Chapter 1 Introduction and review

1.1 Introduction

This thesis describes a theoretical and experimental study of all-optical processing in a $LiNbO_3$ directional coupler. The study brings together three ideas - optical communications, integrated optics and all-optical processing. This chapter reviews these three fields, discussing the motivation behind the research and the state of progress at present.

1.2 Communicating with light

Since signals were first sent electromagnetically, there has been a steady demand for ever-higher information rates. In order for more information to be sent in a given time, the bandwidth of the signal must be increased; higher bandwidths can usually be achieved by using higher frequency signals. In consequence there has been an upward trend in operating frequency which has been punctuated by developments in sources of electromagnetic waves: first radio waves, then microwaves and finally in 1960, laser radiation.

As a stable source of monochromatic radiation, the laser was seen to have an obvious potential for high-speed high-volume communication. By the end of the sixties, all-optical systems had been envisaged with the signals carried in optical waveguides and processed on integrated optical chips. However at that time materials development and fabrication techniques were not sufficiently advanced to realise such a system in practice.

Before addressing the problem of making optical processors, the transmission of optical signals had to be

developed. The following description of a commercially available system for sending laser beams through the atmosphere will demonstrate the need for confinement of signal carrying beams to a material medium for most purposes.

Optel's system (1986), for example, can send digital data and voice signals for a maximum distance of 20 km in good visiblity at 20kb/s or 2km at 10Mb/s. Video signals can also be sent up to 2km. These figures are drastically reduced in poor visibility.

The manufacturers cite several advantages for their system. It is free from electromagnetic interference and hard to tap as the beams used are narrow and, at 800-900nm, invisible. Tapping would also have to be done in the line of sight. Most of all, the system is convenient because it can be installed anywhere, between the tops of buildings or over railways or rivers, without the need to lay cables or conduits.

However, for everyday communication systems,this kind of transmission has its drawbacks - the waves have to travel in straight lines, the transmission distance is very limited, performance of the system varies greatly with the prevailing weather and can be completely disrupted by solid objects, and a determined tapper really only requires to find the beam and place a beam-splitter in it. Finally, stray laser beams are a hazard and if this sort of system were to proliferate, legislation might be required to protect the public, reducing the advantage of do-as-you-please installation. It would seem that while atmospheric communications systems work and are invaluable in certain situations, practical communications require the light to be enclosed and guided.

Although optical fibre waveguides were already in use in the late fifties in a medical instrument called the

fibrescope (Kapany 1967), the attenuation of the silica fibre used was around 500 dB/km, too high to make practical communications systems. The consensus of opinion was that, while some improvement might be made, it would take many years of intensive research to reduce loss in fibre to an acceptable level, and so many researchers suggested alternative methods for guiding light. Detailed descriptions of these methods can be found in Okoshi (1982); a summary of some of the more interesting methods follows.

For instance, waveguiding by passing light through apertures is possible and has been demonstrated with millimetre waves by Mink (1969). This experiment demonstrated that accurate positioning of the apertures is required and the beam cannot deviate from a straight line unless mirrors or prisms are added. Guiding light with mirrors or lenses was proposed (Goubau and Schwering 1961) and quite a lot of experiments were done (Gloge and Steier 1968) until fibres were introduced. Again, mechanical difficulties due to accurately positioning large numbers of lenses or mirrors, mechanical instability and temperature sensitivity were experienced. A system with gas flowing in a hot pipe was proposed (Berreman 1964, Marcuse and Miller 1964) - this produced a gradient refractive index because the gas near the surface of the pipe warmed up while the gas at the centre of the pipe remained cool. Gas lenses could be made in shallow curves, allowing light to be guided round bends, and systems were proposed with glass lenses for straight sections and gas lenses for bends. Again work on this stopped abruptly when optical fibres became practical, but the work done on gradient refractive index media paved the way for future work in glass.

In contrast to the above guiding schemes which could all be described as using discrete optics, there were also proposals for guiding in continuous media, for instance

thin films on glass substrates (Karbowiak 1965) as well as hollow metal (Karbowiak 1958) or hollow dielectric (Karbowiak 1966) waveguides.

Ironically, optical fibres owe most to the discovery of dielectric surface waveguiding which goes back to Tyndall in the 1870s and Hondros and Debye in 1910. Dielectric surface waveguides with a core-cladding structure are used in present-day optical fibres. The waveguides are weakly-guiding, which means that only a very narrow range of frequencies is guided properly and the other frequencies eventually escape. The resulting reduction in dispersion is vital for optical fibre communication.

The alternatives to fibre optics mentioned above now seem clumsy and impractical, but at the time of their invention, few people thought that fibre optics for communications would be available in the near future. However in 1966, Kao and Hockham suggested that there would be a reduction in the loss of silica fibre from 500 to 20 dB/km if the transition metal ion content of the glass could be reduced below certain levels. This suggestion was followed up by Kapron et al of Corning Glass Works, who in 1970 reported the demonstration of 20 dB/km loss in silica fibre. Apart from making the world realise that optical fibres were a useful communication medium, they triggered a race to produce optical fibres with ever lower loss which continues to this day.

Modern systems can transmit signals for many tens of kilometres without significant attenuation at selected wavelengths, eg 1.3 and 1.5μm. While loss in ordinary electrical cables rises steeply as a function of operating frequency, the attenuation in optical fibres is frequency-independent. The frequency ceiling is instead due to dispersion which causes pulse broadening and so limits the speed at which information can be sent. This can be counteracted by using monomode fibres and possibly

by using soliton pulses, where the dispersion in balanced by nonlinear effects (Mollenauer 1985).

Optical fibres have several advantages over conventional cabling. These include;

- they are unaffected by electromagnetic interference or earth loops,

- they can be used safely in environments where an electrical spark from current carrying wires could cause an explosion,

- they are difficult to bug or tap since this would involve breaking the fibre and risking detection,

- they are smaller in diameter, cheaper, lighter and made of more abundant materials than copper conductors.

Optical fibre communication is now a reliable and widely applied technology which looks as if it is here for the forseeable future and which will eventually replace its competitors.

1.3 Integrated optics.

The full signal carrying capacity of optical fibres cannot be attained without multiplexers, demultiplexers, encoders and processors. Also, as optical fibres are increasingly used, there is a growing need to process the optical signals directly, to avoid converting the signal from optical to electrical form and back again every time processing is required. While optical processing can be demonstrated in the laboratory using bulk optics, it is impractical to do so elsewhere as all the discrete devices need to be bolted firmly to a vibration-proof optical bench. Integrated optics attempts to provide solutions to all these problems by processing light directly using integrated circuits with all the necessary components on single small chips.

An optical integrated circuit (see figure 1.1) may contain laser diodes, gratings, couplers and switches as well as optical waveguides. There may also be electrodes to supply control signals to the devices. This is called hybrid optical processing, meaning that the signals are optical but the control is electronic.

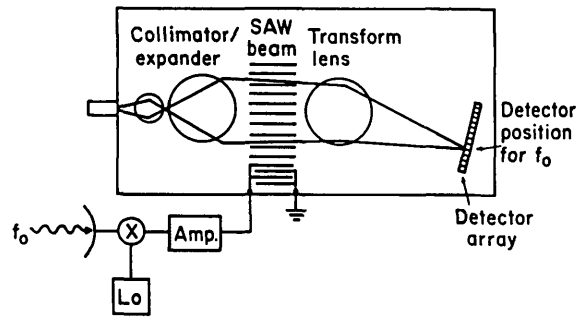

FIGURE 1.1. The integrated optics radio-frequency spectrum analyser (Hunsperger 1982).

In integrated optics fabrication technology at present there are two well-established types of devices; semiconductors, which are capable of producing laser light and $LiNbO_3$ waveguides which cannot. As semiconductor materials permit lasers to be made out of the same material as the substrate, the device can be monolithic - this helps reduce problems of alignment, vibration and temperature sensitivity. $LiNbO_3$ fabrication on the other hand requires less equipment, is easier and the resulting waveguides can carry visible light. The description "hybrid" is again used to distinguish $LiNbO_3$ substrates with electrodes and lasers stuck on from monolithic systems. $LiNbO_3$ fabrication will be discussed further in chapter 6.

1.3.1 Dual-channel directional coupler

In the early days of integrated optics, many researchers had experience in microwave waveguides. Some of the techniques that were used for microwaves could be adapted for use in optics. The integrated optics dual-channel directional coupler derives from the unidirectional couplers used to measure the power in microwave waveguides - these are described in many textbooks on electromagnetism, for instance Feynman (1964). Both devices use evanescent coupling and both treat waves travelling in a chosen direction along the waveguide while ignoring reflected waves.

Ideally the device consists of two channel waveguides which are made so close together that the evanescent tail of a mode propagating in one of the guides overlaps the other (see figure 1.2). In practice, the guiding regions have to start farther apart to ensure that the input goes into one guide only, converge towards the interaction region where they run parallel and diverge again as shown in plan view in figure 1.3.

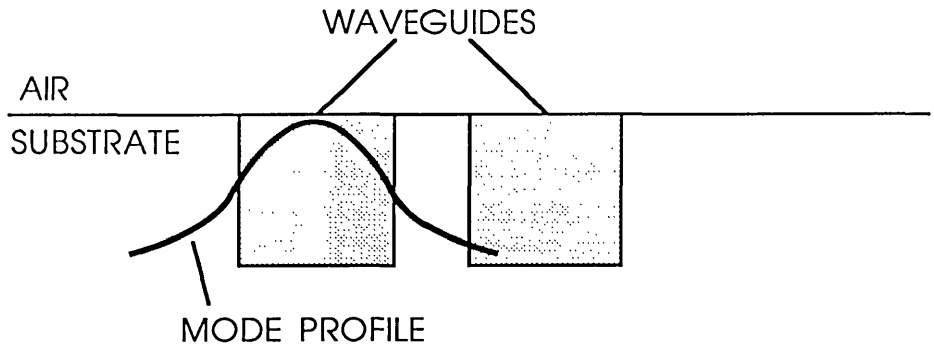

FIGURE 1.2. End view of dual channel directional coupler, showing mode profile.

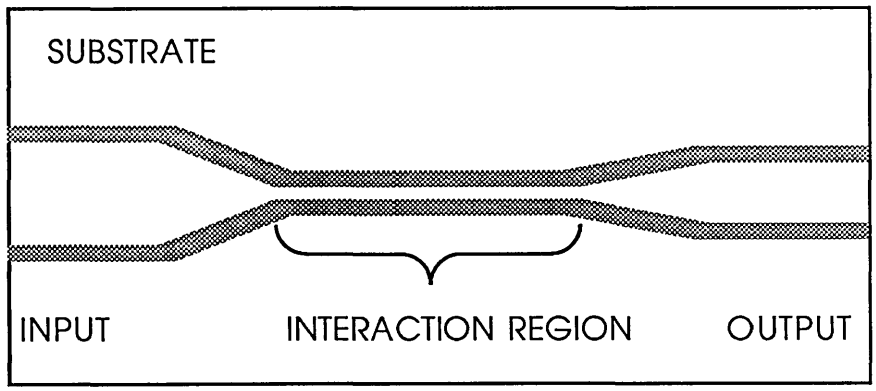

FIGURE 1.3. Plan view of dual channel directional coupler.

The two guides will be referred to as guide 1 and guide 2. If initially light is launched into only one of the guides, say guide 1, the evanescent tail of the mode overlapping guide 2 causes energy to propagate in guide 2 at the expense of guide 1. This energy transfer is coherent - it can only happen if the modes propagating in

the two guides maintain a constant phase relationship. If this is the case, the transfer goes on cumulatively until all the light is propagating in guide 2 and none remains in guide 1 - at least if waveguide loss is ignored. Then the situation is exactly the same as the launch condition with the roles of the two guides reversed, so energy starts to transfer from guide 2 back to guide 1.

There are two approaches to describing the operation of directional couplers - one can consider the modes of the individual waveguides or the modes of the double-waveguide structure itself. The following description of directional coupler operation due to Marcatili (1969) takes the latter course and will also be helpful when considering the X-switch (see 1.3.3).

Consider the directional coupler as a single object rather than two guides. The object has two normal modes - a symmetric mode with equal excitations with equal phase in each guide and an antisymmetric mode with equal amplitude but opposite phase in the two guides (see figure 1.4). These two modes propagate with different propagation constants. If the light is initially launched in one guide only, this can be decomposed into the two normal modes of the system; an equal proportion of the two modes will produce an excitation in one guide and cancel out in the other. In the case of the directional coupler, the two modes are allowed to propagate at different velocities until their phase difference is such that they cancel in the original guide and add constructively in the second guide.

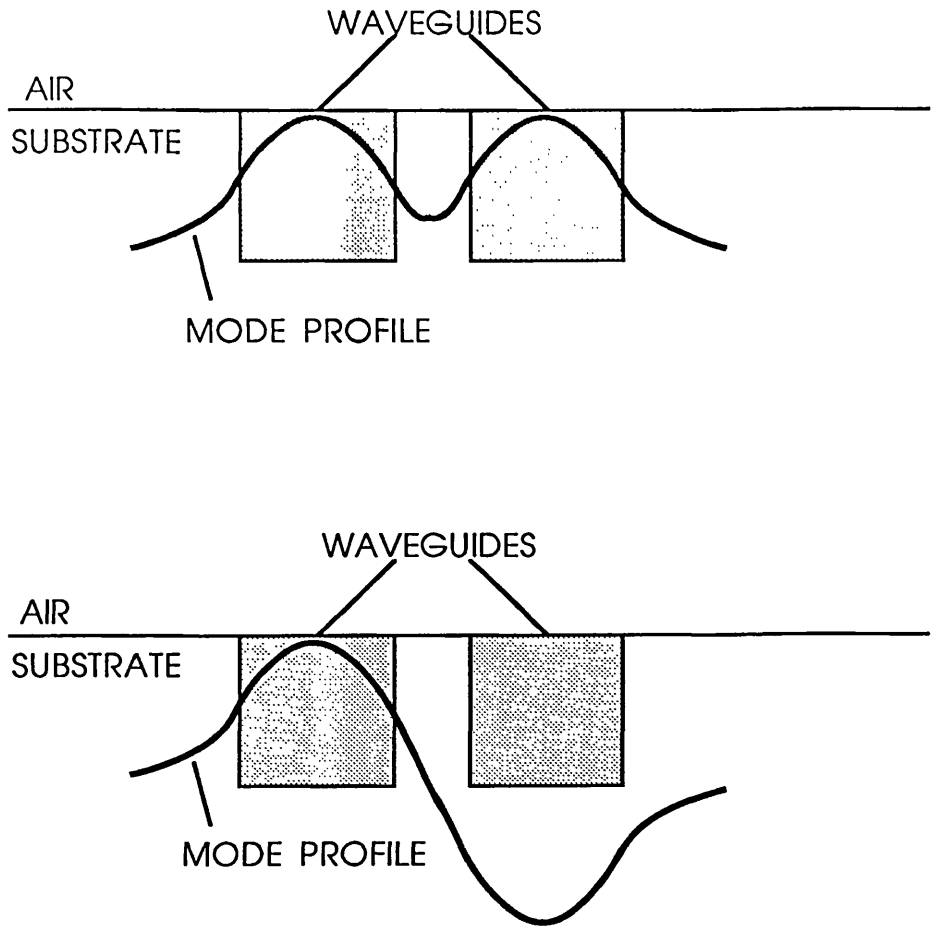

FIGURE 1.4. Symmetric and anti-symmetric modes of dual channel directional coupler.

Another approach is the simple coupled mode theory of Yariv (1973), which considers the mode of a single guide and then adds the coupled field from the other guide via an arbitrary coupling constant. This coupled mode theory is quite suitable for dual-channel directional couplers. However, when it is applied to cases of strong coupling, multiple coupling and waveguide bends, it does not cope well. Syms (1987) found that coupled mode theory could not predict the behaviour of a three-channel coupler. Better coupled mode theories have now been developed, including a scalar theory by Marcatili (1986), a vector theory by Haus et al (1987) and the strong coupling theory of Syms and

Peall (1988).

The simple coupled mode theory is developed as follows. The electric field of a mode propagating in a solitary waveguide is represented by

$$E(x, y, z) = A(z)\, \varepsilon(x, y) \qquad 1.1$$

where A is a complex amplitude containing the phase factor exp $(i\beta z)$ for propagation down the guide and $\varepsilon(x,y)$ is a transverse mode profile for the single guide. There are two contributions to dA/dz; one from the z-dependence of the amplitude and the other from the coupling from another guide. So for the case of the dual-channel directional coupler, the following two coupled mode equations result:

$$\frac{dA_1(z)}{dz} = -i\beta_1 A_1(z) + K_{12}A_2(z) \qquad 1.2a$$

$$\frac{dA_2(z)}{dz} = -i\beta_2 A_2(z) + K_{21}A_1(z) \qquad 1.2b$$

When the two guides are identical, β_1 and β_2 are equal and can be replaced by $\beta = \beta_r - i\alpha/2$ where α is a loss coefficient and α and β_r are real; K_{12} and K_{21} are also equal and consideration of power conservation along the z direction also shows that the coupling coefficient must be purely imaginary. Our two coupled mode equations now become

$$\frac{dA_1(z)}{dz} = -i\beta A_1(z) - iKA_2(z) \qquad 1.3a$$

$$\frac{dA_2(z)}{dz} = -i\beta A_2(z) - iKA_1(z) \qquad 1.3a$$

Where K is real.

Taking the case where light is initially launched into guide 1 and no light launched into guide 2, the boundary conditions are

$$A_1(0) = 1;\ A_2(0) = 0$$

The solution is

$$A_1(z) = \cos(Kz)\ \exp(i\beta z) \qquad 1.4a$$

$$A_2(z) = -\sin(Kz)\ \exp(i\beta z) \qquad 1.4b$$

The power in each guide is the squared modulus of the amplitude, hence

$$P_1 = \cos^2(Kz)\ \exp(-\alpha z) \qquad 1.5a$$

$$P_2 = \sin^2(Kz)\ \exp(-\alpha z) \qquad 1.5b$$

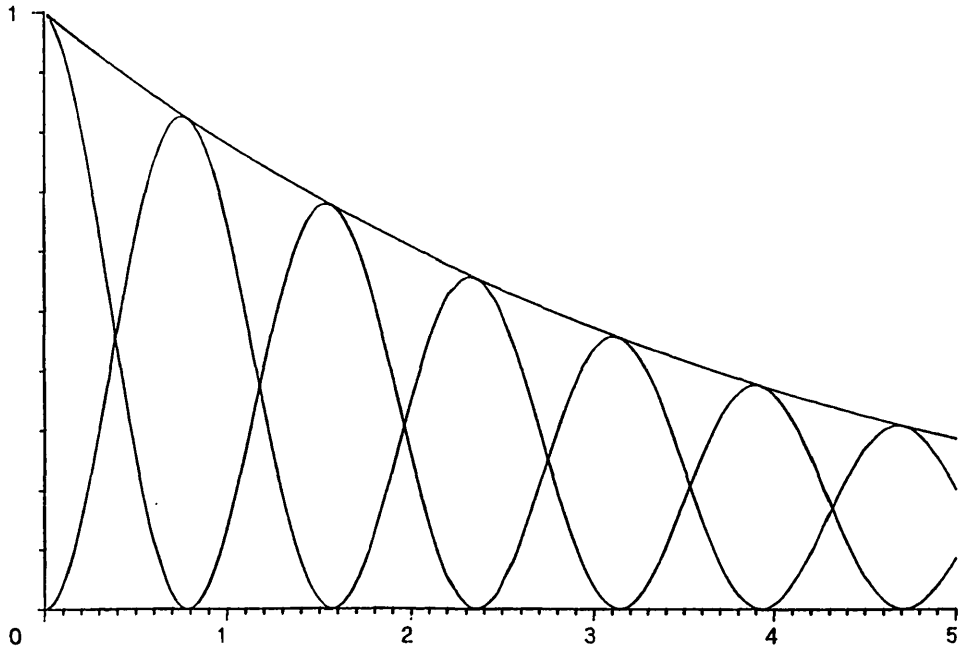

FIGURE 1.5. Solutions of coupled mode equations for directional coupler.

These two functions are plotted versus z in figure 1.5. The characteristics of directional coupler operation are quite evident from this solution; the power in one guide is a maximum when the power in the other guide is zero; the power in each guide varies sinusoidally as a function of distance travelled down the guide; the frequency of the oscillation is proportional to the coupling coefficient K. It can also be seen that linear loss in the guiding medium simply reduces the power in the guides without otherwise affecting the nature of the power transfer.

The degree of coupling depends on fabrication parameters; the coupling is stronger if the separation between the two guides is small, or if there is a large overlap between the evanescent tail of the mode and the other waveguide. In order to derive the coupling coefficients, overlap integrals must be performed on the mode and waveguide profiles; this is straightforward for rectangular profile waveguides but there are no analytic solutions for waveguides of arbitrary profile. The numerical investigations of chapters three and four use alternative methods to study the coupling in linear and nonlinear media.

The length of waveguide required for complete transfer to take place from one guide to the other once is called the coupling length. Devices of different lengths have different properties. For instance a device half a coupling length long is a 3dB coupler or beamsplitter, dividing one input equally between the two outputs. 10 dB couplers can be used to measure the power in a waveguide. Much longer devices have interesting waveguide selection properties due to dispersion.

Directional couplers in which the propagation constant of one of the guides can be varied with respect to the other can be operated as switches. To make a switch, the directional coupler is made in an electrooptic material

and electrodes are arranged around one guide so that its refractive index can be changed with respect to the other. The waveguide length must be an odd number of coupling lengths, so that light entering one guide emerges from the other. In this case an applied field will destroy the phase matching between the two guides and prevent coupling taking place, so that light will emerge from the same guide as the input. In this way a light input can be switched to one of two outputs.

The coupled mode analysis can be repeated with β_1 different from β_2, in equations 1.2a and 1.2b, resulting in the following solutions in terms of $\Delta\beta = |\beta_1 - \beta_2|$ and g where $g^2 = K^2 + (\Delta\beta/2)^2$;

$$A_1(z) = \left(\cos gz - \frac{i\Delta\beta}{2g} \sin gz\right) \exp\left[-i\left(\beta_1 - \frac{\Delta\beta}{2}\right) z\right] \quad 1.6a$$

$$A_2(z) = -\left(\frac{-iK}{g} \sin gz\right) \exp\left[-i\left(\beta_2 + \frac{\Delta\beta}{2}\right) z\right] \quad 1.6b$$

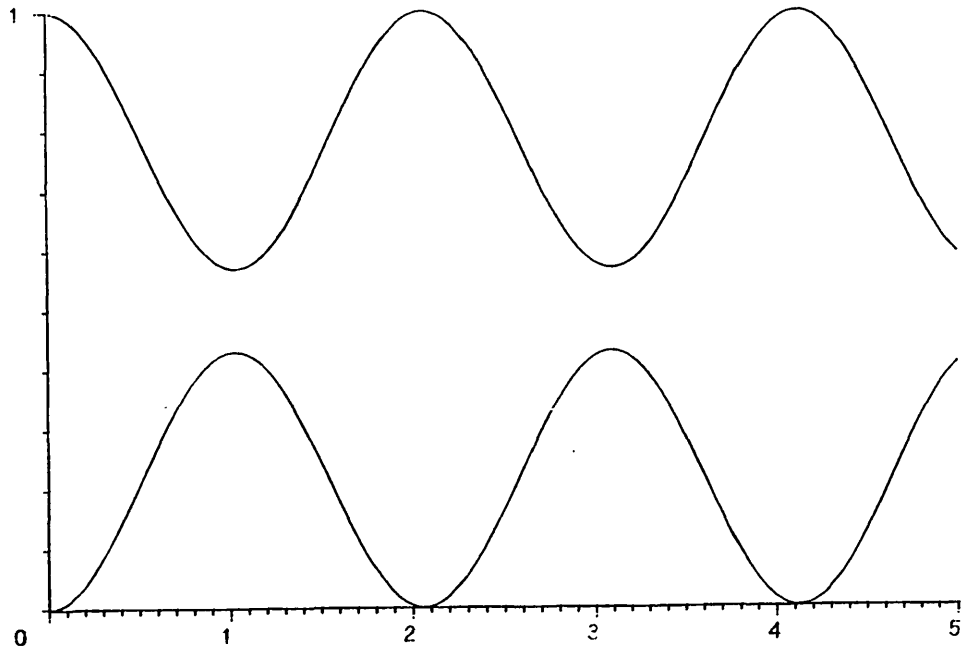

FIGURE 1.6. Solution of coupled mode equations with $\Delta\beta \neq 0$.

These solutions are plotted versus z in figure 1.6, for the case of a lossless medium. It can be seen that coupling still takes place, but the power is never fully coupled from one guide to the other, and the fraction of the power that is coupled decreases as $\Delta\beta$ is increased. More importantly, the frequency of the oscillation increases, and this allows a certain value of $\Delta\beta$ to change the state of the switch from 100% coupling to 0% coupling.

Haus and Molter-Orr (1983) have produced an analysis of directional couplers with an arbitrary number of parallel channels, using simple coupled mode theory. They conclude that with the correct choice of coupling coefficients it will always be possible to transfer power completely from one outermost guide to the other, no matter how many guides there are between them, and also for an odd number of guides, to transfer power completely from the centre guide to the two outermost guides and vice-versa. The authors propose that multiple-channel directional couplers could produce more effective splitting of guided waves than Y-junctions (see figure 1.7).

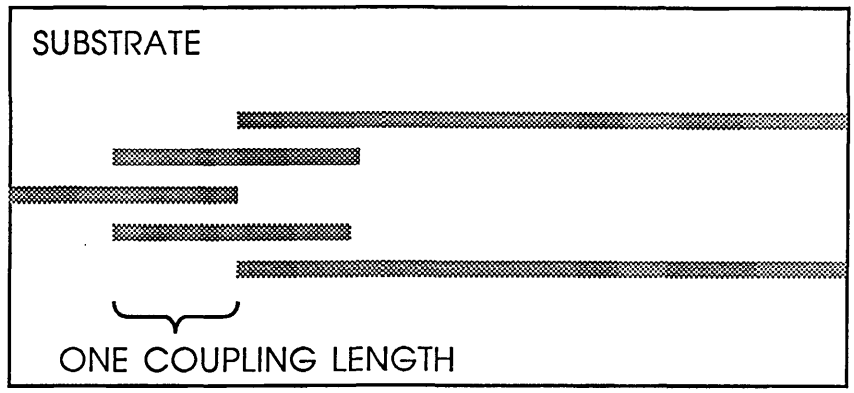

FIGURE 1.7. Y-junction made from multiple channel directional coupler.

While this may be true, the experiments of Syms (1987) gave results for a three-channel coupler that were incompatible with simple coupled mode theory. More accurate theories have been developed by Marcatili (1986), Haus et al (1987) and Syms and Peall (1988).

1.3.2 Mach Zehnder switch

The integrated optics version of the Mach-Zehnder interferometer (fig 1.8) consists of a waveguide which splits into two at a y-junction; the two waveguides continue parallel and some distance apart (so that there is no interaction between the waves in the two waveguides) and then they meet another y-junction and are recombined into one waveguide.

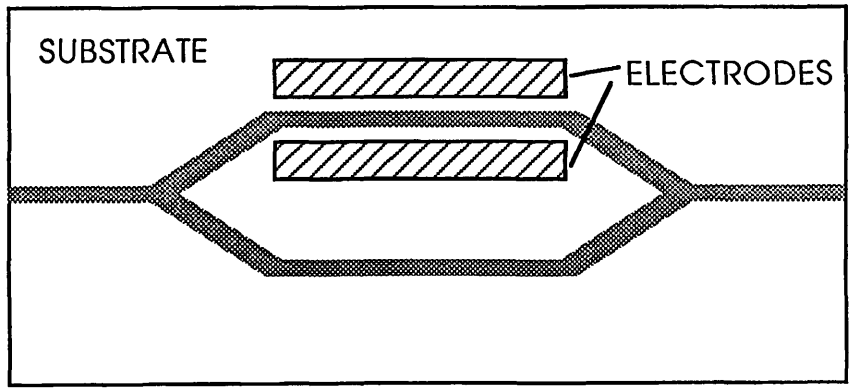

FIGURE 1.8. Mach-Zehnder switch.

The substrate is made in an electrooptic material. Electrodes are placed around the waveguides so that fields

can be applied to change the refractive index and hence the path length in one of the guides. The waveguides are single-mode.

If the two guides are of exactly equal length, the waveguide mode which is split in two at the y-junction will recombine to form the mode at the second y-junction and will appear at the output with little loss. On the other hand, if a π phase difference is introduced between the two modes, the waves recombine to form the next higher order mode, which is antisymmetric; this mode cannot be guided by the single-mode waveguide, so it rapidly dissipates into the substrate. In this way, the appearance of an output can be controlled by a signal on the electrode.

With present day fabrication techniques, even ostensibly identical waveguides may in practice be slightly different and so have different propagation constants - this would ruin a Mach-Zehnder switch as a full output would never be possible. The problem can be solved by applying a purely dc field to one of the guides to tune its propagation constant to that of the other guide.

1.3.3 X-switch

The X-switch or cross-coupler is a four-port device not unlike a directional coupler. It consists of two single-mode waveguides laid across each other typically at an angle α of 1 degree (see fig 1.9).

There are three regions of interest - the input region and the output region behave like directional couplers, except that they are converging and diverging linearly. The interaction region contains an area whose refractive index difference from the substrate is higher than that for the single waveguides, as it has contributions from two

waveguides. This area of higher refractive index increases uniformly in width towards the centre of the device and then decreases uniformly. Meanwhile, the total width of waveguiding region decreases uniformly to w, the width of one of the waveguides, in the centre of the device.

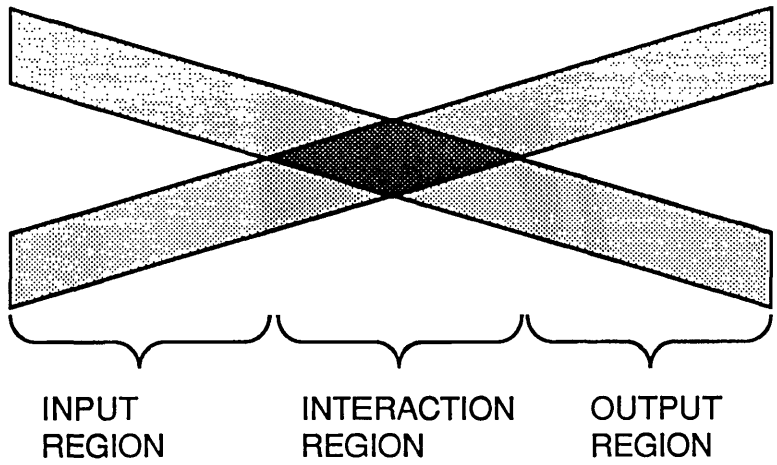

FIGURE 1.9. X-switch.

An input into only one of the guides in the input region can be resolved into the two normal modes of the tapering directional coupler. These two modes, one symmetric and one antisymmetric, are converted approximately losslessly into the fundamental and first antisymmetric mode of the interaction region. These two modes again have different propagation constants, and it is their difference, $\Delta\beta$, which governs the proportion of power staying in the original guide (straight-through mode) to the power emerging from the other guide (crossover mode). In fact,

$$P_C = P_{IN} \cos^2 (\Delta\beta L/2) \qquad 1.7$$

$$P_S = P_{IN} - P_C \qquad 1.8$$

where P_{IN} is the input power, P_C is the crossover power, P_S is the straight-through power and $L = w/\sin(\alpha/2)$ is the length of the interaction region.

Electrodes can be put across the interaction region in such a way that they change the β of the fundamental mode without affecting the β of the antisymmetric mode too much. Thus $\Delta\beta$ varies with applied field.

Neyer (1983) performed a beam propagation analysis of the X-switch and calculated the output power in both the straight-through and crossover modes of the device as a function of applied field - see figure 1.10. It can be seen that a small field is required for tuning, and a voltage of about 2.5 V gives complete switching.

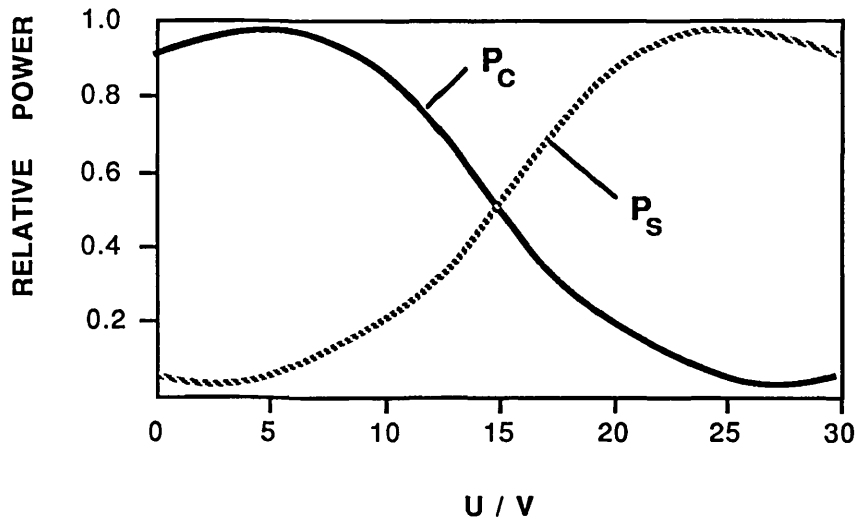

FIGURE 1.10. Output of X-switch (Neyer 1983).

Because the interaction region and so the electrodes are small, the capacitance of the electrodes is also small, allowing switching speeds above 1GHz.

1.4 All-optical devices.

The hybrid optical switches described above allow a number of operations to be carried out on optical signals. However, switching is still controlled by the application of electric fields, and so the natural high-speed capabilities of the devices are lost.

All-optical processing attempts to solve this problem by using light to control light. The field of nonlinear optics could supply many processes that would give switching. However, a little consideration quickly shows that some methods would be unnecessarily complicated. First of all, there should be no net frequency change of the signal on processing. If there is, then optics for two different frequencies are required, and of course multi-stage optical processing would require a number of frequencies to be catered for in the devices. This rules out processes involving harmonic generation, parametric processes and Raman scattering. It is also beneficial for the process to be incoherent, otherwise it is hard to maintain phase coherence over the distances required with the materials available.

Two main approaches have emerged: optical bistability in semiconductor etalons and all-optical waveguide devices. Either of these methods would work perfectly if the ideal material was available. However, as we shall see, with present materials, each has its advantages and drawbacks. Although this thesis concerns waveguide devices, it will be helpful to digress to examine optically bistable devices for the sake of comparison.

1.4.1 Optical bistability.

In an optically bistable device, there are ranges of input power which can give one of two output power values. It is

therefore obvious that some kind of optical nonlinearity is required to produce bistability; in addition, as the switch must have some "knowledge" of the output state, feedback is required.

Over the past few years, optical bistability has been realised in many systems and by many methods; for a comprehensive review see Abraham and Smith (1982). Some examples are absorptive and dispersive bistability in cavities and etalons (Gibbs et al 1976), hybrid bistable devices (Smith et al 1979a), bistability at a nonlinear interface (Kaplan 1976, Smith et al 1979b), bistability due to self-focusing (Bjorkholm et al 1981) and even bistability in a vacuum (McCullen et al, 1983). For the purposes of all-optical processing, it is most instructive to consider bistability in etalons.

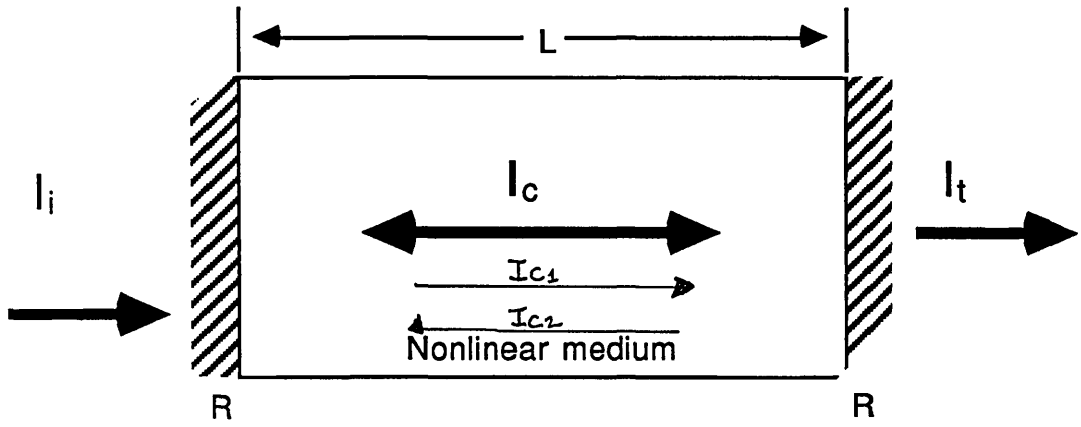

FIGURE 1.11. An optically bistable etalon.

The etalon system consists of two partially reflecting surfaces which reflect a portion R of the incident intensity and transmit T so that R + T = 1 (fig 1.11). In fact the value of R need not be the same for the two surfaces. A nonlinear medium is placed between the two mirrors. In absorptive bistability, this is typically sodium vapour; the possiblity of bleaching the absorber

provides the nonlinearity, while the cavity provides the feedback. In dispersive bistability, a medium exhibiting intensity dependent refractive index is required and again, Na vapour is a candidate. However it is possible to use GaAs or InSb prepared as a semiconductor slab whose surfaces provide the partial reflection.

For practical purposes, the semiconductors are preferable for reasons of ease of fabrication, cost and reliability; one could compare Na vapour versus semiconductor etalons to valves versus transistors.

Optical bistability was first observed in an experiment on absorptive bistability in Na vapour (Gibbs et al 1976). However, the mechanism observed was predominantly dispersive.

In dispersive OB the laser is initially mistuned from cavity resonance, and so little light is transmitted. If the intensity is increased, the nonlinearity changes the optical path length until the laser is tuned to the cavity, and then high transmission is possible. Assuming the usual intensity dependent refractive index,

$$n = n_o + n_2 I \qquad 1.9$$

The optical path length of the cavity is

$$L(n_o + n_2 I_c) \qquad 1.10$$

where L is the length of the cavity and I_c is the intensity in the cavity. It can be seen from the argument so far that switching should be possible. However, to understand how the bistability comes about, it is helpful to look at the graphical solution for the two equations of the Fabry-Perot etalon. The usual etalon equation is (Born and Wolf 1965)

$$\mathcal{T} = I_T/I_I = 1/(1 + F \sin^2 \phi/2) \qquad 1.11$$

where F, the cavity finesse is $4R/T^2$, and ϕ is the round trip phase shift for a linear medium of refractive index n,

$$\phi = 2\pi n\ L\ (2/\lambda) \qquad 1.12$$

For a medium with the intensity dependent refractive index given above,

$$\phi(I_c) = 4\pi n_o L/\lambda + 4\pi n_2 \lambda/L\ I_c \qquad 1.13$$

Substituting this into the etalon equation, we get an expression for $\mathcal{T}$ that is a function of I_c only. This is the Airy function (fig 1.12).

Next, we derive another equation for $\mathcal{T}$ involving the field inside the cavity, I_c. Going back to figure 1.11, we see that I_c has two components, I_{c1} travelling in the same direction as I_I and I_T and I_{c2} travelling in the opposite direction, so that $I_c = I_{c1} + I_{c2}$. An infinite number of internal reflections contribute to I_{c1}; however, each gives rise to a backward travelling reflection of intensity RI_{c1}, which contributes to I_{c2}. Hence $I_{c2} = RI_{c1}$ and

$$I_c = (1+R)\ I_{c1} \qquad 1.14a$$

Similarly, each component of I_{c1} gives rise to a component of I_T, so that

$$I_T = (1-R)\ I_{c1} \qquad 1.14b$$

From 1.14a, I_{c1} can be replaced by I_c / (1+R), giving

$$I_T = I_c\ (1-R)\ /\ (1+R) \qquad 1.15$$

And so

$$\mathcal{T} = I_c(1-R)\ /\ I_I(1+R) \qquad 1.16$$

showing that the graph of $\mathcal{T}$ against I_c is a straight line whose slope is inversely proportional to I_I. Plotting this simultaneously with the Airy function gives fig 1.12.

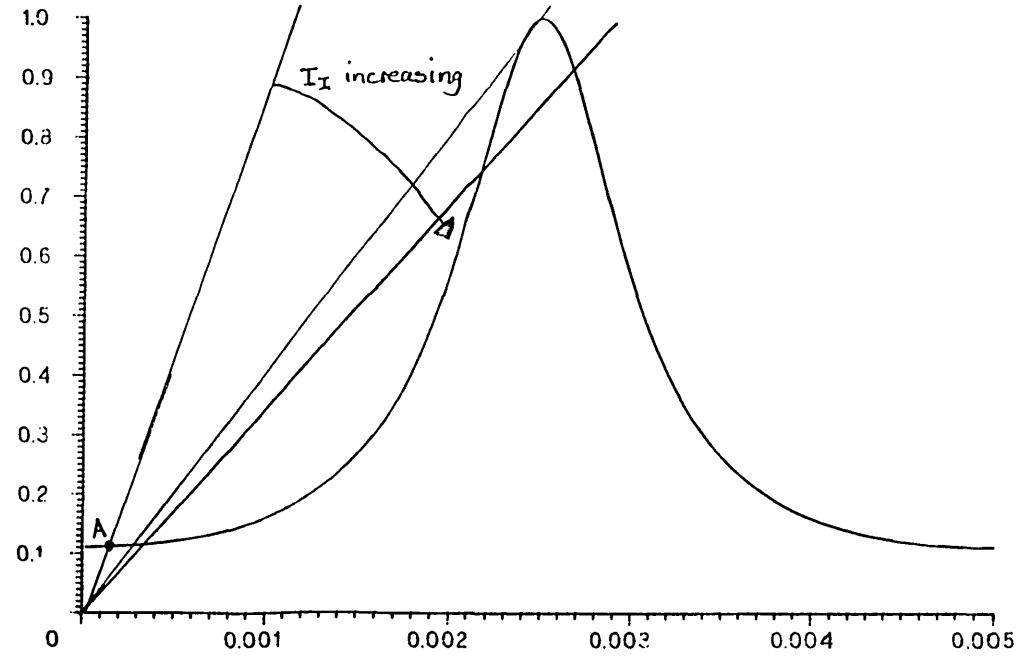

FIGURE 1.12. The two constraints on the output of the etalon.

For a low value of I_I, ie a steep slope of the straight line, there is only one intersection of the two curves, namely point A. Therefore only one value of I_C is possible. As I_I is increased, and the slope of the straight line is decreased, there are eventually two and then three intersections with the Airy function. This situation is more easily understood by plotting τ against I_I instead of I_C (fig 1.13) or better still, multiplying τ by I_I and plotting against I_I. This is effectively a curve of output intensity versus input intensity, and gives the familiar hysteresis curve of optical bistability (fig 1.14). A linear stability analysis (Gibbs et al, 1976) shows that the portions of the curve from A to E and from G onwards are stable, whereas the part between E and G is unstable. Therefore when the input intensity is increased from A onwards, the system progresses along the line to E but then hops up to F. If the intensity is then decreased, the system goes back to G before hopping down to H.

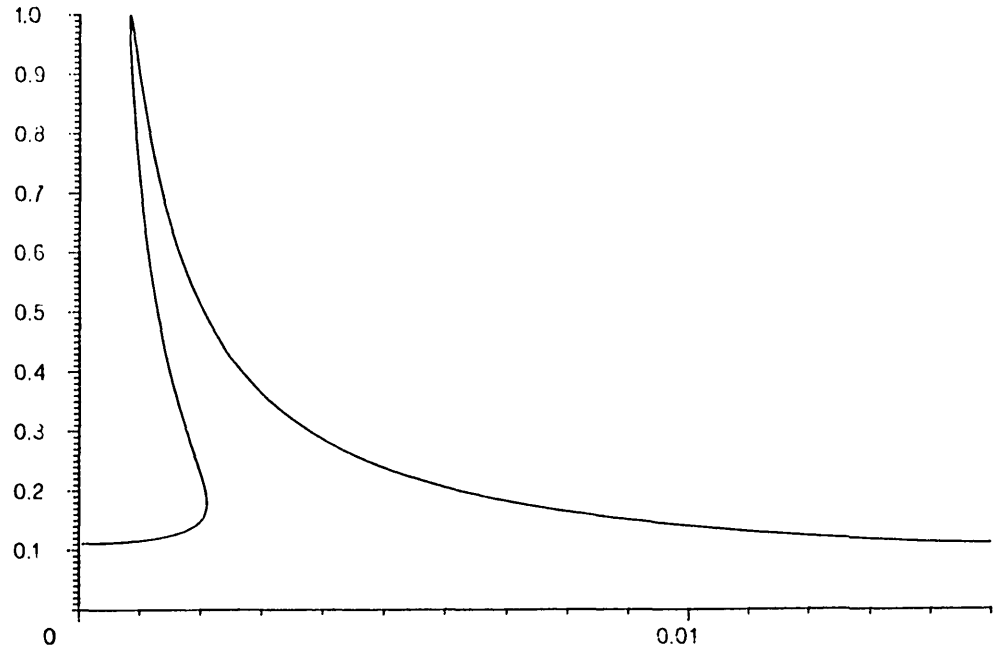

FIGURE 1.13. Transmission of etalon versus input intensity.

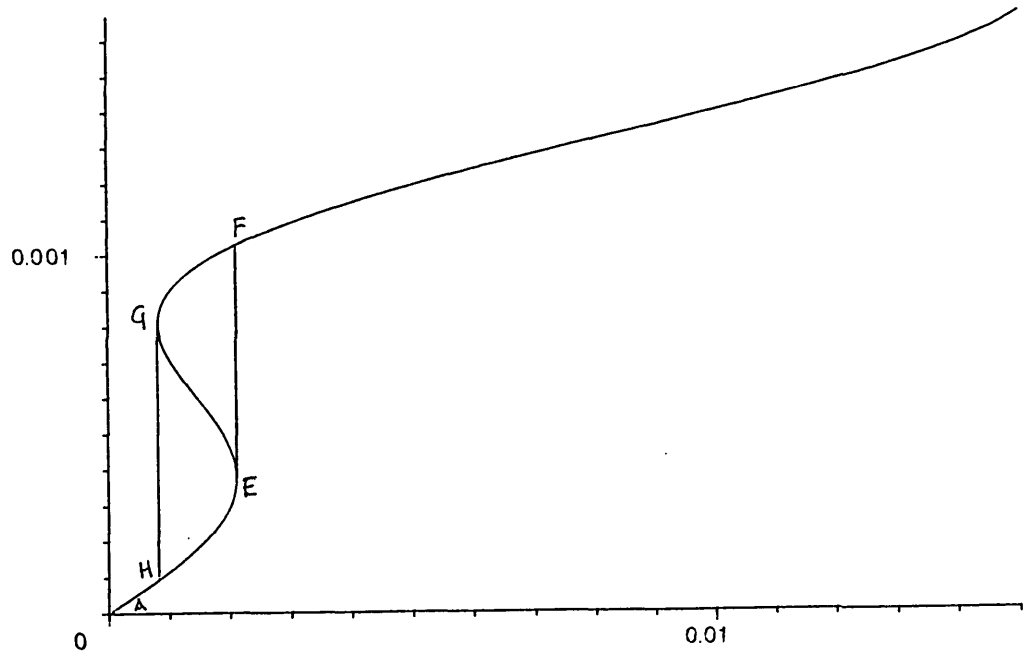

FIGURE 1.14. Output versus input intensity of etalon, showing optical hysteresis.

The width of the bistable region can be altered by

altering the feedback, ie the mirror reflectivity. It is then possible to make different optical components (fig 1.15), for instance bistable device, discriminator/pulse amplifier, differential gain or optical transistor ("transphasor"), clipper and limiter. Here I_o is the biasing input intensity or holding power.

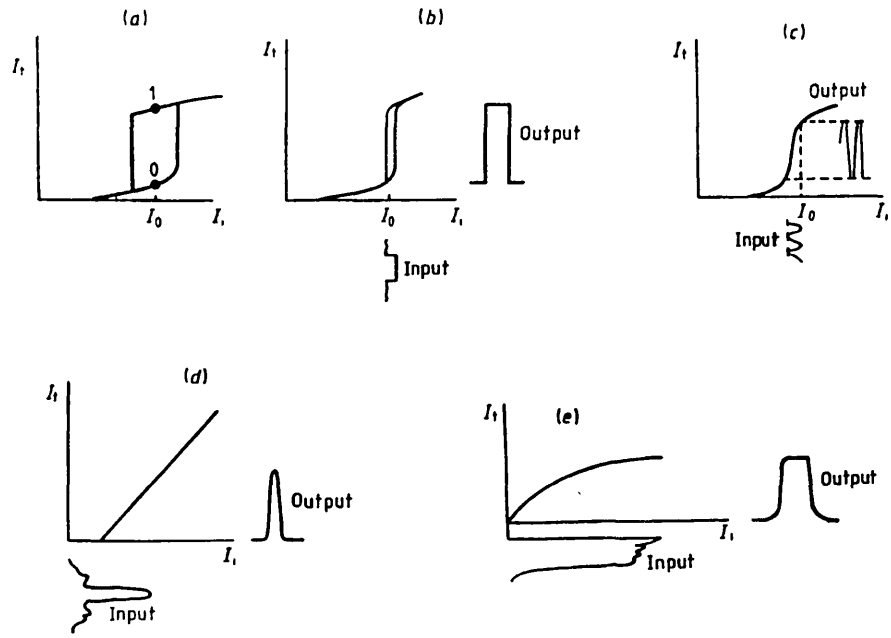

FIGURE 1.15. Various devices made from optically bistable elements. (Abraham and Smith, 1982a)

Finally, it can be seen that optical multistability is also possible. For a high enough input intensity, the straight line intersects with the next peak of the Airy function, or alternatively, the phase shift caused by the intensity dependent refractive index is greater than 2π.

At the present, bistable optical devices are being made and tested with GaAs and InSb. The speed of the devices is limited by relaxation times in the semiconductors and by the cavity relaxation time. In practice, while the devices can switch to an upper state quickly, the long relaxation time of the optical nonlinearity means that the devices

cannot switch back to a lower state immediately. The relaxation time of n_2 in GaAs is strongly dependent on fabrication parameters such as doping, and is typically a number of nanoseconds. For InSb it is even longer, as this material is operated near the bandgap to exploit the anomalously large optical nonlinearlity there. It seems then that these materials would be unsuitable for all-optical processing. However there is one advantage. The slab geometry allows several beams - perhaps hundreds - to enter the device and be processed independently in parallel. This massive parallelism is far simpler in semiconductor etalons than in any other type of device, as all that needs to be done is to focus the beams down into the medium and make sure they are kept separate - no waveguides or electrodes are required.

1.4.2 The all optical gate.

An all-optical waveguide device which has been made and tested is the all optical gate of Lattes, Haus, Leonberger and Ippen (1983). The device is basically a Mach-Zehnder switch combined with two Y-junctions at the input end (fig 1.16).

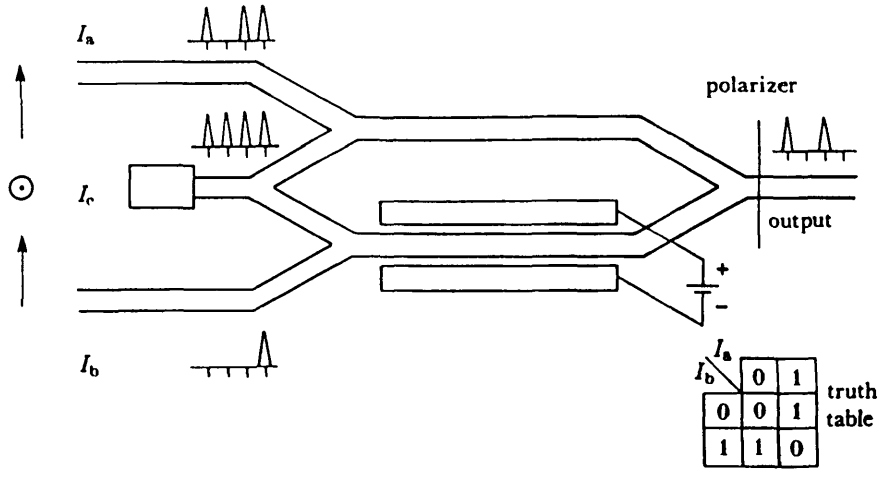

FIGURE 1.16. The all-optical gate (Lattes et al 1983).

The outer two inputs, A and B, take control signals which must be of sufficient intensity to alter the refractive index. The centre input, C, usually takes a stream of pulses. There is a biasing electrode on one arm of the interferometer to allow the phase difference between the two arms to be changed from zero to π. This bias voltage is purely dc and does not detract from the all-optical nature of the switching.

The signal input takes TM pulses and the controls TE. With no control pulses and a π phase-shift on the electrode, the field at the output end of the device is antisymmetric; since single-mode guides are used, however, this mode is not confined and rapidly escapes into the substrate. Now if the TE pulses are introduced down the A control input, with just enough intensity to produce a π phase shift in the other arm, the phase shifts in both arms of the interferometer are equal and the TM pulse emerges. TE and TM pulses can be separated on output with a polariser.

With different combinations of pulses in the inputs and dc bias on the electrodes, the device can become an AND gate, a NOT gate or an XOR gate. For instance, with a π bias, the gate is an AND gate between the A and C inputs; each A input pulse counteracts the π bias, allowing a C pulse to pass simultaneously. An A pulse alone will not pass the polariser and a C pulse alone will be rendered antisymmetric and escape to the substrate. On the other hand if a stream of pulses is input at C then the device gives the XOR of the A and B inputs. An A pulse will equal the π bias, a B pulse will make it a 2π bias - either will allow a C pulse to pass, giving an output. Both or neither A and B will leave the two arms unbalanced, so that no C pulse will pass and the A and B pulses will again be stopped by the polariser.

Fabrication was tried in $LiNbO_3$. However, only modulation was obtained as the nonlinearity is so weak that intensities sufficient for switching result in damage. The device fared better when speed was considered, as it could cope with 10 ps pulses.

For this technology to be practical, a higher nonlinearity is required. Lattes et al report another attempt with GaAs multiple quantum well material, which has a higher nonlinearity than $LiNbO_3$ but a much longer relaxation time of 20ns. The relaxation time was speeded up using carrier diffusion, so that pulse separations of 300 ps were possible. The peak power of 1W compared well with the estimated 1.5 kW for $LiNbO_3$.

Lattes et al think that an improvement in material nonlinearity and relaxation time by a factor of ten would result in a viable technology.

1.4.3 All optical directional coupler.

Another nonlinear waveguide device, the all-optical directional coupler results when a directional coupler is made from a material exhibiting intensity-dependent refractive index. The coupler is made in the same way as the linear directional coupler decribed in section 1.3.1 and behaves linearly for low input light levels. For high input intensity into one guide only, a refractive index change is produced in that guide, and this destroys the phase matching required for complete coupling.

If the coupler is made one coupling length long, so that light input in guide 1 will emerge from guide 2, then a light input of sufficient intensity will change the propagation constant of guide 1 so that coupling into guide 2 will not be possible. This is a perfect all-optical switch - a light beam comes out of one or

other guide according to its intensity. No electrical intervention is necessary, although is is convenient to use a dc bias to tune the guides to each other, as they are likely to have slightly different propagation constants.

Although the device delays pulses because of its physical length, switching times can be sub-picosecond if the optical nonlinearity allows it. The device is said to operate in a pipeline mode, with a number of pulses in the waveguide, separated in time, each being processed according to its intensity and independently of the others.

Li Kam Wa et al (1985) report an all-optical directional coupler in multiple quantum well (MQW) GaAs (see fig 1.17).

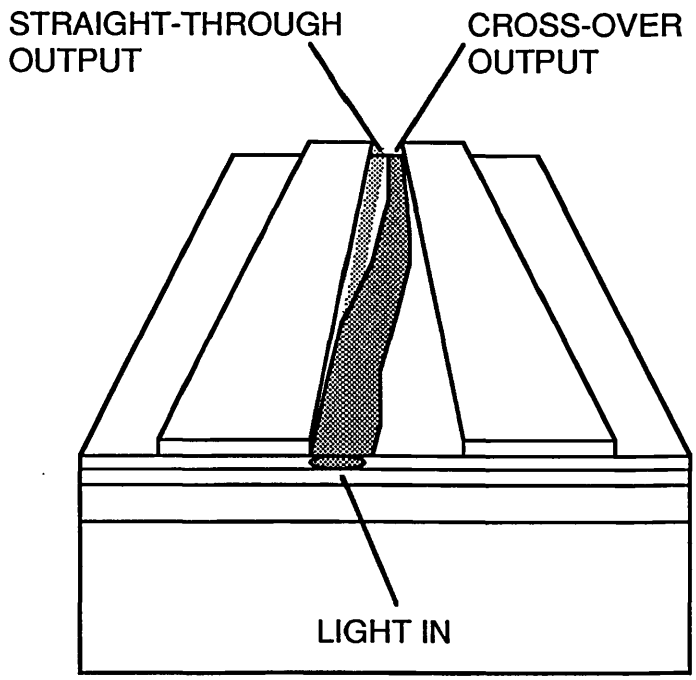

FIGURE 1.17. All-optical directional coupler (Li Kam Wa et al 1985).

First of all a planar waveguide was made in the material. Next gold strips were evaporated onto the surface. On cooling, the gold contracts and sets up a stress pattern along the strip. As the material is photoelastic, a refractive index change is produced in the area of stress, and this results in a waveguide following the gold strip. With two gold strips formed close to each other, the result is a directional coupler. Since the material also exhibits intensity dependent refractive index, the device is nonlinear. Switching powers of only 1mW were achieved with a GaAlAs laser operating at 850 nm. Although the experiment was done at 180 K, it is claimed that it could be duplicated at room temperature with the right laser source. At present there is no indication of the speed of the device.

1.5 Preview of chapters 2-7

The rest of this thesis describes a theoretical and experimental study of directional coupler in $LiNbO_3$. In chapter 2, the simple one-dimensional analysis due to Jensen (1982) is reproduced. In chapter 3, the Beam Propagation Method (BPM) used for the simulations is introduced and developed. The results of the BPM simulations are presented and discussed in chapter 4. Chapter 5 presents the development and results of another computational method based on a computational model of a Gire-Tournois Interferometer. Chapter 6 describes the fabrication of $LiNbO_3$ waveguide devices and the experiments that were attempted. Conclusions and ideas for future developments are presented in chapter 7.

CHAPTER 2

ONE-DIMENSIONAL THEORY OF THE ALL-OPTICAL DIRECTIONAL COUPLER

2.1 Introduction 45

2.2 Discussion of units and values of n_2 49

2.3 Empirical derivations of switching power 51

2.4 Derivation of coupled mode equations 52

2.5 Solutions of coupled mode equations 55

2.6 Predictions for switching power 58
- 2.6.1 Jensen's experiments 58
- 2.6.2 Power predictions for $LiNbO_3$ AODC experiments 59

Chapter 2. One-dimensional theory of the all-optical directional coupler

2.1 Introduction

In this chapter, Jensen's analysis (1982) of the all-optical directional coupler (AODC) is described, and the implications for the computational and experimental investigations presented in the rest of this thesis are discussed.

The AODC was first proposed by Jensen in 1980. His device was similar to the linear directional coupler described in 1.3.1, but was to be made in a material whose refractive index had a component that was proportional to the intensity of light in its waveguides (see fig 2.1). The device would then behave in a nonlinear fashion as described in 1.4.3.

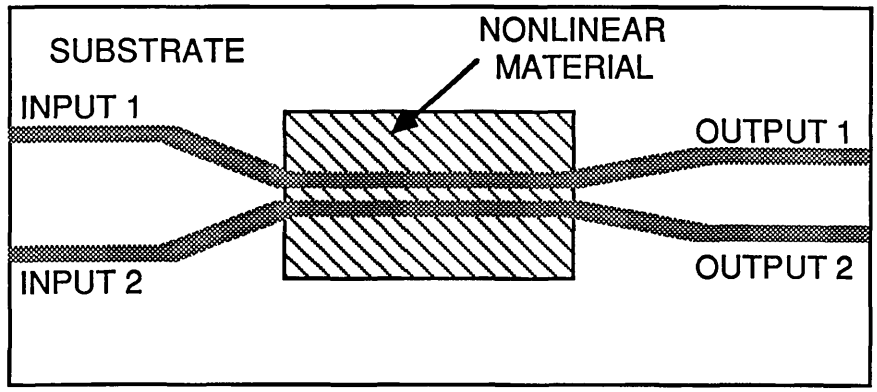

FIGURE 2.1. The all-optical directional coupler.

Jensen claimed that his device would be capable of sub-picosecond switching, provided that the relaxation of the nonlinearity of the material was fast enough. At first, this does not seem to be possible because a light

pulse takes tens of picoseconds to travel through a 5mm waveguide. However, what is of importance for switching speeds is not the time taken for an individual pulse to be processed, but the number of pulses which can be processed in a given time. The AODC is said to operate in a pipeline mode, which means that many pulses can be sent into the device one after the other, and while at any instant there may be tens of pulses in the device, each will be processed individually, according to its power.

It is interesting to compare this behaviour with that of a nonlinear Fabry-Perot etalon (FPE) (see chapter 1.4.1). An FPE with a large cross-sectional area can process many pulses simultaneously in parallel, as long as they are spatially separated. It cannot work in a pipeline mode because pulses which are input at the same point in space but separated in time will be stored in the device for long enough to encounter the same part of the material at the same instant and so cannot be processed independently.

Unfortunately, there is still no suitable material with which to make an AODC. Table 2.1, taken from Chang 1981, shows nonlinearities and relaxation times for several classes of materials. The nonlinearity of $LiNbO_3$ is in the third category, nonlinear electronic polarizability, and has a fast enough relaxation time to realise the full potential of the AODC. On the other hand, its nonlinearity is so weak that the power levels required for switching cause optical damage. Highly nonlinear materials such as GaAs can be switched without risk of optical damage, but the long relaxation time of several nanoseconds makes pipelining impossible.

Physical mechanism	n_2 (esu)	τ (sec)
Molecular-orientation Kerr effect	$10^{-11} - 10^{-12}$	$10^{-11} - 10^{-12}$
Molecular redistribution (libration)	$10^{-12} - 10^{-13}$	~2x10-13
Nonlinear electronic polarizability	$10^{-8} - 10^{-14}$	$10^{-14} - 10^{-15}$
Electrostriction	$10^{-11} - 10^{-12}$	$10^{-8} - 10^{-1}$
Thermal effects	$10^{-4} - 10^{-3}$	0.1 - 1

TABLE 2.1. Properties of some classes of nonlinear materials (Chang 1981).

The rest of this chapter follows Jensen in using a one-dimensional coupled wave model to determine the switching power required for nonlinear operation. This analysis amounts to a description of the state of knowledge at the start of the research programme; the analysis and results in chapters 3, 4 and 5 seek to improve on this model.

To set the stage for the following analysis, section 2 examines the notation for intensity dependent refractive index and reviews numerical values for the nonlinearity and corresponding relaxation times for a number of integrated optics materials. This information is used to make a direct empirical estimate of the switching power in section 3. Section 4 reviews the coupled mode approach to the problem, culminating in a more rigorously obtained prediction for the switching power. Section 5 presents the solutions of the coupled mode equations for comparison

with the computational methods used in chapter 4. Section 6 reviews the results of Jensen's experiments and uses the estimates derived in this chapter to make predictions concerning the experiments described in chapter 6.

2.2 Discussion of units and values of n_2

The relationship between the intensity, I, of light in a material and the refractive index, n, of the material can be expressed either as

$$n = n_o + n_2 I \qquad 2.1$$

or

$$n = n_o + n_2 \langle E^2 \rangle \qquad 2.2$$

Since the numerical value of n_2 is obviously different in these two cases, it is convenient to call n_2 in (2.1) n_2^I and in (2.2), n_2^E.

It seems that authors who prefer to work in MKS use (2.1), although they may express n_2 in cm^2/MW rather then m^2/W. Those who prefer esu use (2.2). As the esu unit of electric field is statvolt/cm, the esu unit of n_2 is $cm^2/statvolt^2$. Unfortunately the great majority of authors quoting n_2 values in esu do not state their units explicitly, nor do they state whether they are in fact using n_2 with reference to equation 2.1 or 2.2. Jensen's papers are assumed to use equation 2.2 because they reference Hellwarth (1977), which gives equation 2.2 explicitly.

To convert a value of n_2^E expressed in esu to n_2^I expressed in MKS it is necessary to convert n_2^E (esu) to n_2^E (MKS) and then convert n_2^E (MKS) to n_2^I (MKS). It is also normal to quote n_2 values in cm^2/MW rather than the true MKS unit, m^2/W. The following conversion factors apply:

$$n_2^E \text{ (esu)} = n_2^E \text{ (MKS)} \times 9 \times 10^8$$

$$n_2^E \text{ (MKS)} = n_2^I \text{ (MKS)} \times n_o c \varepsilon_o / 2$$

$$n_2^I (m^2/W) = 10^{-10} \times n_2^I (cm^2/MW)$$

With this information it is possible to construct the following table of n_2 values for different media given by different authors:

Substance	n_o	λ	n_2(cm^2/MW)	n_2(esu)	Refs
CS_2	1.61	694nm	6.24×10^{-8}	1.2×10^{-11}	1
$LiNbO_3$	2.25$_e$	840nm	3×10^{-7}	8×10^{-13}	2
GaAs	3.2	10μm	3.7×10^{-7}	14×10^{-11}	3
InSb	3.75	10μm	1.8×10^{-5}	804×10^{-11}	3
SF-59 glass	1.95	650nm	8.8×10^{-9}	2.0×10^{-12}	4
SF-6 glass	1.85	650nm	4.2×10^{-10}	9.3×10^{-13}	4
Fused SiO_2	1.45	650nm	3.5×10^{-10}	6.0×10^{-14}	4
PDA	1.88	>750nm	10^{-6}	2.2×10^{-10}	5

TABLE 2.2. Values of n_2 for different materials. References: 1 - Paillette (1969), 2 - Lattes et al (1983), 3 - Chang (1981), 4 - Thomazeau et al (1985), 5 - Carter et al (1983).

A good review of third-order nonlinearities, including n_2, can be found in Hellwarth (1977), while the values of n_2 for various materials are reviewed in Chang (1981).

2.3 Empirical determination of switching power

An empirical estimate of the switching power required for nonlinear operation can be made as follows. From the discussion above, it is evident that switching takes place when the phase change for a wave travelling through the device at high power differs from that at a low power by some factor of π. Hence,

$$2\pi L\Delta n/\lambda \sim m\,\pi \qquad 2.3$$

where L is the device length, Δn is the induced refractive index change, λ is the wavelength and m is an integer, is the condition for switching.

This condition on Δn can be used to find the critical intensity, I_c and the critical power, P_c, as follows;

$$\begin{aligned}\Delta n &= n_2 I_c \\ &= n_2 P_c/A \end{aligned} \qquad 2.4$$

where A is the cross-sectional area of the waveguide.

And so we obtain;

$$P_c = m\lambda A/2Ln_2 \qquad 2.5$$

Substituting the values λ = 1μm, A = 3μm^2, $^{m=1,}_{1}$L = 5mm and n_2 for $LiNbO_3$ = 3 x 10^{-9} cm^2/MW, the critical intensity of 33GW/cm^2 results, with a corresponding P_c of 1 kW.

This empirical estimate gives the same order of magnitude for the switching power as the more sophisticated methods described later. However, the result must be compared with the damage threshold for $LiNbO_3$, which is 600 MW/cm^2 (Normandin et al 79). The decision to go ahead with the experiments in the face of these figures is justified in chapter 6.

2.4 Derivation of coupled mode equations.

The coupled mode equations of Jensen (1982) are derived with reference to Snyder (1972), (Yariv 1973) and (Marcuse 74).

We start from Maxwell's curl equations;

$$\nabla \wedge \underline{E} = -\mu \, \partial \underline{H}/\partial t \qquad 2.6$$

$$\nabla \wedge \underline{H} = \partial \underline{D}/\partial t \qquad 2.7$$

$$\text{where } \underline{D} = \varepsilon_o \, \underline{E} + \underline{P} \qquad 2.8$$

There are several contributions to $\underline{P}$; these can be treated as the usual linear $\underline{P} = X\varepsilon_o\underline{E}$ plus a series of perturbations. Of these, another three main terms need be considered. A second linear contribution arises from the interaction of the mode in one guide with the presence of the other guide. The two major nonlinear terms are due respectively to the nonlinear interaction of the wave in one guide with itself and with the mode in the other guide. It is convenient to call these last three terms $\underline{P}_{NL}$ and amalgamate the linear part of $\underline{P}$ with $\underline{E}$. The other nonlinear terms can be ignored. Hence

$$\underline{D} = \varepsilon \underline{E} + \underline{P}_{NL} \qquad 2.9$$

$$\text{where } \varepsilon = (1 + X_E) \, \varepsilon_o \qquad 2.10$$

Next, we split the $\underline{E}$, $\underline{H}$ and $\underline{P}$ vectors and the ∇ operator into transverse parts, subscripted "T" and longitudinal parts, subscripted "Z". Some manipulation of (2.6) and (2.7) leads to the following two equations (in esu).

$$\nabla_z \wedge \underline{E}_T - \frac{ic}{\omega} \nabla_T \wedge \nabla_T \wedge \underline{H}_T - \frac{i\omega}{c} \underline{H}_T = \frac{4\pi}{\varepsilon} \nabla_T \wedge \underline{P}_{z\,NL} \qquad 2.11$$

$$\nabla_z \wedge \underline{H}_T - \frac{ic}{\omega}\nabla_T \wedge \nabla_T \wedge \underline{E}_T + \frac{i\omega\varepsilon}{c}\underline{E}_T = -\frac{i4\pi\omega}{c}\underline{P}_{NL} \qquad 2.12$$

After expanding the $\underline{E}_T$ and $\underline{H}_T$ in ideal modes

$$\underline{E}_T = \sum_\nu a_\nu(z)\ \underline{E}_T^\nu \qquad 2.13$$

and using the orthonormality relation for waveguide modes

$$\int dx\ dy\ \underline{k} \cdot \underline{E}_T^\nu(\underline{r}) \wedge \underline{H}_T^{\nu'}(\underline{r})^* = 2\pi P_o\ \delta_{\nu\nu'}/c \qquad 2.14$$

where P_o is the normalised power, we obtain

$$-i\ \frac{\partial a^\nu(z)}{\partial z} = \frac{\omega}{P_o}\int dx\ dy\ \underline{E}_\nu(r)^* \cdot P_{NL}(r) \qquad 2.15$$

To apply this equation to the case of the nonlinear directional coupler, we treat single modes in two waveguides running parallel and close to each other, and identify the components of $\underline{P}_{NL}$.

The presence of the second guide changes the propagation constant of the first guide. This is equivalent to a change in susceptibility of, say, δ, so $\underline{P}_{NL}$ has a term $\delta\underline{E}$. The wave in the second guide can add coherently to the wave in the first guide, giving rise to $\underline{P} = (\varepsilon+\delta)\underline{E}'$ where ε is the susceptibility of the unperturbed guide. The two nonlinear terms arise from

$$\underline{P} = n_o n_2/4\ |\underline{E}|^3$$

and $$\underline{P} = n_o n_2/2\ |\underline{E}|\,|\underline{E}'|^2$$

Hence we can write down the two nonlinear coupled mode equations for the system in terms of a and a', the two mode amplitudes.

$$-i\,\frac{\partial a}{\partial z} = Q_1 a + Q_2 a' + (Q_3|a|^2 + 2Q_4|a'|^2)a \qquad 2.16a$$

$$-i\,\frac{\partial a'}{\partial z} = Q_1 a' + Q_2 a + (Q_3|a'|^2 + 2Q_4|a|^2)a' \qquad 2.16b$$

where

$$Q_1 = \frac{\omega}{4\pi P_o}\int dx\,dy\,\delta|E|^2 \qquad 2.17a$$

$$Q_2 = \frac{\omega}{4\pi P_o}\int dx\,dy\,(\varepsilon + \delta)EE'^* \qquad 2.17b$$

$$Q_3 = \frac{n_o n_2 \omega}{\pi P_o}\int dx\,dy\,|E|^4 \qquad 2.17c$$

$$Q_4 = \frac{n_o n_2 \omega}{\pi P_o}\int dx\,dy\,|E|^2\,|E'|^2 \qquad 2.17d$$

2.5 Solutions of coupled mode equations

As the two guides are identical, and the linear interactions of the waves are coherent, Q_2 has no phase mismatch and can be chosen to be real. This allows the solutions of the coupled mode equations to be expressed in terms of elliptic integrals. A considerable simplification is introduced if all the power is initially launched into one guide, say guide 1. Then the power remaining in the guide with distance z is

$$P_1(z) = P_1(0) \{1+ cn (2z|m)\}/2 \qquad 2.18$$

where $m = P_o^2 / P_c^2$ and the critical power $P_c = 4Q_2/Q_3-Q_4$; hence m is a measure of the input power relative to the critical power. The function cn (u|m) is approximately cos (u) when $m \sim 0$ (low input power compared to the critical power) and sech (u) for m approaching 1 (at critical power) (Abramowitz and Stegan 1965, Milne-Thomas 1956).

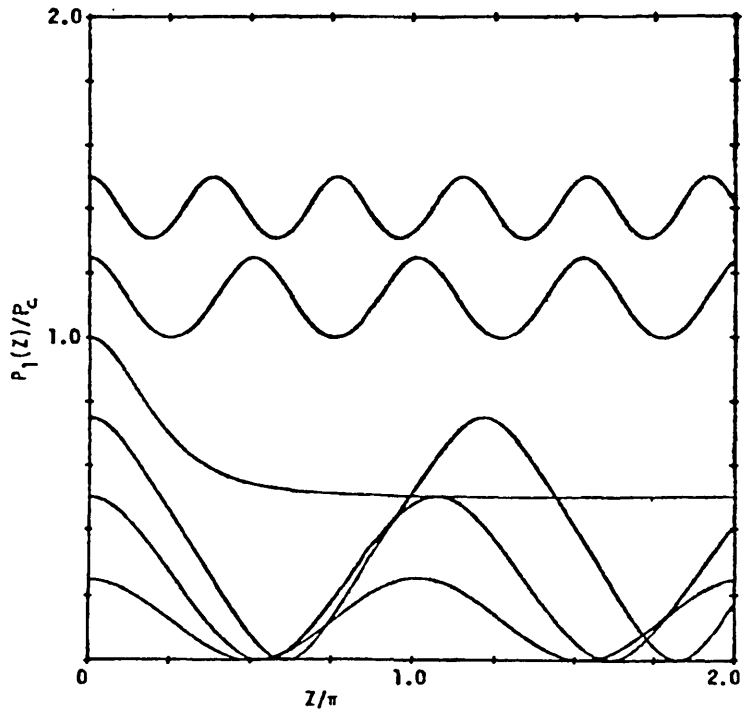

FIGURE 2.2. Power remaining in input guide of AODC versus distance. (from Jensen 1980a).

Jensen produced two diagrams of the solutions to demonstrate the use of the NLDC as an all-optical switch. The first (fig 2.2) is a plot of power remaining in the input guide versus distance. The power is normalised so that the critical power is one unit and distance is normalised so that one coupling length is $2/\pi$. For an input power low enough to be in the linear region, the curve is a simple sinusoid, shifted vertically so that its minima touch the x axis. This shows that all the power launched into the guide is transferred out of it completely into the other guide and then completely back again every coupling length. As the input power is increased, the coupling length becomes longer, but 100% coupling is still achieved. For input power equal to the critical power, a curve which is a vertically shifted sech is obtained, falling to the value $^1/_2$ as an asymptote, indicating that in this situation, the launched power is divided equally between the two guides and no further cross-coupling takes place. Finally, for input powers above the critical power, a sinusoidal z-dependence is again obtained, but now only a fraction of the input power is ever coupled to the other guide.

Linear and nonlinear behaviour can be distinguished by a factor of 2 in input power level. This is useful for binary logic, as it would be possible to indicate "0" by one pulse and "1" by two pulses.

Another way to present the solutions is to plot normalised input/output power curves for devices of various lengths (fig 2.3). The device lengths, L, are such that $Q_2L = \pi/2$, π, $3\pi/2$ and 2π.

Study of these curves demonstrates how the devices could be used as logic gates. For instance, the curve marked on the diagram as "$kL = \pi$" gives a high output for inputs around 2 units and a low output for inputs just below 4 units. If two sources of power 2 units were merged into

one of the device inputs, then the output would be zero if both or neither sources were present and high if either source were present - this is the operation of an XOR gate. It is also instructive to observe the difference between these curves and the familiar input/output curve for optical bistability (fig 1.14).

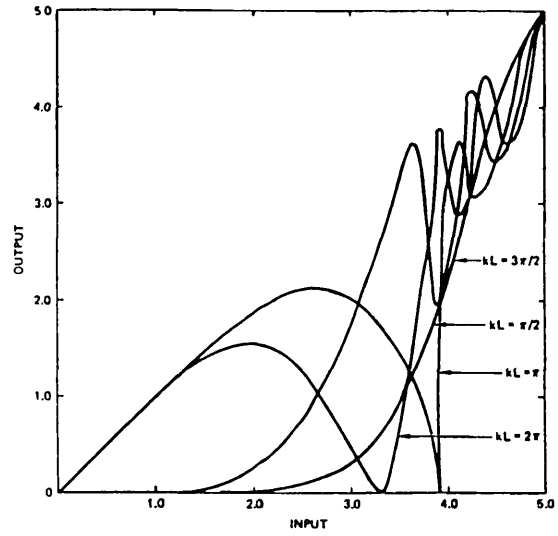

FIGURE 2.3. Input-output curves for four AODCs. (Jensen 1980a)

2.6 Predictions for switching power

We already have $P_c = (4Q_2/Q_3-2Q_4)$, so to find P_c we need Q_2, Q_3 and Q_4. We make the (oversimplified) assumption that the mode of one of the guides consists of a plane wave inside and zero elsewhere. This means that Q_4 is zero and Q_3 reduces to

$$Q_3 = 8\pi^2 n_2 P_o/(\lambda n_o c A) \qquad 2.19$$

so that $$P_c = Q_2 A(\lambda n_o c/(2\pi^2 n_2)) \qquad 2.20$$

Q_2 is identified with $\pi/2$ times the exchange length.

From here it is now possible to predict the power level for nonlinear operation once the crossover length is known. Jensen (1982) calculated a critical power of 3.65 W for a device with 0.5cm exchange length, area 3 μm^2 and λ = 0.85 nm, n_o = 3 and $n_2 = 10^{-7}$ esu. However, he did not say which material was in fact intended.

2.6.1 Jensen's experiments

In Jensen (1980) there is a report of an experiment on a $LiNbO_3$ directional coupler with 3μm wide waveguides 3μm apart over a 3mm distance. However, light at 514 nm was used as the source to encourage photorefractive damage (Ashkin et al 1966, Glass 1978, Glass et al 1980), and this was used as the nonlinear optical effect rather than nonlinear refractive index. Photorefractive damage does cause a refractive index change, but the relaxation time is a matter of hours, unless the damage is annealed out. The result was that a low intensity output of 46% dropped to 19% for high input intensity, for a device of normalised length $\pi/4$. This result did not compare well with the theoretical analysis - the experimenters claimed that better results would require higher powers, but that

higher powers would degrade the waveguides.

2.6.2 Power predictions for $LiNbO_3$ AODC experiments

When the values of the parameters in equation are substituted with those for the proposed $LiNbO_3$ device, the critical power density is 100GW/cm^2. Again, this should be compared with the optical damage threshold in $LiNbO_3$ of 600 MW/cm^2 (Normandin et al 1979). The justification for going ahead with the experiments can be found at the beginning of chapter 6.

CHAPTER 3

THE BEAM PROPAGATION METHOD

3.1 Introduction 61

3.2 Derivation of the BPM 63

3.3 Limitations of the BPM 67

3.4 Setting up the BPM 69

3.5 Testing the BPM 71

Chapter 3. The Beam Propagation Method

3.1 Introduction

The propagation of light waves through a uniform medium can be described by diffraction theory (Hecht and Zajac 1974). However, for propagation in a medium which is non-uniform, birefringent or nonlinear, a numerical model must be used to predict the effects of the material properties on the wave. Two material properties can be modelled simultaneously by treating the medium as consisting of layers in each of which only one of the properties in modelled.

In the case, for instance, of pulse propagation in a dispersive medium exhibiting self-phase modulation (Fisher and Bischel 1975), the medium is divided into alternate dispersive and self-phase modulating slabs. While the self-phase modulation can be applied to the pulse directly in the time domain, the dispersion is easiest to apply to each frequency component of the pulse separately. For this reason the pulse must be Fourier transformed into the frequency domain on entering the dispersive slab, the dispersion applied and the pulse Fourier transformed back into the time domain before entering the self-phase modulating slab.

Each step of the propagation then requires two Fourier transforms; while these can be implemented using the Fast Fourier Transform (FFT) algorithm (Cooley and Tukey 1965, Brigham 1974), considerable amounts of computer time are required, especially for long propagation distances or pulses containing many points of the computational grid. Problems of numerical accuracy and spectral aliasing must also be taken into consideration.

A similar model, the Beam Propagation Method (BPM) was

developed by Fleck, Morris and Feit in 1976, to investigate propagation of laser beams through the atmosphere. In this case, the transverse spatial profile of the beam was considered, requiring a treatment of diffraction; this was achieved by Fourier transforming into reciprocal space, applying diffraction to each spatial frequency of the beam and Fourier transforming back into real space. The model also took into account self-focusing and various effects due to wind and atmospheric turbulence.

Soon the method was applied to the rather simpler case of beam propagation in material media such as optical fibres and waveguides (Feit and Fleck 1978, 1979, 1980a, 1980b, 1980c, 1981, 1983], Fleck and Feit 1983, Baets and Lagasse 1983, Hermansson et al 1984, Thylen 1983 and Van Roey et al 1981).

In the rest of the chapter the derivation and use of the BPM will be discussed and tests of the method for situations with known analytical solutions will be demonstrated.

3.2 Derivation of the BPM

This section reviews the derivation of the three-dimensional BPM found in Feit and Fleck (1978) and Van Roey et al (1981). Since the object of the BPM is to follow waves propagating in a material medium, we start with the wave equation for a scalar field E;

$$\nabla^2 E(x,y,z,t) = \frac{n^2}{c^2} \frac{\partial^2}{\partial t^2} E(x,y,z,t) \qquad 3.1$$

where n, the refractive index of the medium is assumed at present to be any function of x, y and z and c is the speed of light in vacuo. Assuming a time dependance of exp(iωt), the solution for E will have the form

$$E(x,y,z,t) = E(x,y,z) \exp[-i[\omega t]] \qquad 3.2$$

where E is a complex and includes a phase function. And so the wave equation becomes

$$\nabla^2 E(x,y,z) + \frac{\omega^2 n^2(x,y,z)}{c^2} E(x,y,z) = 0 \qquad 3.3$$

This is the scalar Helmholtz equation, which is valid for strictly monochromatic light and takes no account of effects involving the polarisation of the waves. We now wish to express the solution at z = Δz in terms of the field at z = 0. If we make the abbreviation

$$\frac{\partial^2}{\partial x^2} + \frac{\partial^2}{\partial y^2} = \nabla^2_\perp$$

then 3.3 becomes

$$\frac{\partial^2}{\partial z^2} E + (\nabla^2_\perp + \frac{\omega^2 n^2}{c^2}) E = 0 \qquad 3.4$$

By inspection, integrating 3.4 along the z direction from $z = 0$ to $z = \Delta z$ gives

$$E(x,y,\Delta z) = \exp\left[i\Delta z(\nabla^2_\perp + \omega^2n^2/c^2)^{1/2}\right] E(x,y,0) \quad 3.5$$

The BPM requires the square root to be replaced by a so-called symmetrised split operator of the form

$$\exp(-i\Delta za)\ \exp(-i\Delta zb)\ \exp(-i\Delta za) \quad 3.6$$

where the operator a involves $\nabla^2_\perp$, b involves ω^2n^2/c^2 and the symmetrisation is introduced to minimise errors.

It is this approximation which renders the BPM accurate only to second order. Effectively, rather than treating diffraction and the transverse refractive index variation simultaneously, we must allow the beam to diffract through a medium of constant refractive index and then treat the refractive index variation as a passage through a thin lens.

To derive the exact form of the symmetrised split operator, we write

$$\left[\nabla^2_\perp + \frac{\omega^2n^2}{c^2}\right]^{1/2} = \frac{\nabla^2_\perp}{\left[\nabla^2_\perp+\frac{\omega^2n^2}{c^2}\right]^{1/2}+\frac{\omega n}{c}} + \frac{\omega n}{c} \quad 3.7$$

To proceed further, the n on the right hand side denominator must be taken to be the constant n_o, as this is the part that will be treated in reciprocal space. This approximation immediately restricts the BPM to cases with small refractive index variations. In other words, rather than treat a general profile $n(x,y)$, n is assumed to be approximately n_o and the difference, Δn is treated as a perturbation.

Writing $k = n_o\omega/c$ and $X(x, y) = k[n(x, y)/n_o - 1]$ equation 3.7 becomes

$$\left[\nabla^2_\perp + \frac{\omega^2 n^2}{c^2}\right]^{1/2} = \frac{\nabla^2_\perp}{(\nabla^2_\perp + k^2)^{1/2} + k} + k + X(x,y) \qquad 3.8$$

Next, a time dependence of $\exp(i\omega t)$ is assumed, so Let

$$E(x, y, z) = E'(x, y, z) \exp(-ikz)$$

This turns equation 3.5 into

$$E'(x,y,\Delta z) = \qquad 3.9$$

$$\exp\left\{-i\Delta z\left[\frac{\nabla^2_\perp}{(\nabla^2_\perp + k^2)^{1/2} + k} + X(x,y)\right]\right\} E'(x,y,0)$$

To solve this equation numerically, the part involving X must be treated in real space and the part with the derivatives in reciprocal space. However, splitting the operators is a source of error as they do not commute. This error is kept to a minimum if the operators are symmetrised; if we abbreviate the first term in the multiplier of $i\Delta z$ in (3.9) to K, the symmetrised version of (3.9) is

$$E'(x,y,\Delta z) = \qquad 3.10$$

$$\exp\left[\frac{-i\Delta z K}{2}\right] \exp(-i\Delta z X) \exp\left[\frac{-i\Delta z K}{2}\right] E'(x,y,0)$$

The propagation part of the above is dealt with by transforming E_{MN}, the Fourier components of $E(x,y)$ according to

$$E'_{MN}(\Delta z) = E'_{MN}(0) \exp\left\{i\Delta z\left[\frac{K_x^2 + K_y^2}{(k^2 - K_x^2 - K_y^2)^{1/2} + k}\right]\right\} \qquad 3.11$$

where $K_x = 2\pi M/L$ and $K_y = 2\pi N/L$ where M and N are integers

covering the number of points in the grid and L is the length of the grid in the units being used (microns or metres). The refractive index part is simply a multiplication of $E(x, y, \Delta z,)$ by $\exp(-i\Delta z\ X(x,y))$.

3.3 Limitations of the BPM

As has been pointed out, the BPM requires small transverse refractive index variation. In its simplest form, as presently described, it cannot cope with any variation of index along the propagation direction, because this would set up a backward propagating wave which could not be treated with the present forward propagating algorithm. Also, the above derivation was for a single frequency. Treatment of pulses requires each frequency present to be treated separately (Feit and Fleck 1979, 1980c). For anisotropic media a full vector derivation must be developed, leading to a set of vector Helmholtz equations (Feit et al 1983).

The boundary of the computational mesh causes problems. Owing to the discrete nature of any computational Fourier transform we are really setting up an infinite array of computational grids, and waves leak from each to its nearest neighbours. It then appears that waves are reflected from the boundary, and these waves, if unchecked, will travel back into the area of interest and interfere with the computation.

To deal with this, it is often suggested that strong absorbers are placed on the boundary (Feit and Fleck 1978), (Thylen 1983). However, the exact nature of these absorbers seems to be up to the individual. For instance, Thylen suggests returning the outer 20 points of the mesh to zero every step. If anything, this exacerbates the problem as the transition between points which are returned to zero and those which are not becomes a reflecting boundary which is closer to the centre of the grid.

Instead, one can apply a much more gentle "roll-off" towards the edges. For instance, the outer 20 points can be multiplied by a broad sech profile of height 1 towards

the centre of the grid and going down to 0.1 at the edge. Even such a small alteration still causes some scatter, although the situation is improved. It seems that the best solution would be to use a vastly increased computational grid, so that stray waves never reach the boundary over the propagation times being used. However, there is a trade-off with computer cpu time, which increases with the size of the grid used, and economy suggests using the smallest possible grid.

3.4 Setting up the BPM

In order to use the BPM, it is necessary to set up a computational grid, a refractive index profile, a profile for the field launched into the guide and to consider boundary conditions.

When setting up the grid, one must decide on the number of points and the spacing. In practice the number of points is limited to a power of 2 in many FFT algorithms. The grid must have adequate extent and resolution not only for the real space field distribution but for the Fourier space spatial frequency distribution, and this can be checked by looking at plots of both of these distributions during the propagation.

Single-mode waveguides are the most exacting application of the BPM and it is particularly important to ensure that the grid is adequate both in real space and reciprocal space. According to Feit and Fleck (1978), this can be done by considering the relationship between the numerical aperture (NA) of the waveguide and the grid;

$$N\pi/L > k \sin \theta_{MAX} \qquad 3.12$$

where θ_{MAX}, the waveguide NA, is approximately the square of the difference between the maximum and minimum refractive index of the waveguide. With $L = N\Delta x$ and $k = n_o 2\pi/\lambda$, this implies that

$$\lambda > 2 n_o \theta_{max} \Delta x \qquad 3.13$$

For the waveguides which we are about to discuss, this condition holds when λ and Δx are approximately equal.

One would think that the smaller Δx is set, the more accurate the method would be, but there is a restriction on reducing Δx. For the root in the denominator of the

reciprocal space phase change factor in (3.9) to be real,

$$k^2 > k_x^2 \qquad 3.14$$

which implies that

$$\lambda < 2\, n_o \Delta x \qquad 3.15$$

These conditions do not appear to be very restrictive. More exacting requirements for the set-up can be found in Thylen (1983) and Van Roey et al (1981). For instance Thylen, following Van Roey et al, derives the following four conditions on various parameters for the BPM to operate accurately;

$$\left[\frac{2\Delta n}{n}\right]^2 + \left[\frac{s}{k}\right]^4 + \left[\frac{2\Delta n}{n}\right]\left[\frac{s}{k}\right]^2 + \left[\frac{2\Delta n}{n}\right]\left[\frac{p+s}{k}\right]^2 \ll \frac{8\Delta n}{n} + 4\left[\frac{s}{k}\right]^2 \qquad 3.16a$$

$$\Delta z \ll \left[\frac{8\pi}{k}\right]\left\{\left[\frac{s^2}{k^2} + \frac{\Delta n}{n}\right]^2 + \left[\frac{2\Delta n}{n}\right]\left[\frac{s+p}{k}\right]^2\right\}^{-1} \qquad 3.16b$$

$$\Delta z \ll (12n/\Delta n)^{1/2}\,(s+p)^{-1} \qquad 3.16c$$

$$\Delta z \ll 6k(s+p)^{-2} \qquad 3.16d$$

where s is the highest spatial frequency of the field, p is the highest spatial frequency of the refractive index distribution, Δn is the maximum refractive index difference from the substrate and $k = 2\pi n_o/\lambda_o$.

The two papers disagree on the form of 3.16a but agree on the others. Thylen shows that it does not matter much if one of 3.16b-d is not met so long as Δz is not ten times bigger than the quantity on the right hand side of the inequality. However he bases this judgement on the results of rather short propagations of 10-100μm, some of them consisting of only ten steps, which does not seem to be a very stringent test of a BPM program.

3.5 Testing the BPM

It is possible to test the BPM in a number of situations where an analytic solution exists. The first is the case of simple diffraction theory, where a Gaussian beam spreads out from a focus.

To carry out this diffraction in a vacuum, the refractive index distribution is set to 1 everywhere. The field distribution is proportional to $\exp(-x^2/w_o^2)$ with a uniform phase - the conditions at a focus. Here w_o is a width parameter. Siegman (1982) gives the following expression for the width at any distance z from the focus as

$$w(z) = w_o [1 + (z\lambda/\pi w_o)^2] \qquad 3.17$$

A two-dimensional (one transverse, one longitudinal dimension) test was carried out with total propagation distance 1000μm, wavelength 1.06μm, mesh spacing 0.98μm, 256 points in the grid and a sech roll-off applied to the outer 30 points of the grid. The width parameter of the field was 10μm. From (3.15) with these figures, an increase in the width of the curve by a factor of 3.52 can be expected. Figure 3.1 shows a linear plot of the initial and final field distributions (respectively the taller and shorter of the two curves); the two horizontal lines mark their half heights. Figure 3.2 is a plot of the Fourier transforms of these two curves, showing good containment of the spatial frequencies during the propagation. The "cutoff" function used is plotted in figure 3.3; it is a sech at the outer edges and has a uniform value of 1 in the centre. From direct measurement of the plot, the width of the distribution at half height, which is proportional to w(z), increases over this distance by a factor of 3.5 ± 0.08.

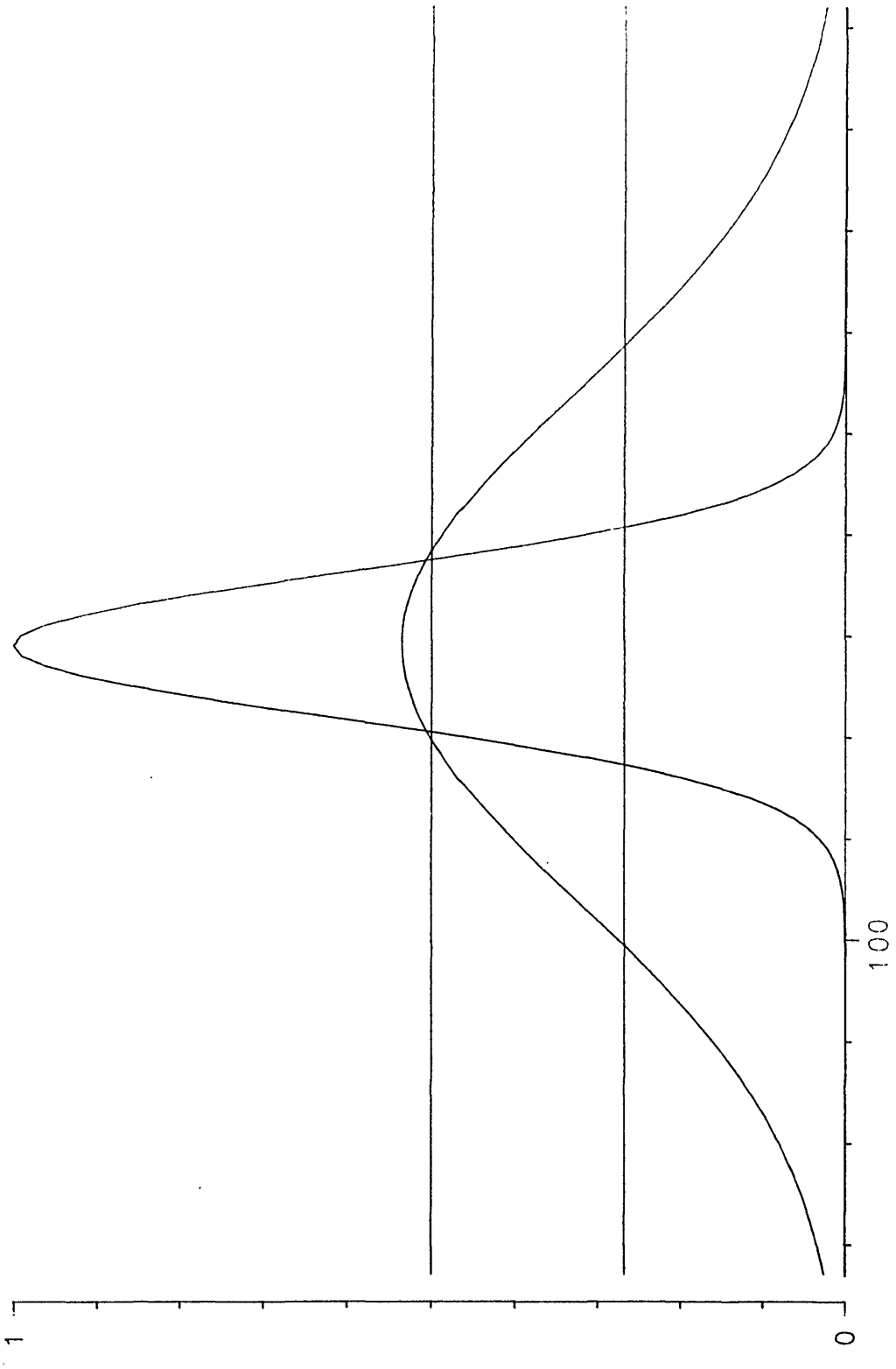

FIGURE 3.1. Field distribution before and after propagation through 1mm of free space.

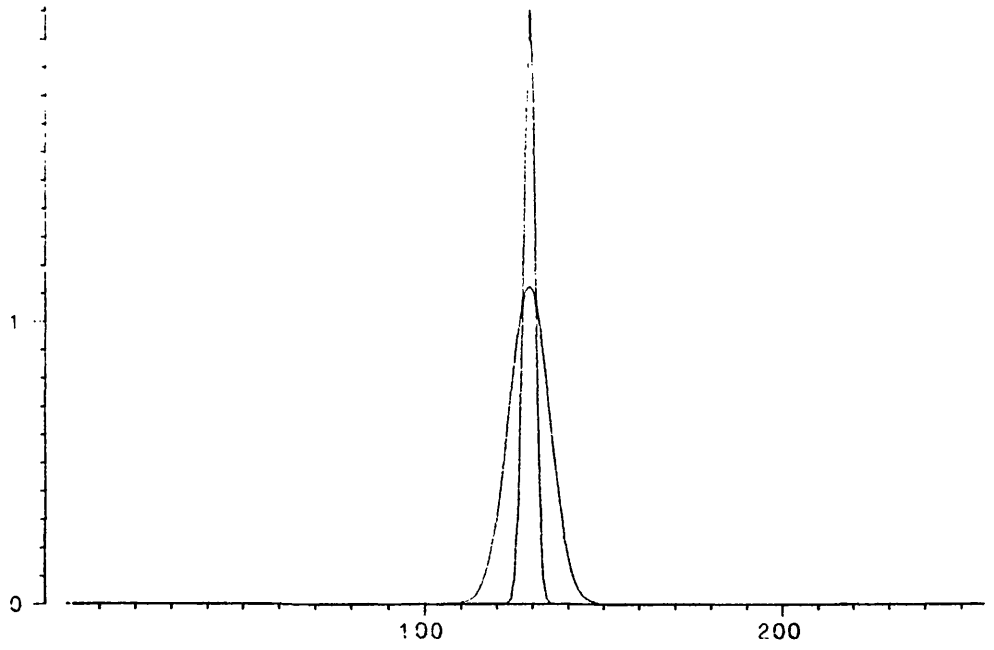

FIGURE 3.2. Spatial Fourier transform of fig 3.1, showing that the spatial frequencies are well contained within the computational mesh.

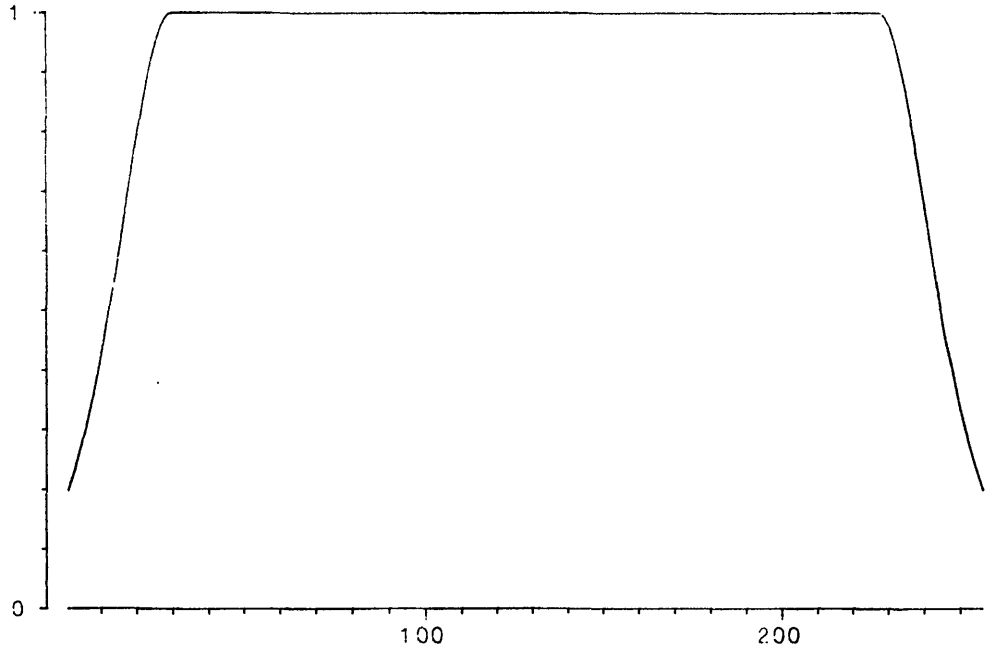

FIGURE 3.3. The field is multiplied by this function each step to avoid interaction with the boundary.

In conclusion, this first test of the BPM shows that diffraction is modelled as expected. However, the test as it stands is not very accurate.

A more exacting test is to check the model's treatment of diffraction against its treatment of refractive index, using a waveguide refractive index profile with an exact analytic solution. Adams (1981) gives a number of examples of analytic solutions for different waveguides. The Epstein-layer profile was chosen for the tests because it seemed similar in shape to the actual profile of Ti in-diffused waveguides in $LiNbO_3$, which is given by the empirical formula (Fukuma et al 1978, Andonovic 1983),

$$n(y,z) = \qquad 3.18$$

$$n_{SUB} + \Delta n(0)\ \exp\left[\frac{-y^2}{2D_y^{\,2}}\right] \operatorname{erf}\left[\frac{w+2z}{2D_z}\right] \operatorname{erf}\left[\frac{w-2z}{2D_z}\right]$$

where n_{SUB} is the refractive index of the substrate, D_y and D_z are diffusion depths which quantify the diffusion of Ti along the respective crystal axes of the $LiNbO_3$ in a given time. The peak refractive index change, $\Delta n(0)$, can be found from

$$\Delta n(0) = A\tau/D_y$$

where A is a constant relating the amount of Ti in the substrate to the refractive index change and τ is the initial thickness of the titanium layer before diffusion.

The symmetric Epstein-layer profile has refractive index

$$n^2(x) = n_2^2 + 2\Delta n_1^{\,2}/\cosh^2(x/a) \qquad 3.19$$

where n_2 is the refractive index of the medium without the waveguide, n_1 is the index at the peak of the distribution, $2\Delta n_1^{\,2} = n_1^{\,2}-n_2^{\,2}$ and a is the parameter

governing the width of the guide. This function is plotted in figure 3.4.

The profile supports a zero-order mode with field distribution (see figure 3.5)

$$\Psi \propto 1/\cosh^{w}(x/a) \qquad 3.20$$

Adams uses normalised quantities to describe waveguide operation. To find w in the above formula, it is necessary to know the normalised frequency, v, and the normalised propagation constant b. The former is found directly from

$$v^2 = 2\Delta n_1^2 k^2 a^2 \qquad 3.21$$

The eigenvalue equation gives

$$b = \left| \frac{(1 + 4v^2)^{1/2} - (2N + 1)}{2v} \right|^2 \qquad 3.22$$

where N=0 for the lowest order mode. The parameter w can then be found from

$$b = w^2/v^2 \qquad 3.23$$

Runs with this refractive index profile and initial mode profile, both with a = 5μm show the shape of the mode remains unaltered over six orders of magnitude on a logarithmic plot after propagation over 300 steps of the algorithm, amounting to 1.26mm. Linear and log plots of this propagation are presented in figures 3.6 and 3.7.

In figures 3.8 and 3.9 the width parameter for the field and the waveguide are mismatched. The field distribution has a = 5μm and the waveguide has a = 20μm. Because the field is not a single mode of the waveguide, but a combination of several, some of which are guided and some of which are not, energy is lost; this can be seen from the log plot, where energy rises in the wings and then is

removed by the cutoff function. The amplitude of the field distribution varies with time instead of being constant as it would be for a guided mode. Since the cutoff function actually removes energy from the numerical model, the propagation should eventually settle down to a combination of guided modes; however this would require very much longer propagation distances.

Figures 3.10 and 3.11 show qualitatively similar behaviour when a for the field is 5μm and for the guide is 20μm.

The next mode has mode profile

$$\Psi \propto \sinh(x/a) / \cosh^{w+1}(x/a) \qquad 3.24$$

To calculate w this time, N=1 must be used in the eigenvalue equation (3.20). It can be seen that this mode will not propagate unless a > 3.5 λ. Figures 3.12 and 3.13 demonstrate accurate propagation when a is 5 μm.

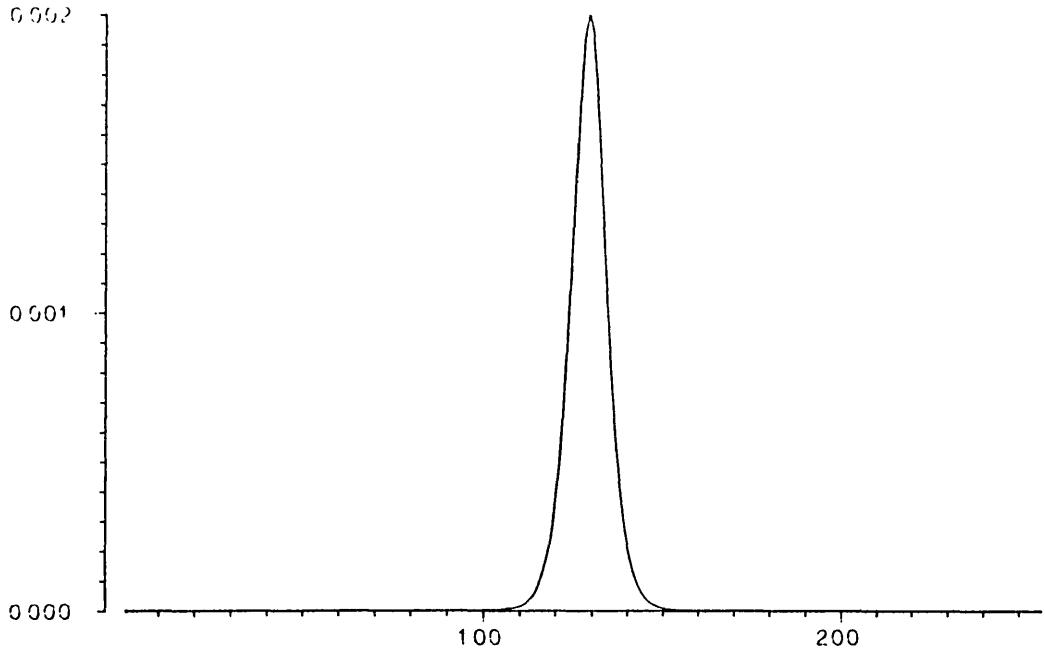

FIGURE 3.4 Refractive index distribution for the Epstein layer profile.

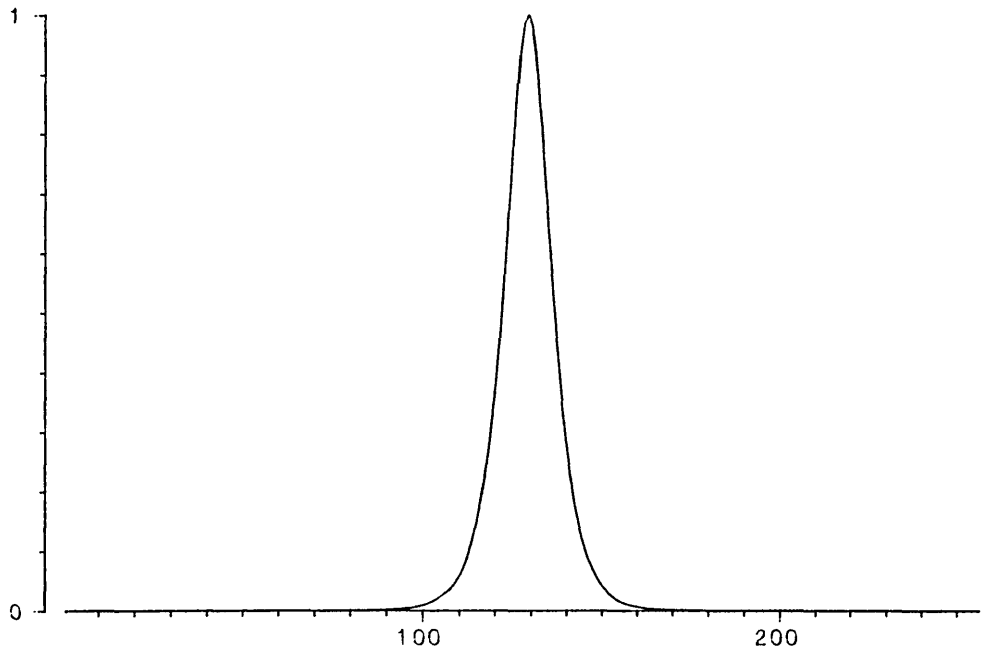

FIGURE 3.5 Modal field distribution for the Epstein layer profile.

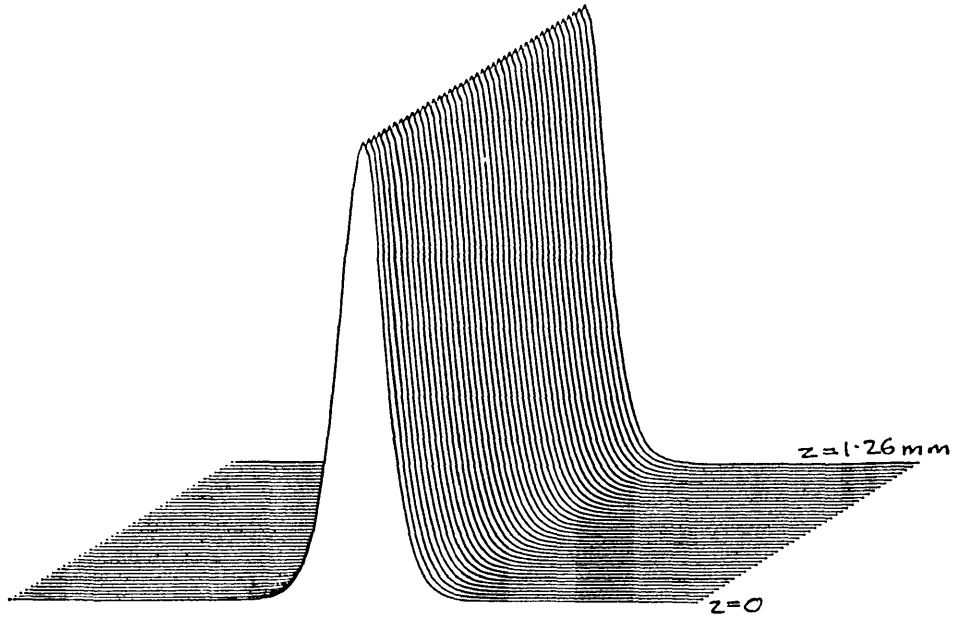

FIGURE 3.6 Intensity distribution during the Epstein layer profile test. Δx = 0.49μm, Δz = 5μm, plots from z=0 to z = 1.26mm. Centre 128 points of computational grid.

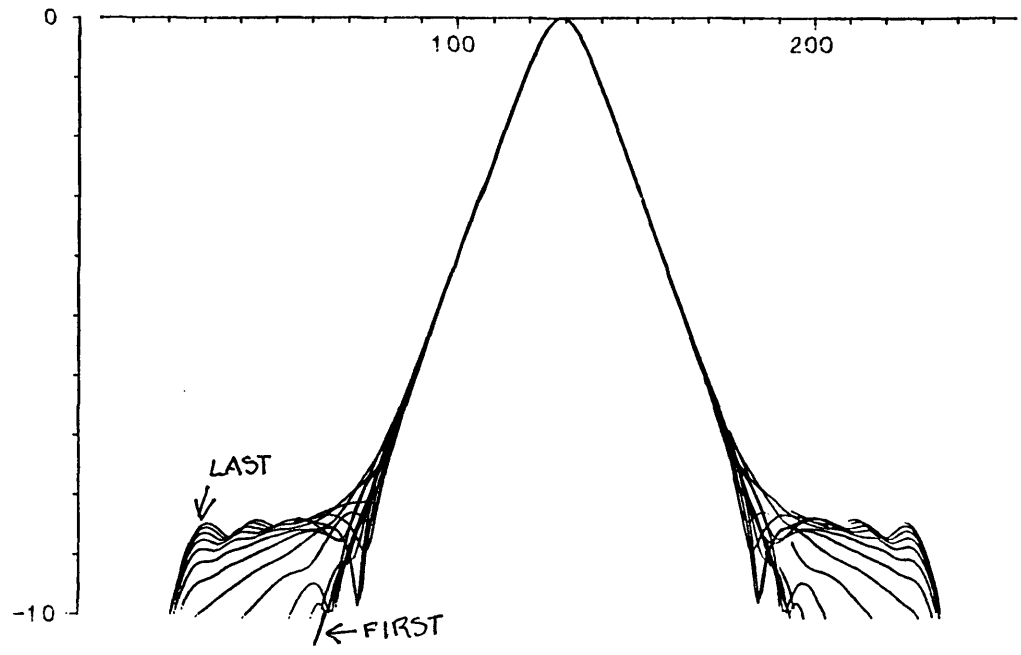

FIGURE 3.7 Log intensity throughout the propagation, showing accuracy over 8 decades.

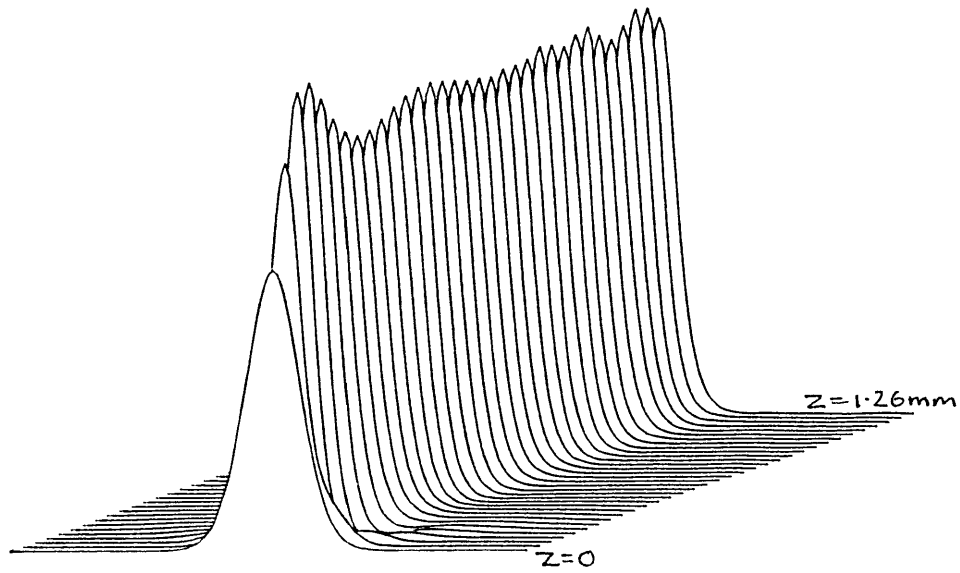

Figure 3.8 As figure 3.6, but with width parameter of waveguide 20μm and for field 5μm.

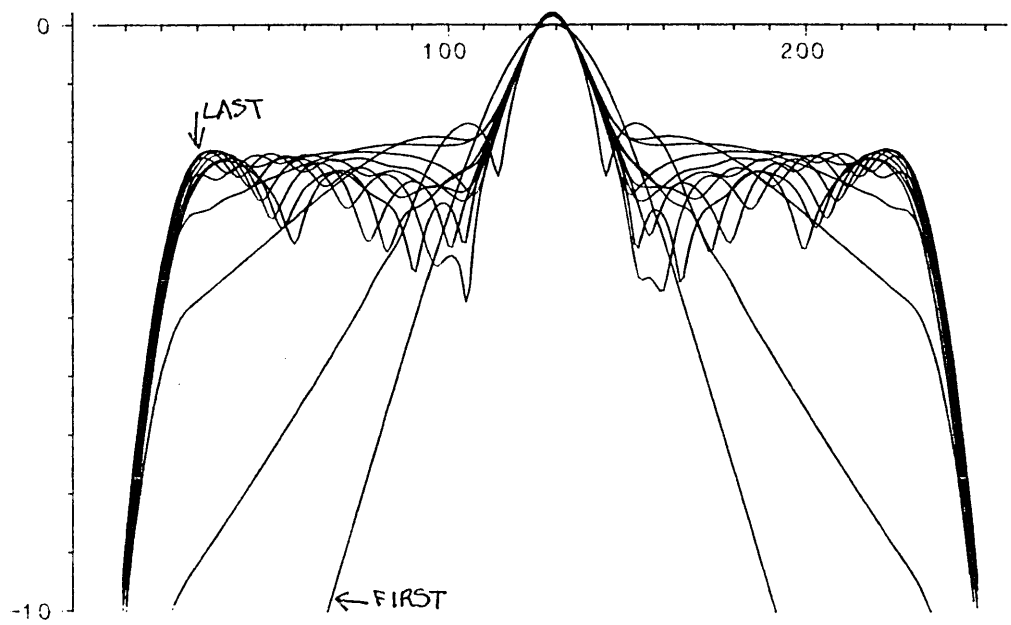

FIGURE 3.9 Log intensity of figure 3.8.

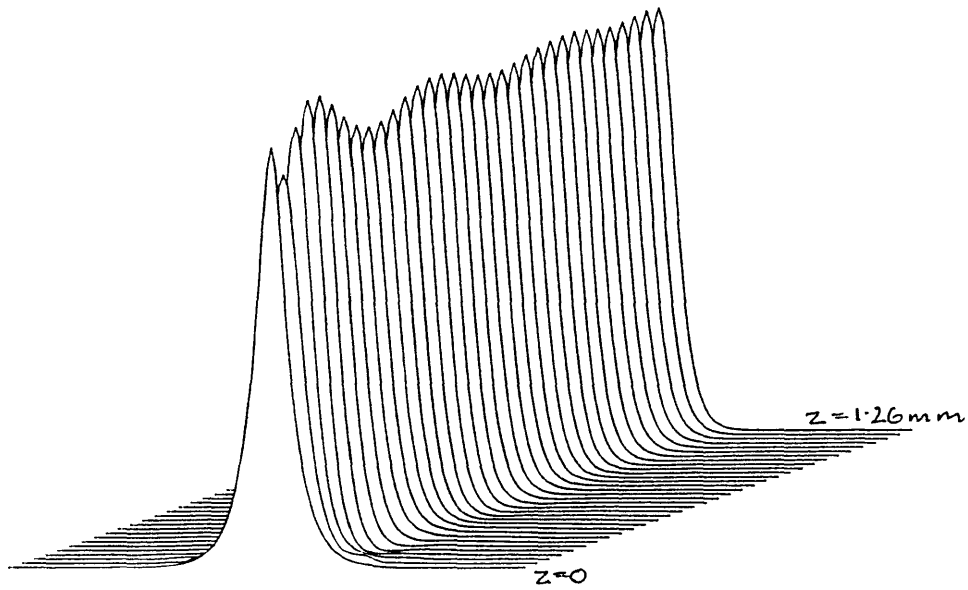

FIGURE 3.10 As figure 3.6 with width parameter of field 20μm and waveguide 5μm.

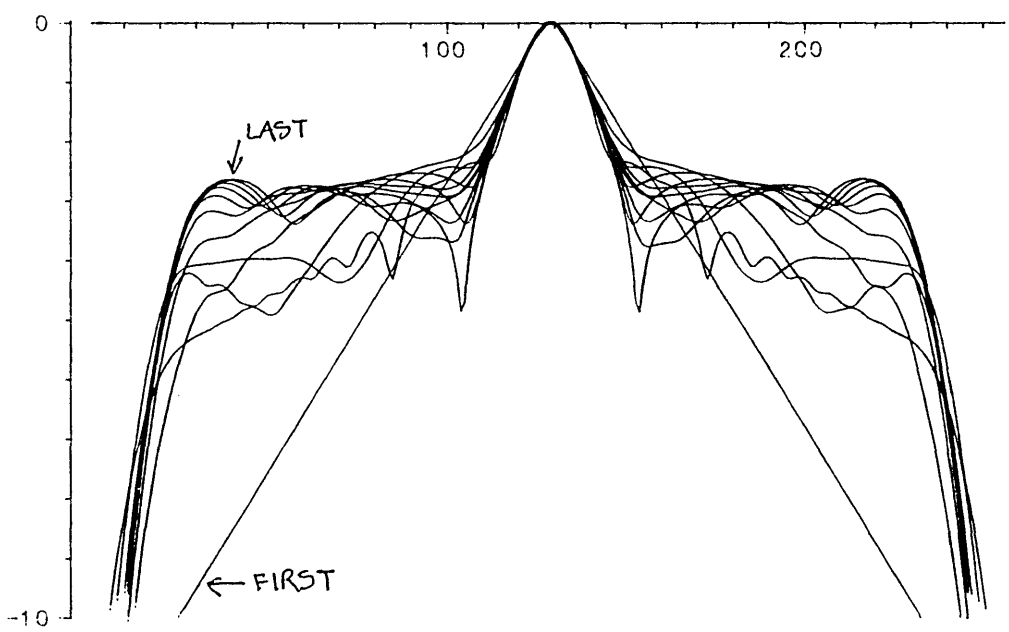

FIGURE 3.11 Log intensity of figure 3.10.

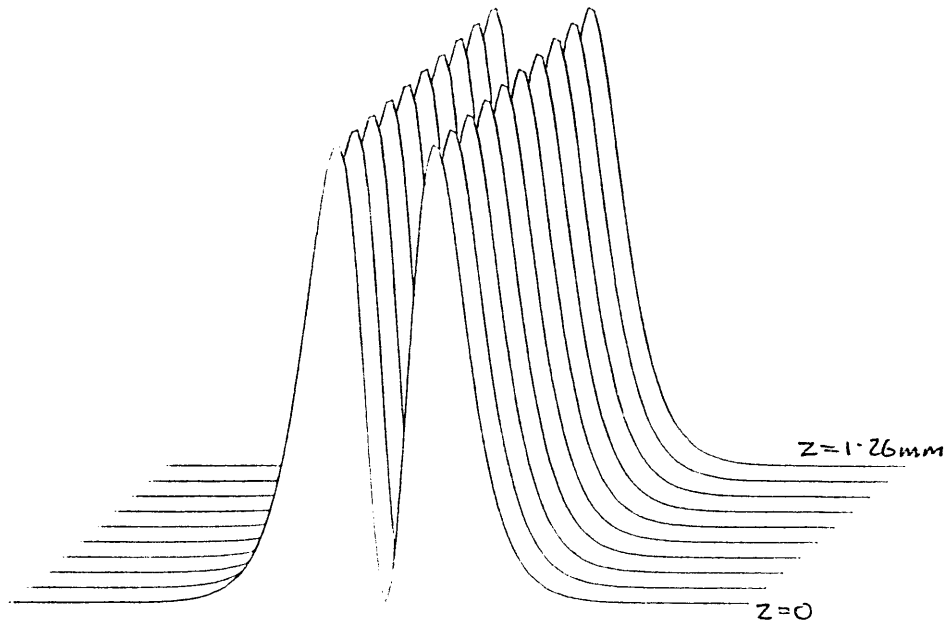

FIGURE 3.12 As figure 3.6 for N=1 mode with a=5λ.

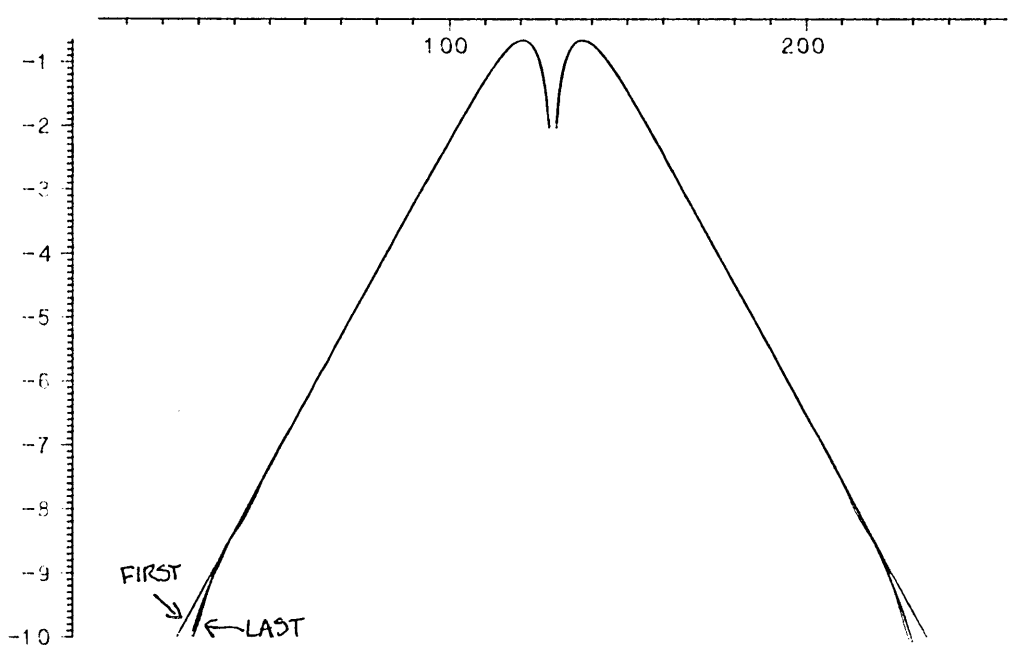

FIGURE 3.13 Log intensity of figure 3.12, showing accurate propagation.

CHAPTER 4

RESULTS OF THE BEAM PROPAGATION METHOD

4.1 Introduction 83

4.2 Modification to model a directional coupler 83

4.3 Modification to model nonlinearity 86

4.4 Runs and results 87

4.5 Conclusions 106

Chapter 4 Results of the beam propagation method

4.1 Introduction

In this chapter, the beam propgation method is used to model an all-optical directional coupler. The model is two-dimensional, with one transverse and one longitudinal dimension, and is equivalent to two parallel planar Epstein-profile waveguides (see eqn 3.18).

Sections 4.2 and 4.3 describe the modifications to the program described in chapter 3 and appendix A that were required. Section 4.4 describes the runs of the computational model that were carried out and presents the results. Conclusions are drawn in section 4.5.

4.2 Modification to model directional coupler.

The BPM program described in chapter 3 used an Epstein-layer refractive index profile for the waveguide, whose centre coincided with the centre of the computational mesh. In order to set up a directional coupler, two such waveguides must be superimposed. This was achieved by setting the refractive index profile to an Epstein profile centred a number of mesh points to the left of the centre and then adding to each array element the value for a refractive index profile centred the same number of mesh points to the right of the centre.

The offset of each waveguide from the centre determines Jensen's Q_2 coupling coefficient (Jensen 1980, 1982) (see eqns 2.17b, 2.20), and so the coupling length of the AODC. The larger the offset, the smaller the coupling coefficient and the lower is Q_2. Since the critical power predicted by Jensen is proportional to Q_2, it ought to be reduced for larger offset. Offsets of 10, 12, and 15 were used for the

runs presented in this chapter. The corresponding refractive index profiles are shown in figures 4.1a, b, and c.

The initial field distribution launched into the AODC was the same as for a single waveguide (see equation 3.19 and figure 3.5) but offset to the left by the same amount as one of the waveguides.

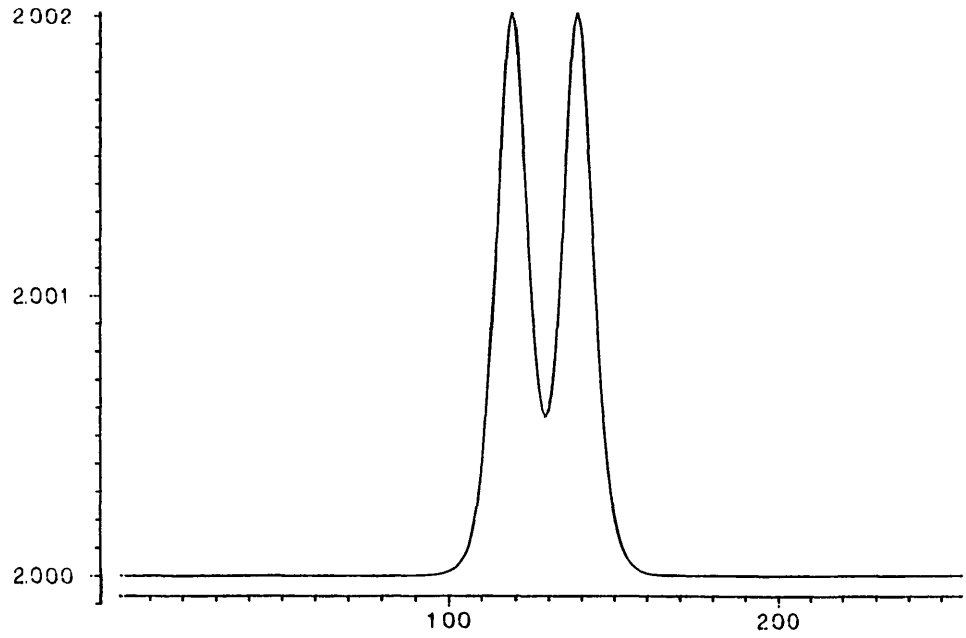

FIGURE 4.1a. Refractive index profile for offset = 10.

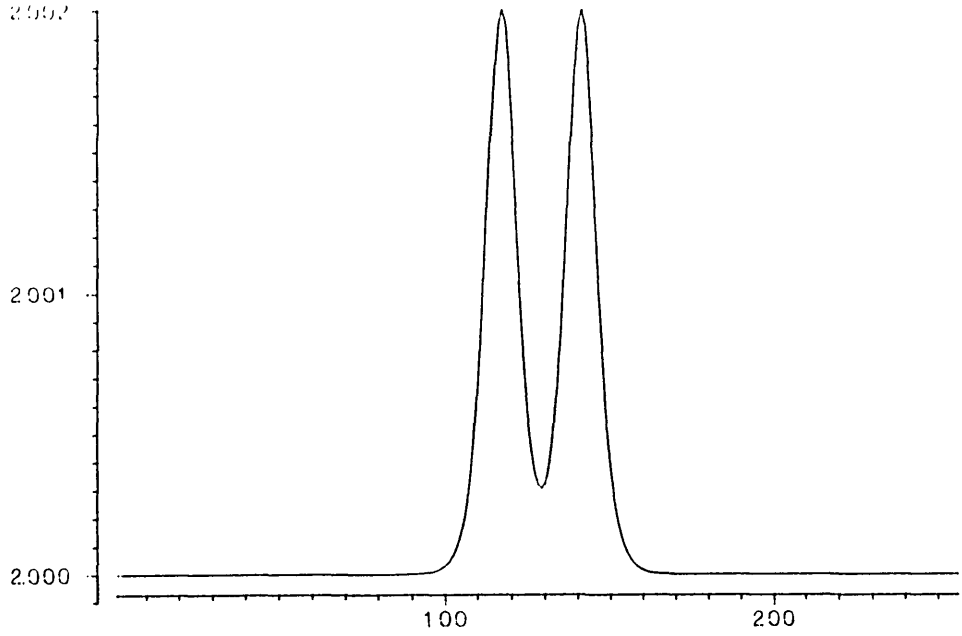

FIGURE 4.1b. Refractive index profile for offset = 12.

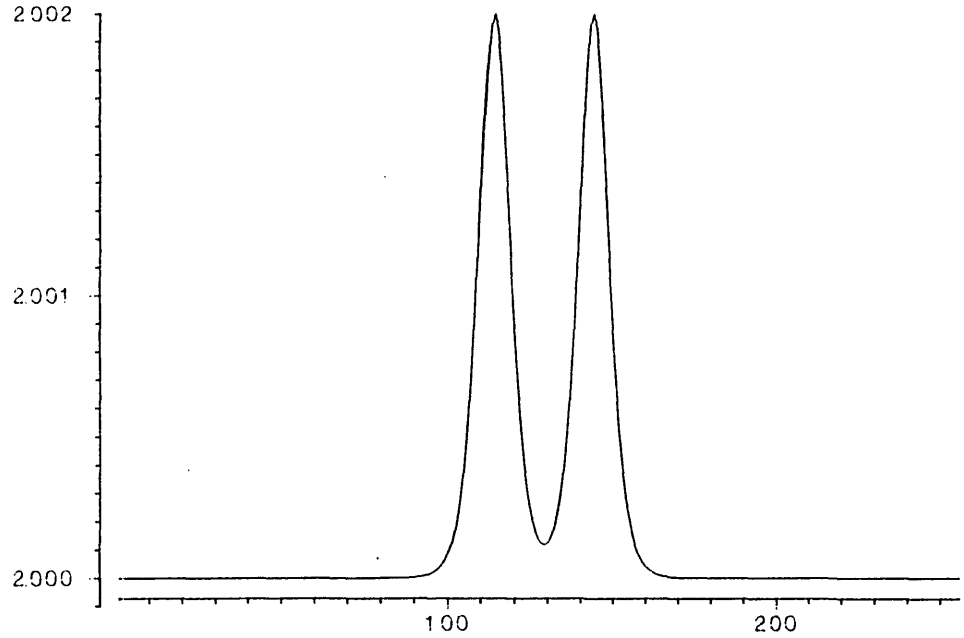

FIGURE 4.1c. Refractive index profile for offset = 15.

4.3 Modification for non-linear refractive index.

The only other modification required to the program was for the nonlinear refractive index. Each element of the array for the refractive index (subscripted by J) was modified according to

$$n'_J = n_J + (n_2 \times I_J) \qquad 4.1$$

where n_2 is the nonlinear refractive index and I_J is found form E_J, the element of the complex array for the field according to

$$I_J = n_o c \varepsilon_o |E|^2 / 2 \qquad 4.2$$

This modification to the refractive index is carried out within every refractive index step.

4.4. Runs and results.

This section presents the results of several runs of the AODC program for a variety of parameters. The parameters that were constant throughout are:

Number of mesh points:	$n = 256$
Transverse mesh spacing:	$\Delta x = 0.49\mu m$
Propagation step size:	$\Delta z = 5\mu m$
Epstein's a coefficient:	$a = 3\mu m$
Vacuum wavelength of light:	$\lambda = 1.06\mu m$
Substrate refractive index:	$n_o = 2.0$
Maximum refractive index:	$n_1 = 2.002$
Nonlinear refractive index:	$n_2 = 3 \times 10^{-19}\ m^2/W$

The value of n_2 is taken from table 2.2, ie the experimental result of Lattes et al (1983). The parameters that were varied were the offset of the waveguides from the centre and the peak intensity of the input.

As a preliminary, directional coupler operation was demonstrated for the linear case. Figure 4.3a shows the results of the propagation when the offset was 10 mesh points and the peak input intensity was $1GW/cm^2$, which was found, by comparison with runs at higher power, to be linear. There were 361 program steps, each containing six Δz steps of $5\mu m$, so the total propagation distance was 10.8mm. The centre half of the intensity profile (ie mesh points 64-192) is plotted every 0.3mm. As with all the three-dimensional plots in this thesis, the horizontal axis is the transverse direction of the coupler, the vertical axis is the intensity and the direction into the paper is the propagation direction. The plot shows an input into a guide on the left coupling into a guide on the right and it can be seen that there are a little over four coupling lengths in 10.8mm for this offset.

Next, nonlinear operation of the device was investigated.

Figure 4.3b shows a nonlinear run with offset = 10. Instead of power coupling fully into the right-hand guide as in 4.3a, we see that only a fraction of the power is coupled. Also the distance between maxima in the right-hand guide has decreased. This corresponds to the behaviuor of an input above the critical power as seen in figure 2.2.

Figures 4.4a-d and 4.5a-f show runs with offset 12 and 15 respectively. The parameters of the runs are summarised in table 4.1; D is the total propagation distance, d is the distance between plots, I_{MAX} is the peak input intensity and the coupling length L is estimated by counting curves on the figures.

Figure	D	d	L	I_{MAX} (GW/cm^2)
4.3a	10.8mm	0.3mm	2.7mm	1
4.3b	10.8mm	0.3mm		20
4.4a	10.8mm	0.18mm	5.4mm	1
4.4b	10.8mm	0.18mm		5
4.4c	10.8mm	0.18mm		7.5
4.4d	10.8mm	0.18mm		10
4.5a	28.8mm	0.45mm	17.1mm	1
4.5b	28.8mm	0.45mm		3
4.5c	28.8mm	0.45mm		4
4.5d	28.8mm	0.45mm		5
4.5e	28.8mm	0.45mm		7
4.5f	28.8mm	0.45mm		10

TABLE 4.1. Parameters for figures 4.3 - 4.6.

Before discussing figures 4.4 and 4.5, it would be helpful

to consider how to extract the power remaining in the input waveguide for each step and plot it against the step number. The power remaining in the input guide cannot be measured directly because of the overlap with the other guide, Instead it can be estimated by doubling the power in the half of the input guide farthest away from the other guide - that is, the shaded part of figure 4.2. This method is not very accurate when the guides are close, presumably because there is an overlap beteen the left halves of the guides, but it is useful for offset = 12 (figure 4.4e) and works well for offset = 15 (figure 4.5g). Figure 4.4e gives power-distance plots for figures 4.4a-d and figure 4.5g is the same for 4.5a-e. These should be compared with Jensen's calculated power-distance plots (figure 2.2).

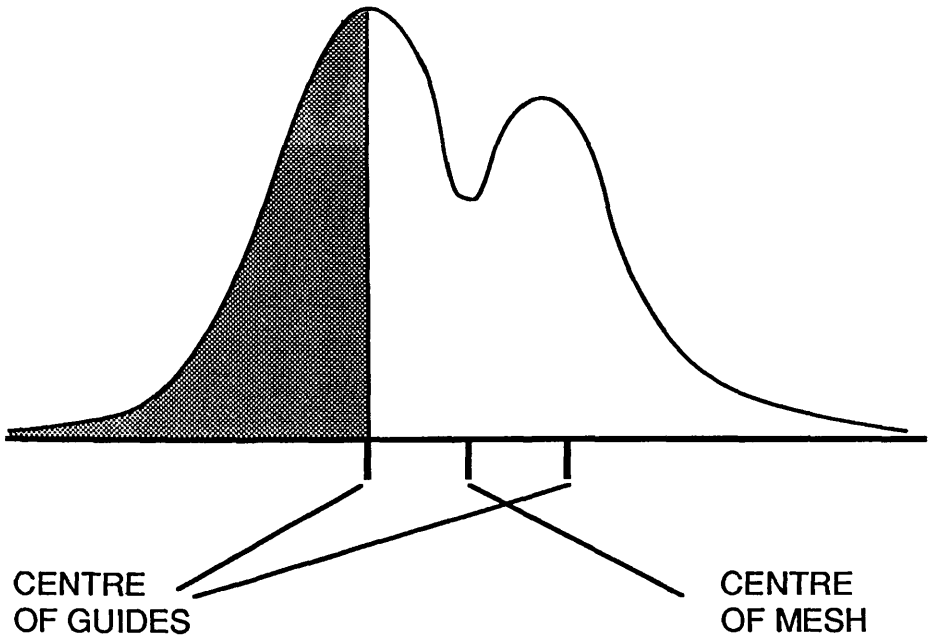

FIGURE 4.2. Estimation of the power left in the input guide.

In figure 4.4, 4.4a and 4.4b show approximately two coupling lengths of propagation. The pictures have been

plotted from different viewpoints but are otherwise almost identical. It is just possible to see that while at the end of 4.4a the power has reached the peak value again, at the end of 4.4b the peak value has not been reached. This can be confirmed by examining the corresponding plots in 4.4e. Figure 4.4c shows a more extreme increase in the coupling length and is obviously just below the critical power. Figure 4.4d is just above the critical power and shows that full coupling is not achieved. Figure 4.4e bears some resemblance to figure 2.2, although the inaccuracy mentioned above is evident.

In figure 4.5, 4.5a shows almost two coupling lengths. 4.5b shows behaviour typical of input power just below the critical power. At critical power, according to figure 2.2, the power in the input guide falls to half of its initial power asymptotically. In this run, the power stays level around the half-way value and then continues to fall. Figures 4.5c-f show the effect of increasing power above the critical power: the power coupled into guide 2 decreases and so does the spacing between successive maxima in guide 2, in accordance with figure 2.2. In figure 4.5f, the power coupled into guide 2 can barely be seen, although the variation in the input guide power level is more evident. Figure 4.5g is qualitatively a very close match for figure 2.2 if allowance is made for the fact that the powers relative to the critical power are different in the two pictures.

An overall comparison of figures 4.3 - 4.5 reveals the dependance of the critical power on the offset. For instance, fig 4.4a shows linear operation of the model and 4.4b does not appear very different, although a glance at 4.4e shows that the coupling length has increased slightly. Figure 4.4c shows the coupling length increasing noticeably and 4.4d is obviously nonlinear as full coupling is no longer achieved.

In the figure 4.5 series, 4.5d, with the same intensity as 4.4b is in the nonlinear regime already, 4.5b appears to be just below the critical intensity and 4.5f shows only a vestigial trace of coupling for the same input intensity as 4.4d. However, figure 4.3b is similar to 4.4d but at 5 times the input intensity.

These results are consistent with the linear dependence of critical power on Q_z, which is in turn inversely dependent on the coupling length. The coupling length increases with the offset in a way determined by the overlap integral in equation 2.17b.

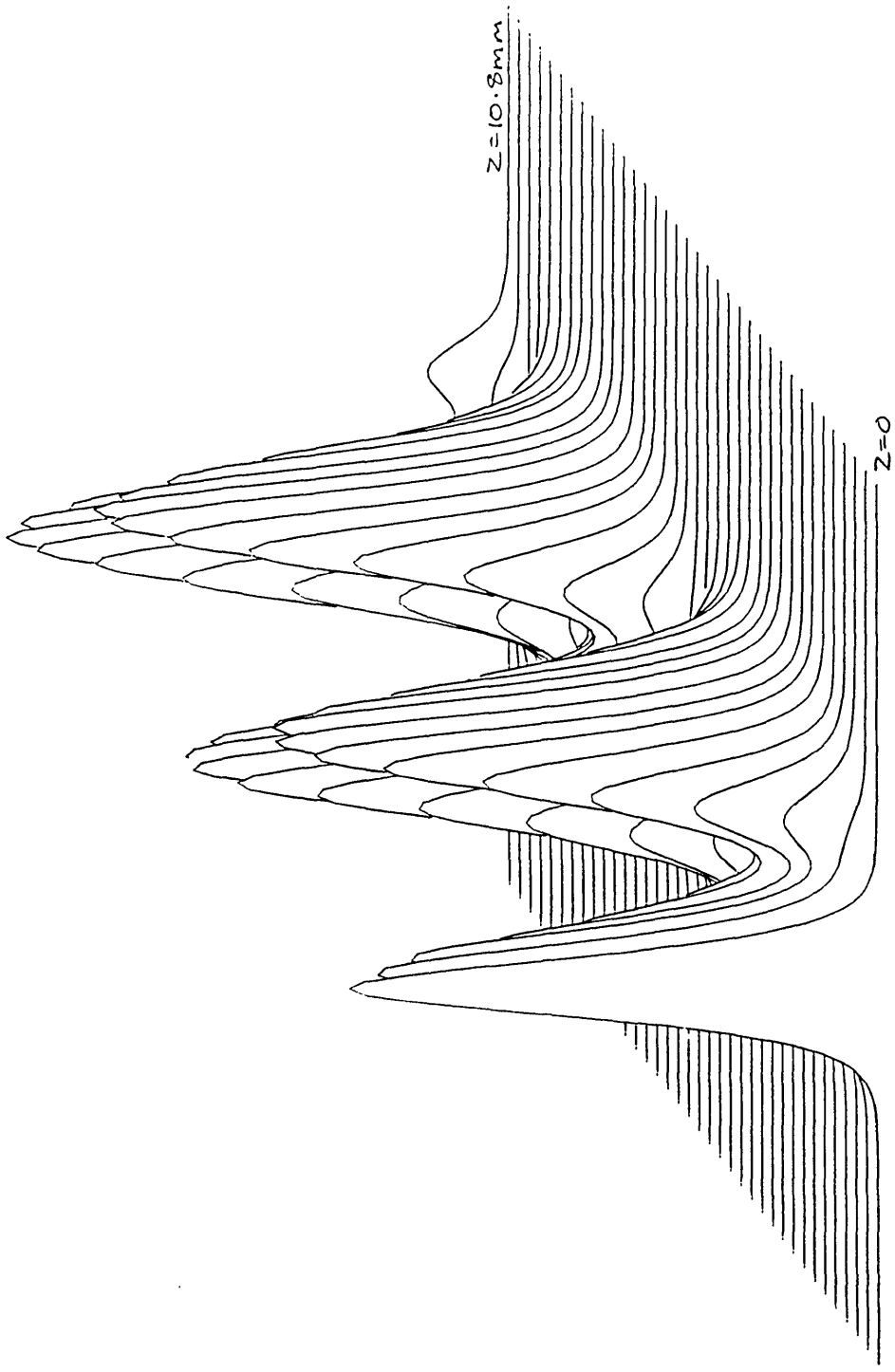

FIGURE 4.3a. I_{MAX} = 1 GW/cm^2, propagation distance = 10.8mm, offset = 10.

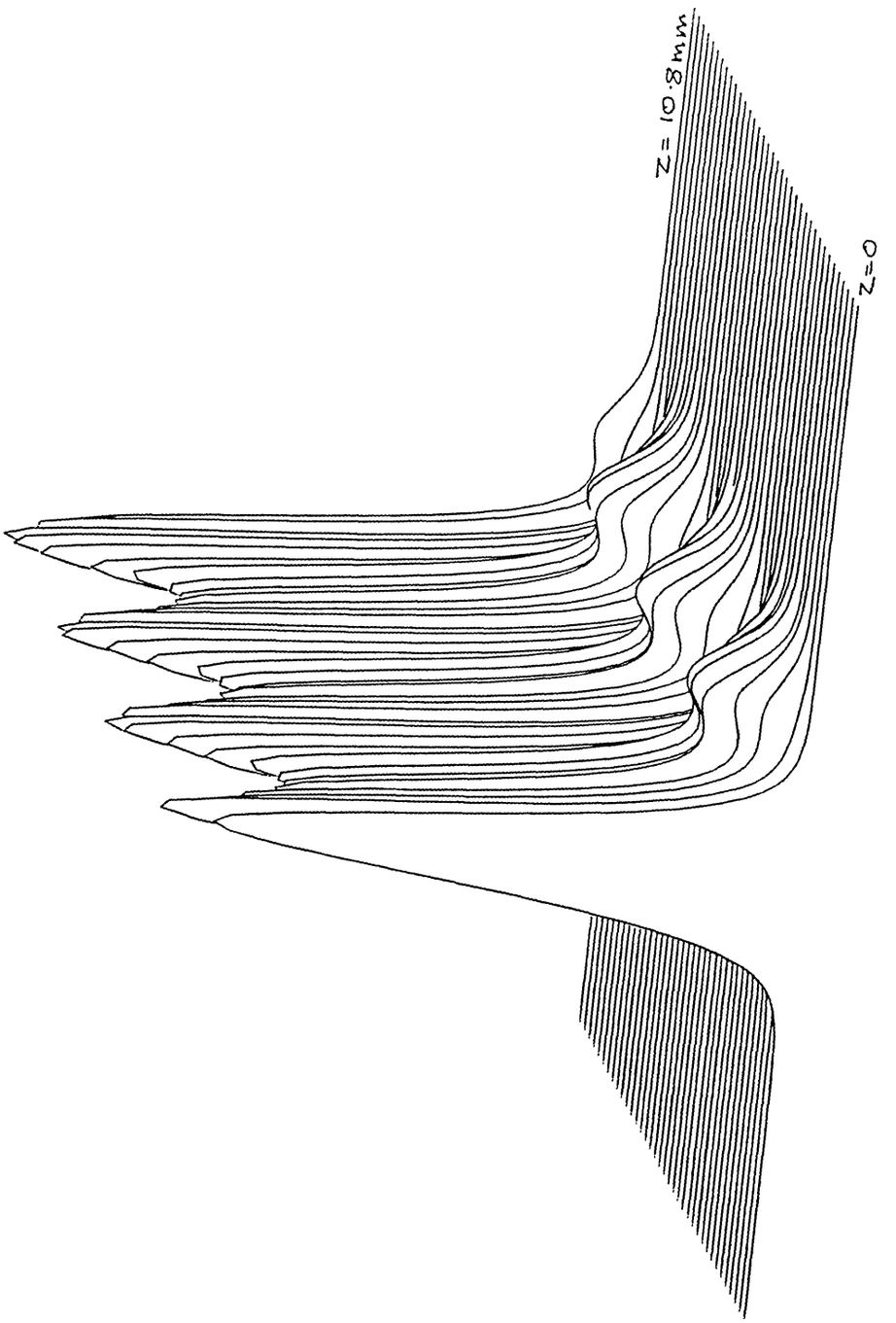

FIGURE 4.3b. I_{MAX} = 20 GW/cm^2, propagation distance = 10.8mm, offset = 10.

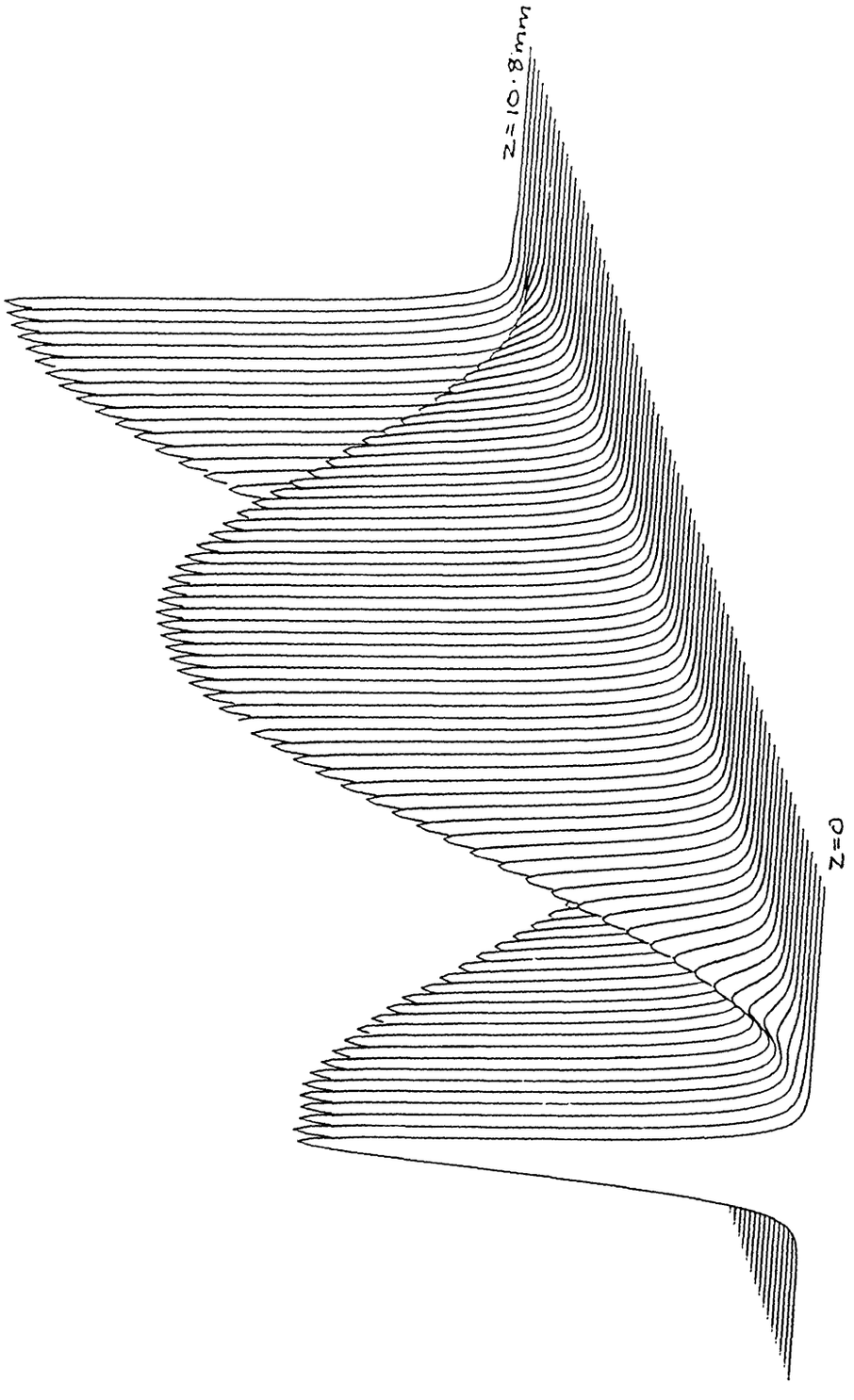

FIGURE 4.4a. I_{MAX} = 1 GW/cm^2, propagation distance = 10.8mm, offset = 12.

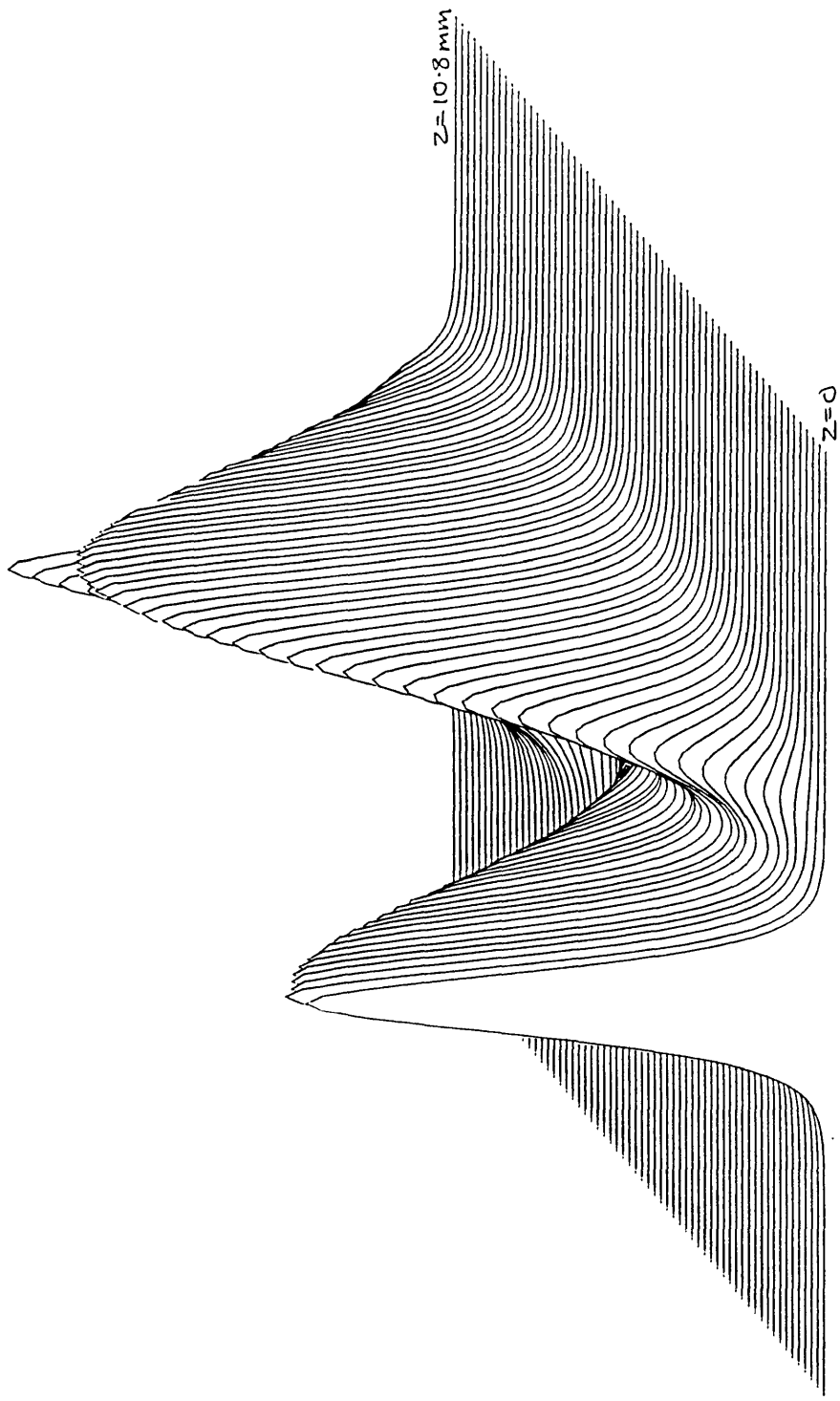

FIGURE 4.4b. I_{MAX} = 5 GW/cm^2, propagation distance = 10.8mm, offset = 12.

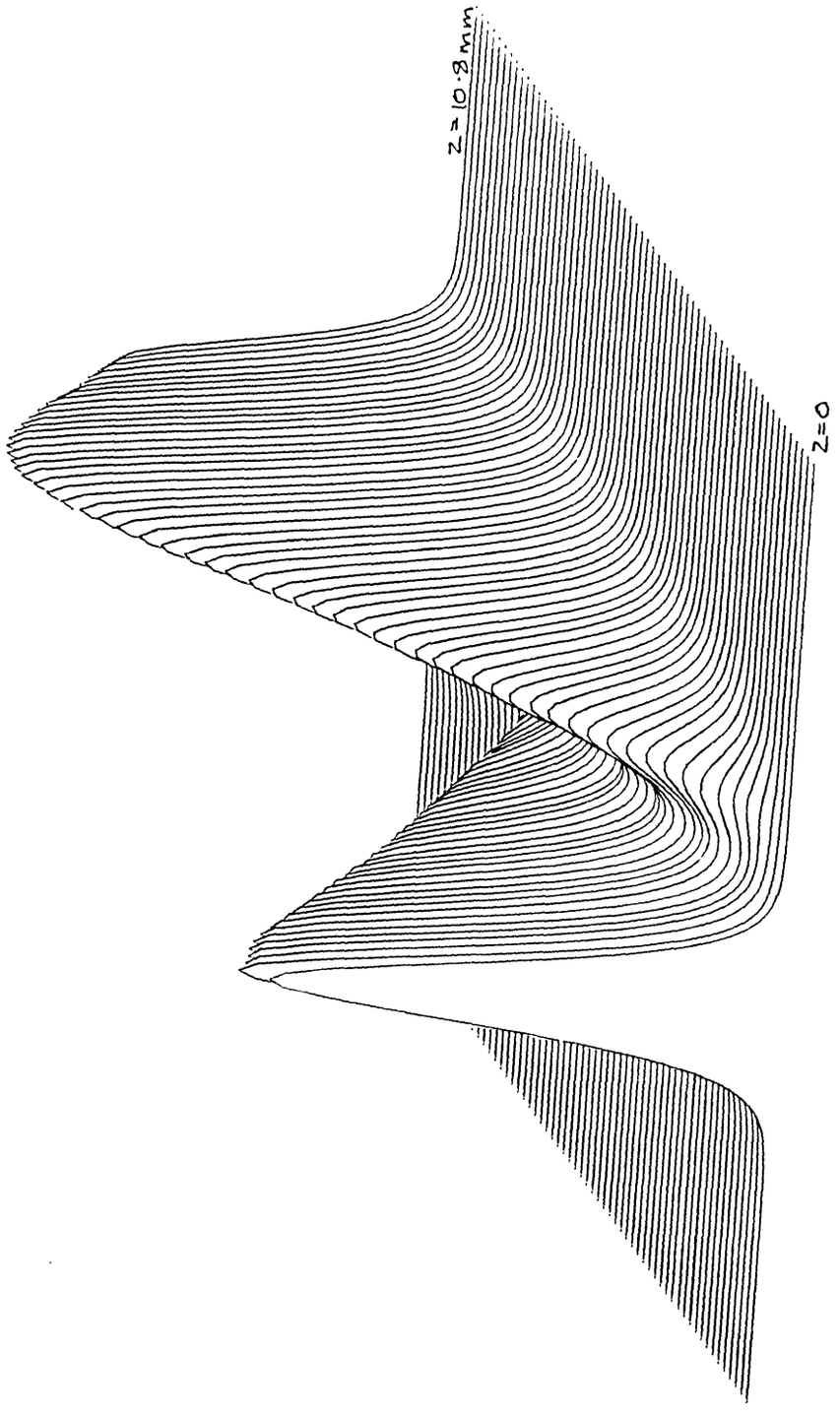

FIGURE 4.4c. I_{MAX} = 7.5 GW/cm^2, propagation distance = 10.8mm, offset = 12.

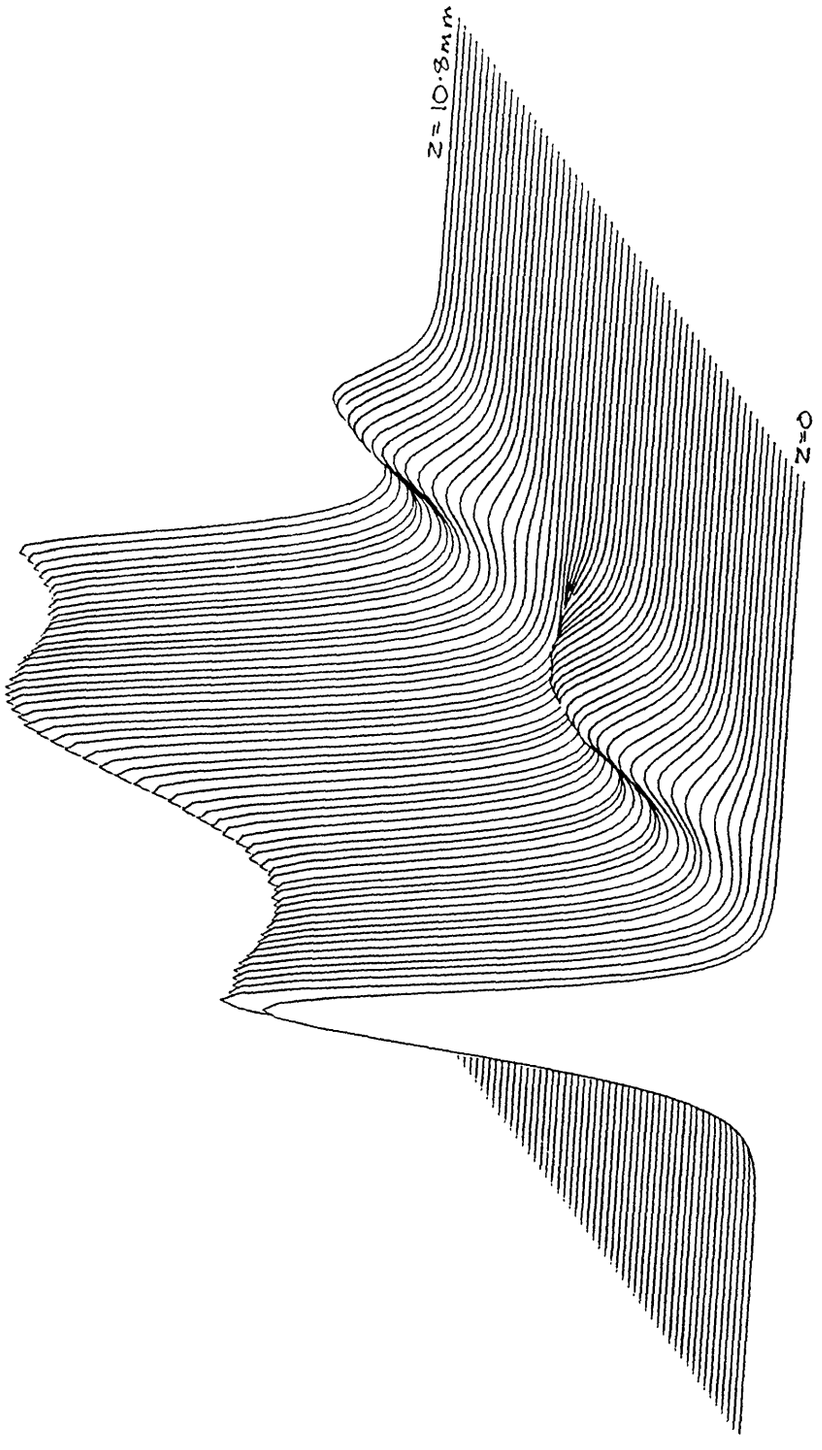

FIGURE 4.4d. I_{MAX} = 10 GW/cm^2, propagation distance = 10.8mm, offset = 12.

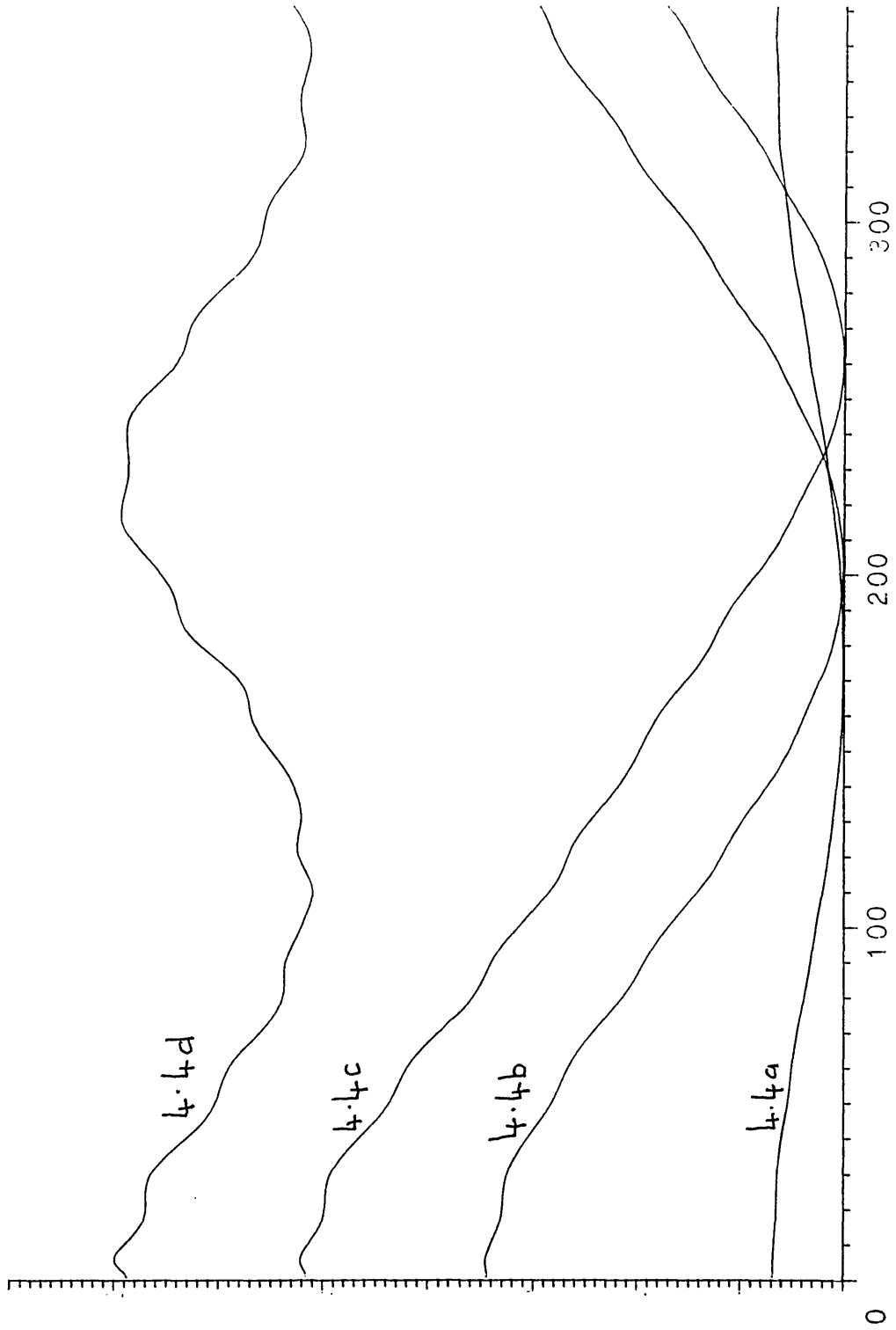

FIGURE 4.4e. Power-distance plots for figures 4.4a-d.

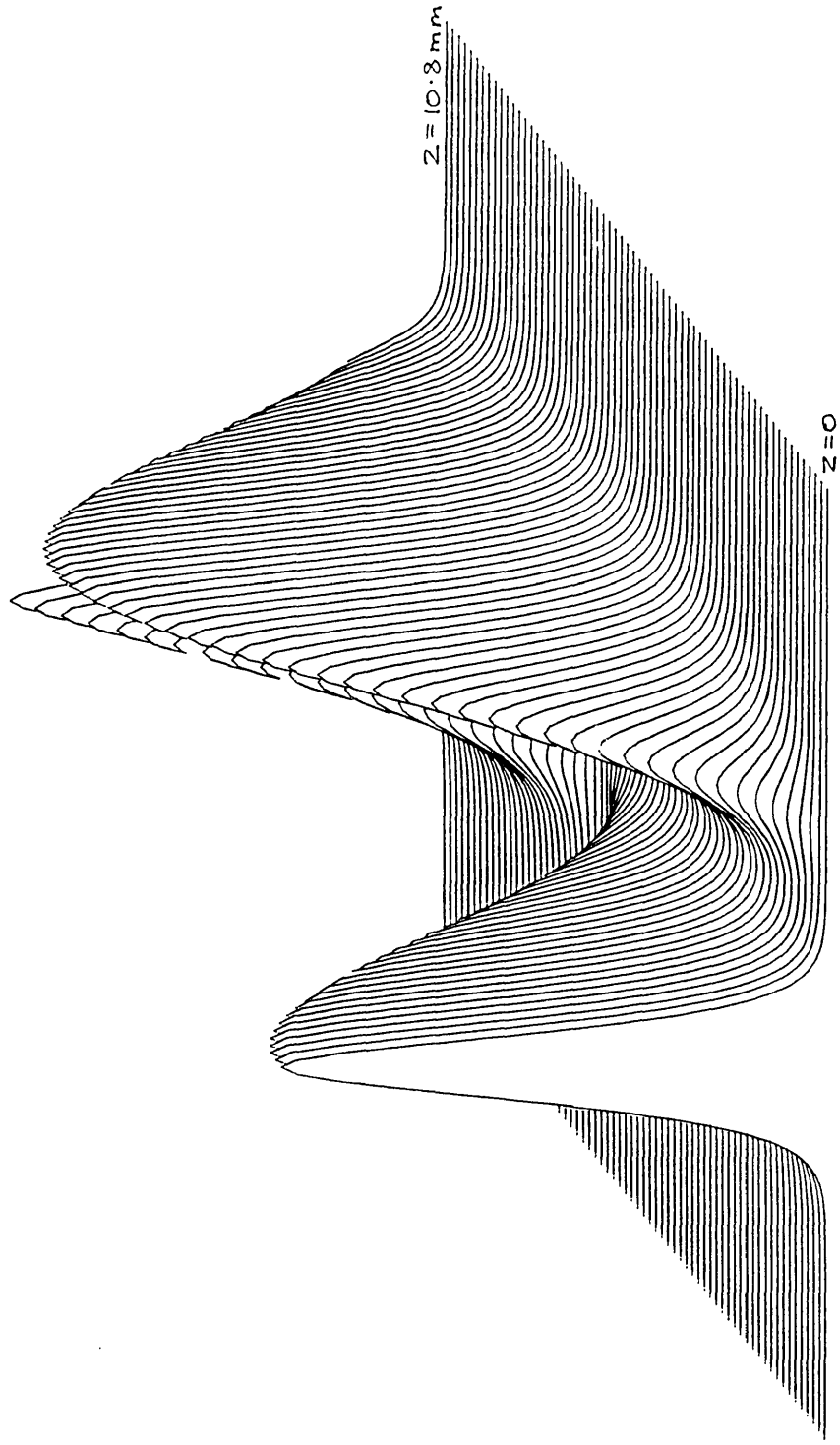

FIGURE 4.5a. I_{MAX} = 1 GW/cm^2, propagation distance = 28.8mm, offset = 15.

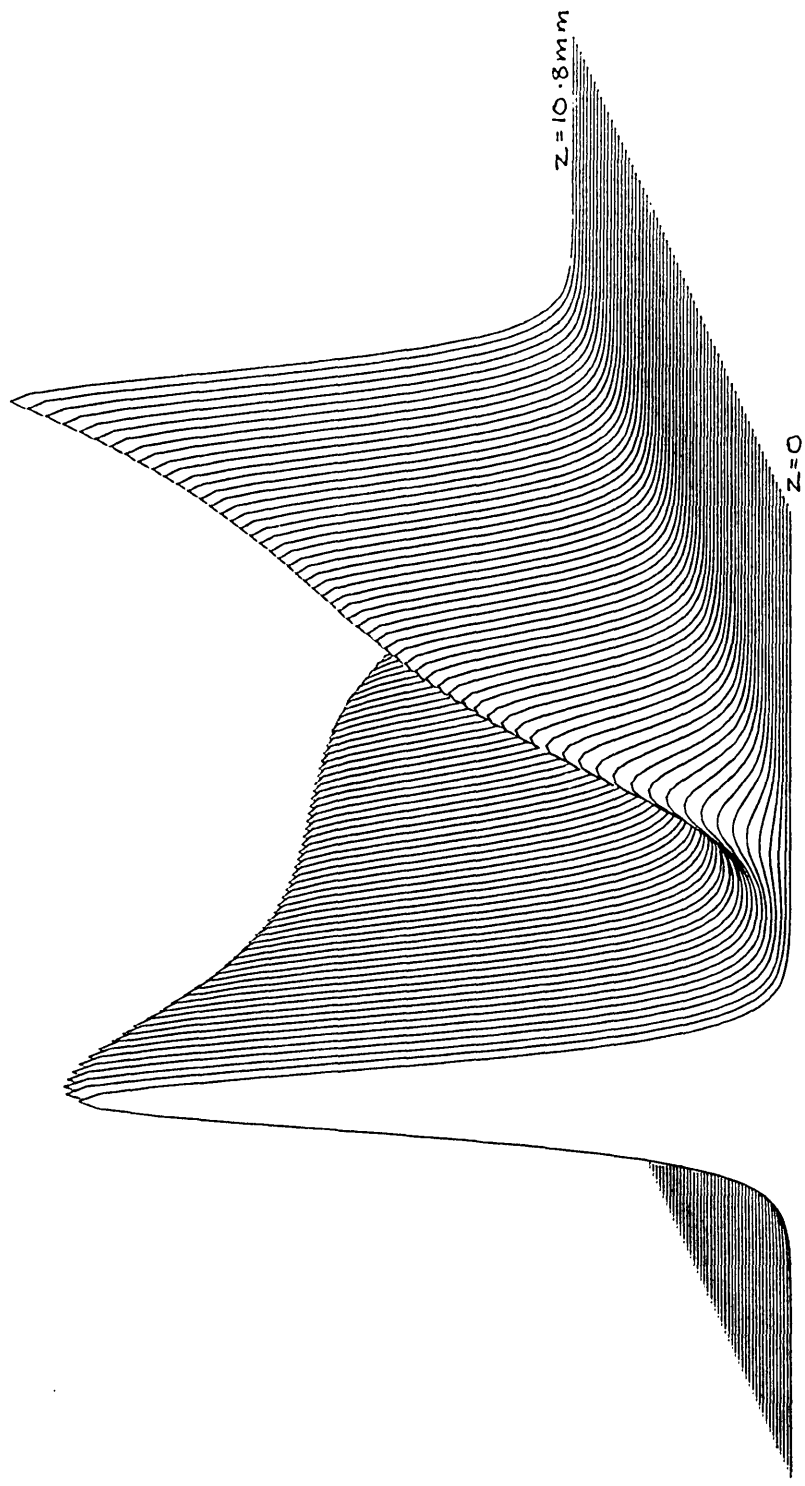

FIGURE 4.5b. I_{MAX} = 3 GW/cm^2, propagation distance = 28.8mm, offset = 15.

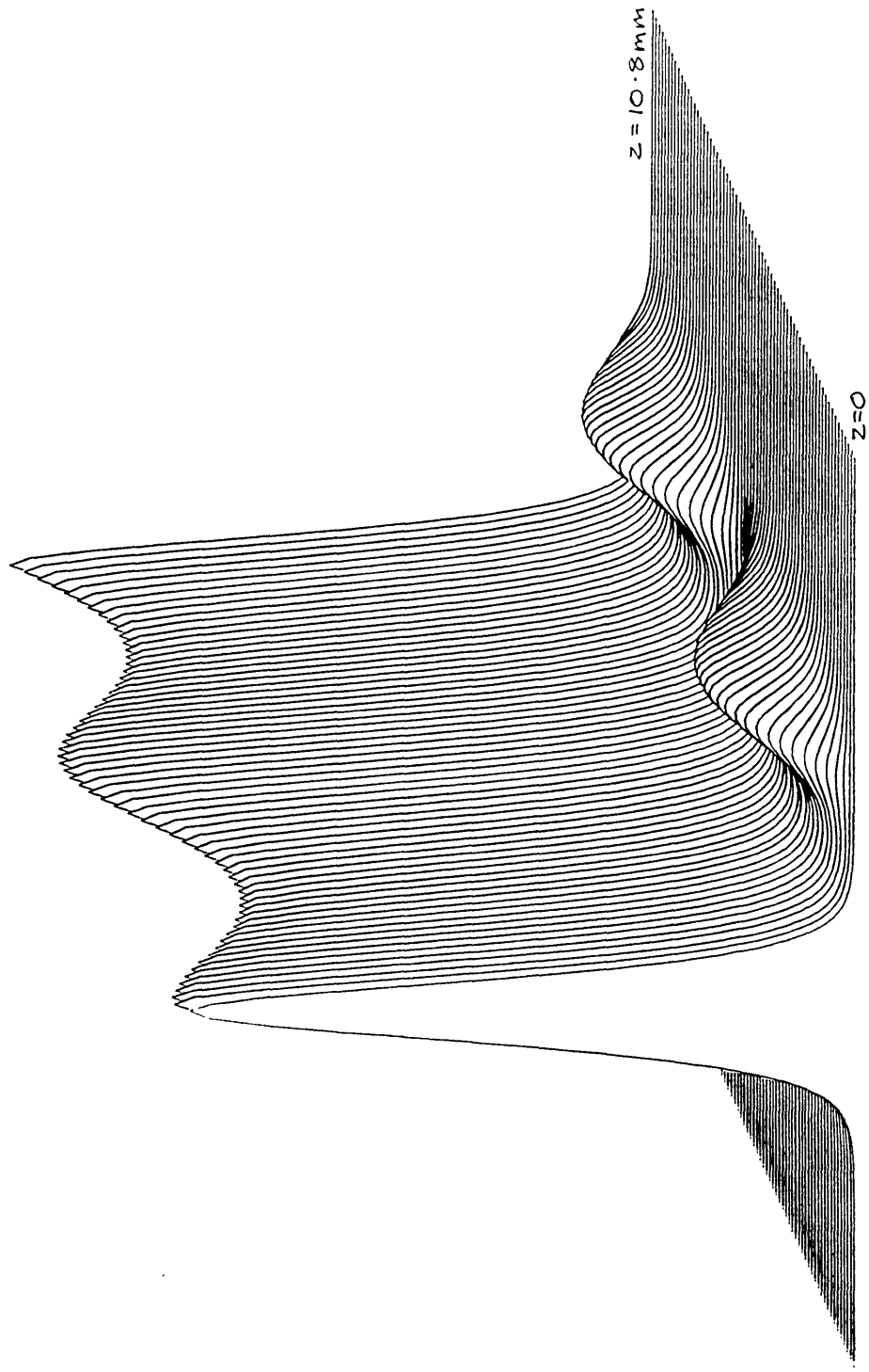

FIGURE 4.5c. I_{MAX} = 4 GW/cm^2, propagation distance = 28.8mm, offset = 15.

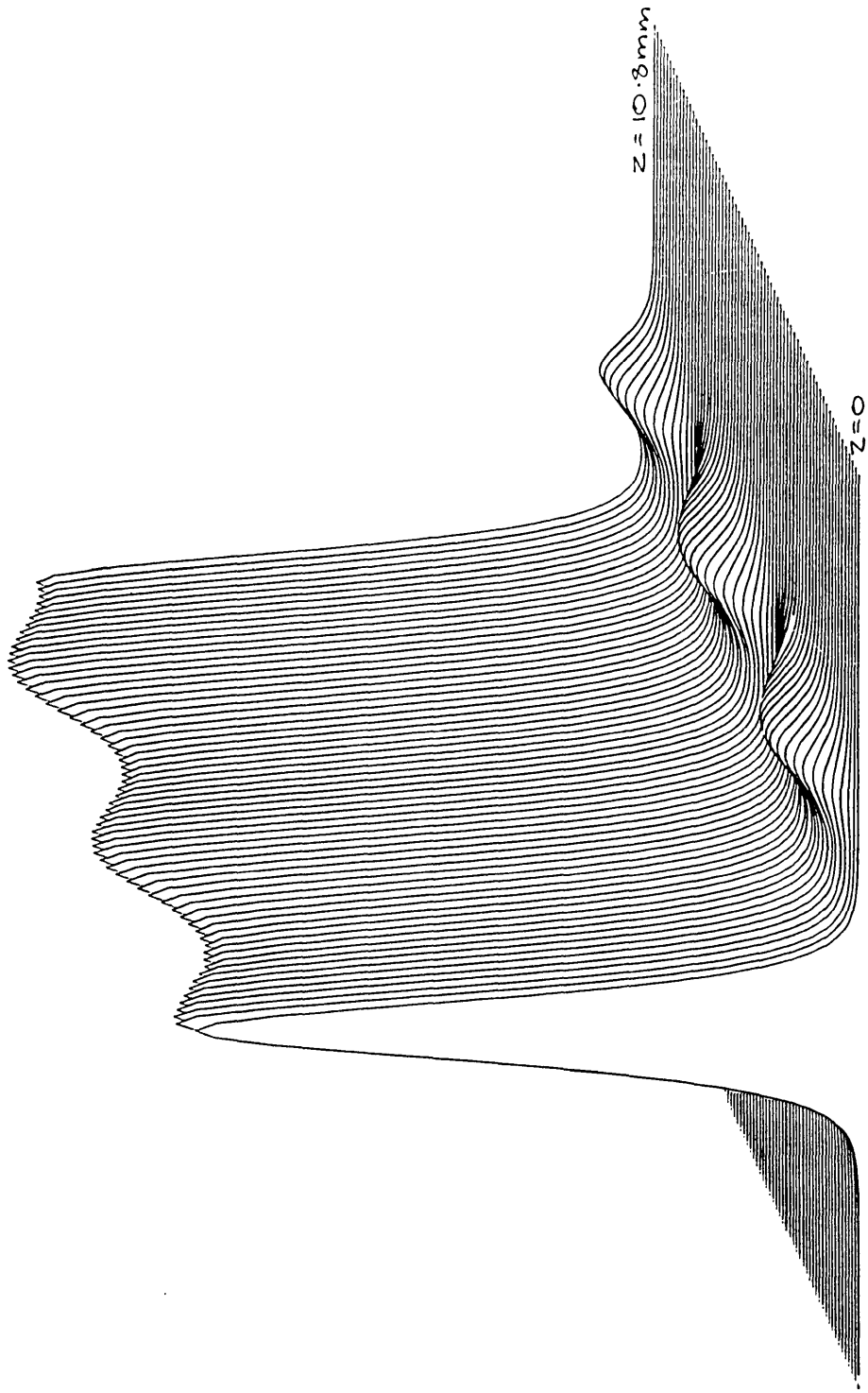

FIGURE 4.5d. I_{MAX} = 5 GW/cm^2, propagation distance = 28.8mm, offset = 15.

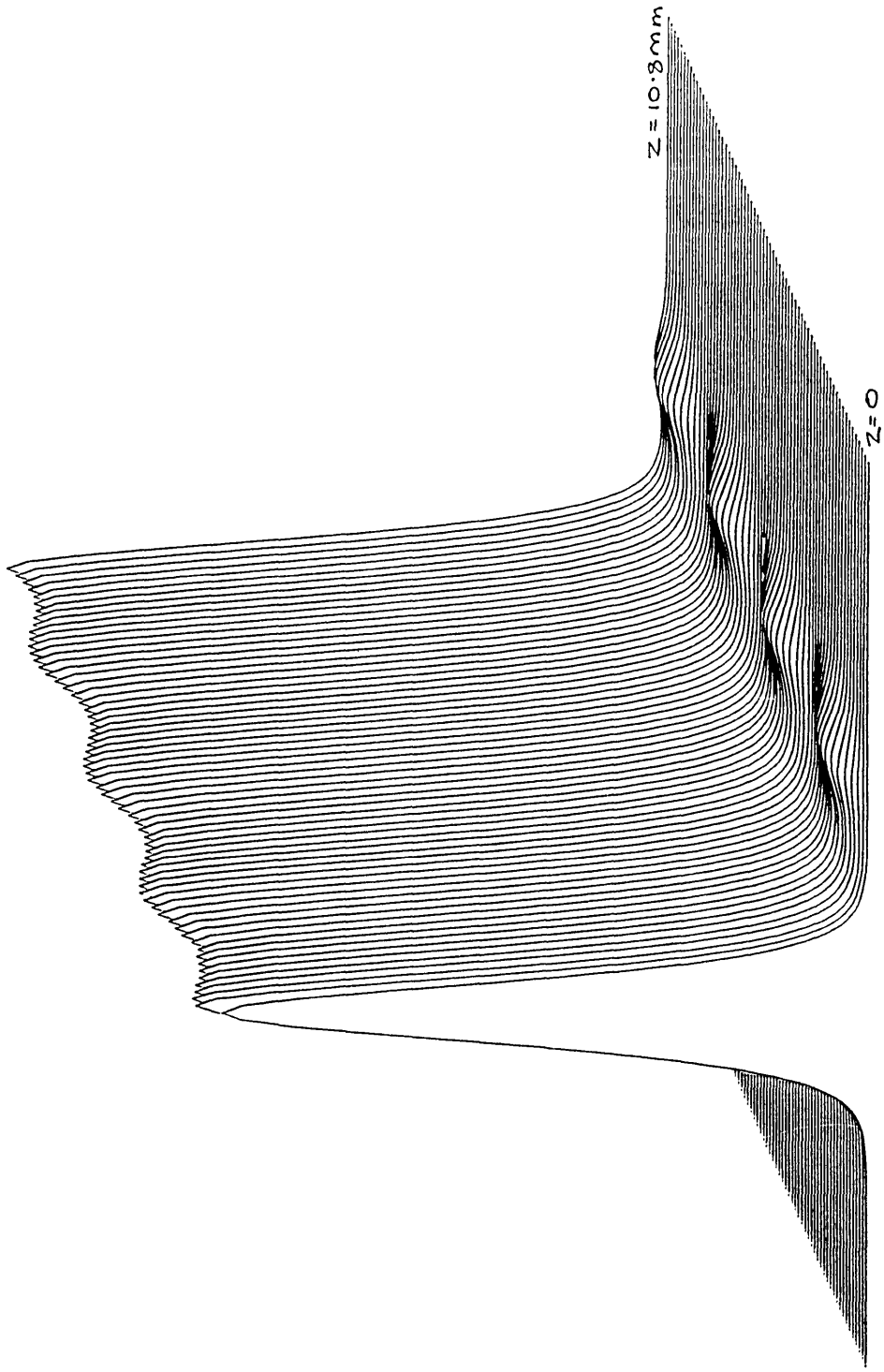

FIGURE 4.5e. I_{MAX} = 7 GW/cm^2, propagation distance = 28.8mm, offset = 15.

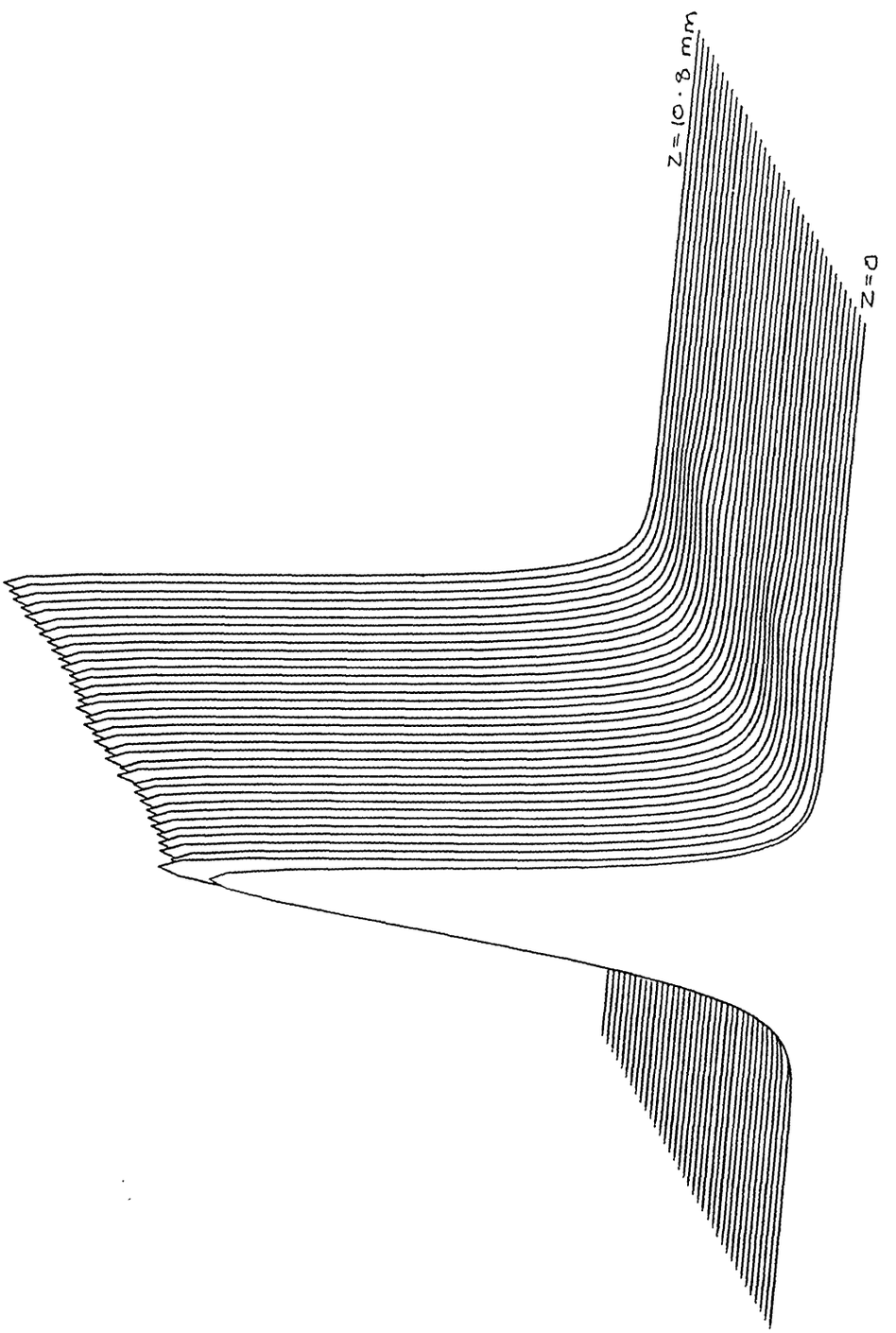

FIGURE 4.5f. I_{MAX} = 10 GW/cm^2, propagation distance = 28.8mm, offset = 15.

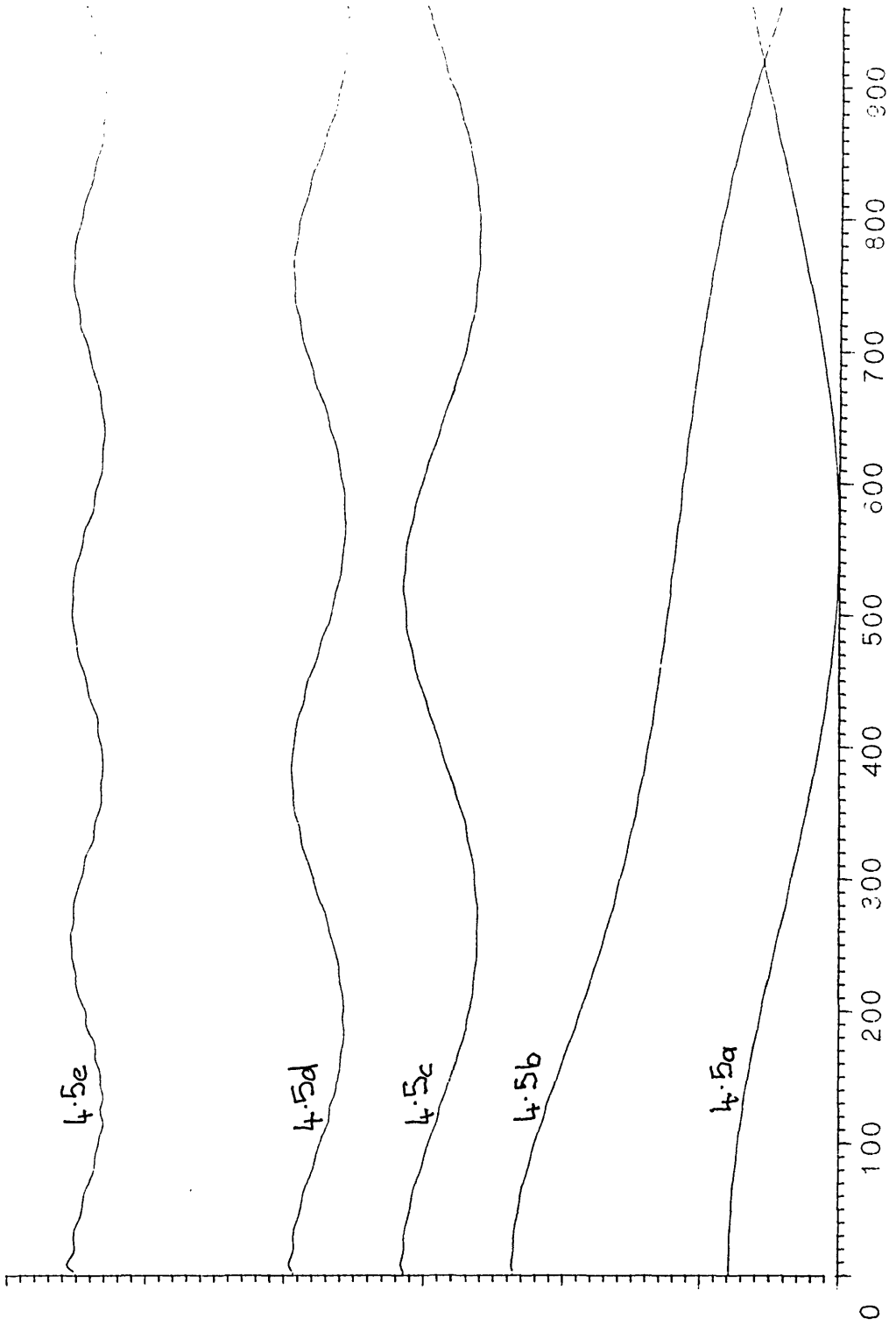

FIGURE 4.5g. Power-distance plots for figures 4.5a-e.

4.5 Conclusions

The BPM has been used to develop a model of the all-optical directional coupler. The model demonstrates nonlinear behaviour and the dependence of the critical power on the distance between the waveguides. The power remaining in the input guide versus distance agrees with Jensen's one-dimensional model.

To summarise, table 4.2 shows the dependence of the intensity required for nonlinearity on centre-to-centre waveguide separation by comparing three similar results. However, although the model used the same n_2 as $LiNbO_3$, it must be emphasised that this result is for two planar Epstein-profile waveguides and not two channel waveguides with the experimentally-derived profile of Fukuma (1978) and eqn 3.17.

Separation	Intensity
9.8 mm	20 GW/cm^2
11.76 mm	10 GW/cm^2
14.7 mm	4 GW/cm^2

TABLE 4.2. Dependence of nonlinearity on waveguide separation.

CHAPTER 5

THE GIRES TOURNOIS INTERFEROMETER TRANSFORM

5.1 Introduction 108

5.2 Overview of the Gires Tournois Interferometer 108

5.3 Derivation of the GTI transform for the dispersive case 110

5.4 Conversion to the diffractive case 112

5.5 Programming details 113

5.6 Results 114

5.7 Conclusions 119

Chapter 5 The Gires Tournois Interferometer transform

5.1 Introduction

This chapter introduces a newly developed computational algorithm which can be used for BPM-style calculations which do not use Fourier transforms. It can be applied in cases where the paraxial approximation holds. The algorithm was developed for the Gires Tournois interferometer (GTI) (Gires and Tournois 1964), a dispersive device similar to the Fabry-Perot Etalon (FPE). A description of the device and its application is followed by an outline of the derivation of the model used in the dispersive case. The model is then converted to the diffractive case and results of using the model for a single Epstein profile waveguide are given and compared with the BPM.

5.2 Overview of the GTI

The GTI is like an FPE but with one wall of the cavity fully reflecting. The material in the cavity can be air or a medium such as glass. The advantage of the GTI as a dispersive element is that its output intensity is independent of input frequency. In an FPE, wanted frequencies are transmitted and unwanted frequencies are reflected. Since the GTI has 100% reflection at one of its walls, it is clear that the intensity cannot be changed by the device. Only the phase of the input can be affected.

The GTI has been used in laser cavities to control dispersion (Duguay and Hansen 1969, French et al 1986a, 1986b, Gomes et al 1986, Heppner and Kuhl 1985, Kuhl and Heppner 1986), since it can be tuned to introduce positive or negative dispersion to render the dispersion of the whole cavity zero. Normally dispersion of a laser pulse is

modelled by Fourier transforming the pulse shape from the time domain to the frequency domain, altering each of the frequencies and Fourier transforming back to the time domain. However Avramopoulos and New (Gomes et al 1986 and to be published) have invented an algorithm which models the GTI without Fourier transforms. Instead, two coupled iterative equations are run along the length of the pulse and back again in the time domain.

This model has a wider application than modelling the GTI. It can be viewed as a mathematical transform which introduces dispersion. The transform is governed by just two parameters, the reflection coefficient of the non 100% mirror and the distance between the two. The GTI is considered to operate in normal incidence but the geometrical problems resulting from the fact that light is totally reflected by the GTI can be ignored; if it is necessary or convenient, the reflection coefficient of the other wall can be made negative. The GTI has been used in this way to model dispersion in optical fibres.

The study of dispersion of pulses in fibres is similar mathematically to the case of beam propagation - the time profile of the pulse corresponds to the spatial profile of the beam and dispersion, which alters the frequency components, corresponds to diffraction, which alters the spatial frequencies. The algorithm was converted to the beam propagation application and tested against the BPM.

5.3 Derivation of GTI transform for the dispersive case.

The following derivation is taken from the unpublished work of Aeramopoulos and New.

The GTI algorithm is defined in the dispersive case by

$$E_I^{OUT} = -r\, E_I^{IN} + t\, E_I^{MEM} \qquad 5.1a$$

$$E_{I+1}^{MEM} = (r\, E_I^{MEM} + t\, E_I^{IN}) \exp(-i\theta) \qquad 5.1b$$

where t_E is the etalon round trip time, ω is the carrier frequency and $\theta = \omega t_E$. The E_I are complex fields. The equations define the two unknowns, E^{OUT} and E^{MEM} in terms of E^{IN}. In order to initialise the iteration, we need values for E_1^{IN}, E_1^{MEM}, r and c. E_1^{IN} can be obtained from the input pulse shape. However, E_1^{MEM} cannot be determined from the second equation because there are no E_0. To get the GTI algorithm started off, this value must be guessed somehow. This can be done by extrapolation.

If a real GTI was being modelled, r and θ would be measured and substituted into the iteration equations. In the present case, r and θ must be chosen to provide a given dispersion. In order to discover the required values, we need to find two equations in r and θ to solve simultaneously. In order to do this, we can consider successive derivatives of ϕ with respect to θ.

The first derivative is proportional to the group time delay, $-d\phi/d\omega$ as $\theta = \omega t_E$. It is not helpful to constrain the GTI to match this derivative as it merely represents a shift of the pulse along the time axis and gives no information about dispersion. The second derivative corresponds to linear dispersion and so must be matched to the known dispersion of the glass. Making this constraint gives one equation in r and θ. The second equation is derived by setting the third derivative of ϕ with respect to θ to zero; this corresponds to constraining the dispersion to be linear - a valid constraint as the dispersion of glass is almost linear for a pseudo-monochromatic pulse. The following derivation first develops these two equations and then discusses their solution.

First we need to find the steady-state solution of the two GTI equations, 5.1a and 5.1b. If E^{OUT}, E^{IN} and E^{MEM} are all set to constants, the equations reduce to

$$E^{OUT} = \frac{(-r + \exp(-i\theta))\, E^{IN}}{(1 - r \exp(-i\theta))} \qquad 5.2$$

The factor in round brackets is used to define four parameters u, v, w and ϕ as follows.

$$\frac{E^{OUT}}{E^{IN}} = \frac{u + iv}{w} = \exp(i\phi) \qquad 5.3$$

The values of u, v and w are

$$u = (1 + r^2)\cos\theta - 2r \qquad 5.4$$

$$v = -(1-r^2)\sin\theta \qquad 5.5$$

$$w = (1 + r^2) - 2r\cos\theta \qquad 5.6$$

Energy conservation is obvious from 5.2 and implies that

$$u^2 + v^2 = w^2 \qquad 5.7$$

The linear dispersion condition implies that the derivatives of ϕ with respect to θ go up to second order only. The third derivative is

$$\frac{d^3\phi}{d\theta^3} = 2r\,\frac{(1-r^2)}{w^2}\,(w\cos\theta - 4r\sin^2\theta) \qquad 5.8$$

and equating this to zero gives

$$\cos\theta = \frac{-(1 + r^2) + ((1 + r^2)^2 + 32r^2)^{1/2}}{4r} \qquad 5.9$$

From the second derivative we get

$$\phi_2 = \frac{d^2\phi}{d\omega^2} = 2rt_E^2\,\frac{(1 - r^2)}{w^2}\sin\theta \qquad 5.10$$

where, in the case of dispersion, ϕ_2 is obtained from the known value for the dispersion of the glass.

5.4 Conversion to the diffractive case

To use the same method for diffraction, the following substitutions are made;

t_E becomes Δx, the transverse mesh spacing, and
ω becomes κ, the transverse spatial frequency.

The phase change for each spatial frequency is

$$\exp(-i\kappa^2\Delta z) \,/\, (\sqrt{(k^2-\kappa^2)} + k) \qquad 5.11$$

where Δz is the step length in the propagation direction and $k = n\omega/c$. In the paraxial approximation, this reduces to

$$\exp(-i\kappa^2\Delta z/2k) \qquad 5.12$$

From this it can be seen that ϕ_z in the dispersion equations ought to be replaced by $\Delta z/k$. Without the paraxial approximation, no replacement for ϕ_z is possible.

And so the two equations for the diffraction case are

$$\cos\theta = -((1 + r^2)/4r) + [((1 + r^2)/4r)^2 + 2)]^{1/2} \qquad 5.13$$

$$\frac{2r\Delta x^2\,(1-r^2)\,\sin\theta}{(1 + r^2 - 2r\cos\theta)^2} - \frac{\Delta z}{k} = 0 \qquad 5.14$$

The iteration method used to solve these equations for r and θ must be chosen carefully as some methods are unstable for certain values of r. A bisection method was used to obtain values for the model. The method is summarised by the following outline;

```
start with r = 0.5 and step = 0.25;
repeat
    solve (5.13) to get θ;
    substitute r and θ into (5.14)
    if the first expression on the left of (5.14) > 0
    then change r to r - step
    else change r to r + step;
    divide step by 2
until r and θ converge.
```

5.5 Programming details

The GTI program was similar to the BPM programs described in chapter 3 and appendix A, with the important difference that the k-space phase change procedure in the BPM was changed to a GTI procedure, based on equations 5.1a and 5.1b.

Two small problems were met. The necessity to guess the first values of E^{MEM} was overcome by using exptrapolation to get a value for E_o. Also the fact that the GTI shifts the working array along by one element was overcome by using arrays one element longer than usual and doing two GTI transforms, flipping the array after each one. This gave the net result of a GTI transform leaving the array in the same position.

Listings of the parts of the GTI code that are different from the BPM code are inserted inside the back cover.

5.6 Results

The GTI program was compared with the BPM program used in chapter 3 and a paraxial BPM program to model a single Epstein-profile waveguide with the following parameters

number of points in array: $n = 256$
transverse mesh spacing: $\Delta x = 0.98\mu m$
Epstein's a coefficient: $a = 3\mu m$
vacuum wavelength of light: $\lambda = 1.06\mu m$
substrate refractive index: $n_o = 2.0$
maximum refractive index: $n_1 = 2.002$
step length for BPM: $\Delta z = 10\mu m$
step length for GTI: $\Delta z = 2.5$, 5 and $10\mu m$.

The total propagation distance in each case was 1.2 mm or 120 10 μm steps. The following table summarises the time taken for the calculations.

method	Figure	Δz	steps	cpu time
BPM	5.1a	10 μm	120	25 cpsec
Paraxial BPM	5.1b	10 μm	120	26 cpsec
GTI	5.2a	10 μm	120	13 cpsec
GTI	5.2b	5 μm	240	27 cpsec
GTI	5.2c	2.5 μm	480	53 cpsec

TABLE 5.1. Summary of GTI test results.

The resulting beam profiles were plotted superimposed at 0.2 mm propagation intervals - see figures 5.1 - 5.5. Over

the propagation distance, both versions of BPM remained accurate over seven orders of magnitude, and the difference between paraxial and non-paraxial versions of the program was barely noticeable. With the same step length, the GTI took half the cpu time to perform the calculation but was less accurate. With half and quarter the step length, so that twice and four times the cpu time were used, there was some improvement in accuracy, but not enough to make the GTI transform comparable with the BPM.

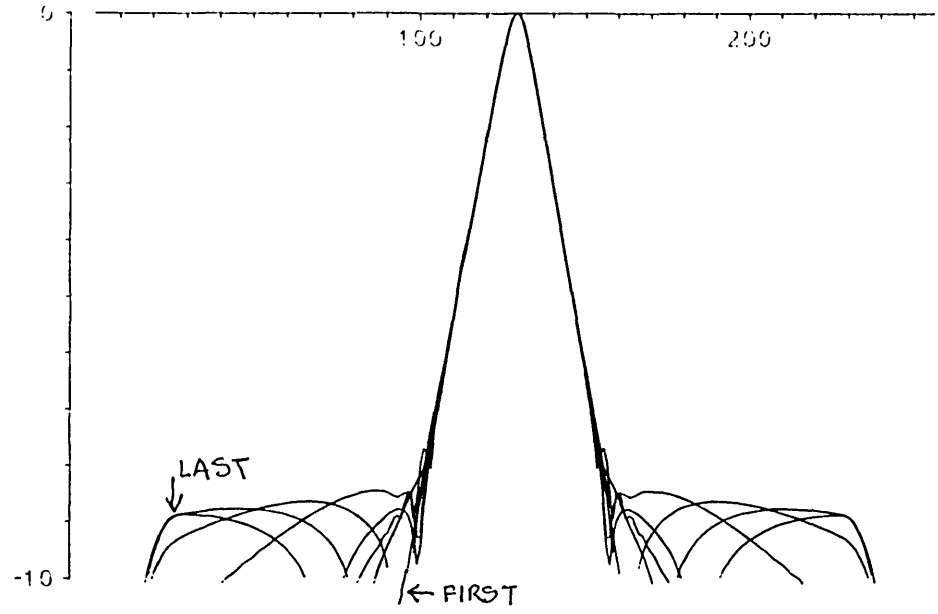

FIGURE 5.1a. BPM propagation test over 1.2mm (log plots).

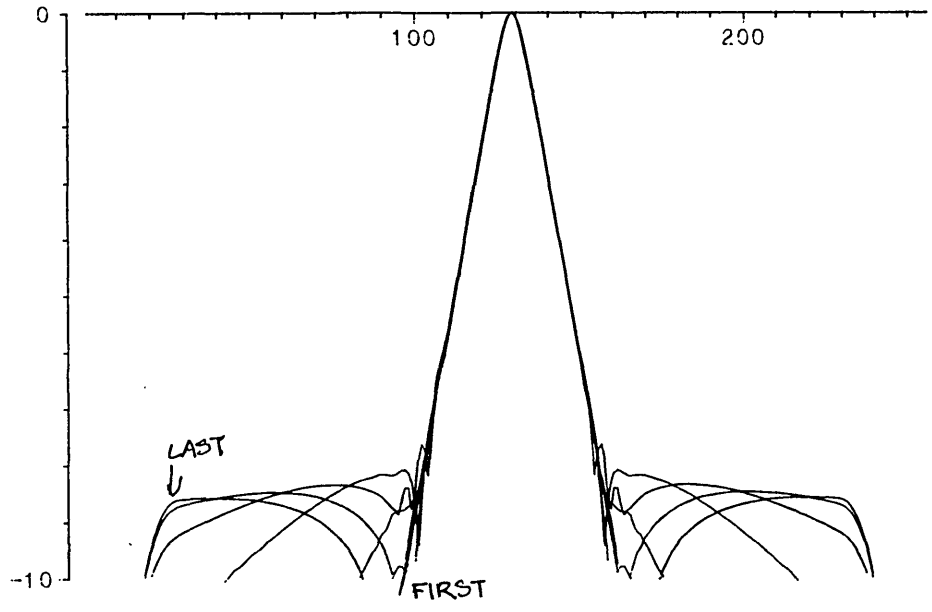

FIGURE 5.1b. Paraxial BPM propagation test over 1.2mm (log plots).

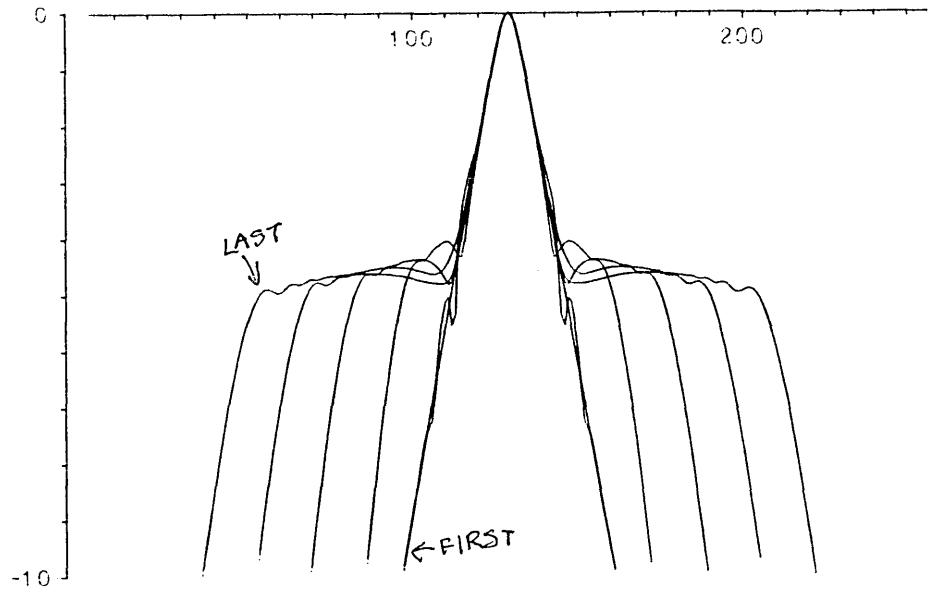

FIGURE 5.2a. GTI propagation test, z step = 10 μm.

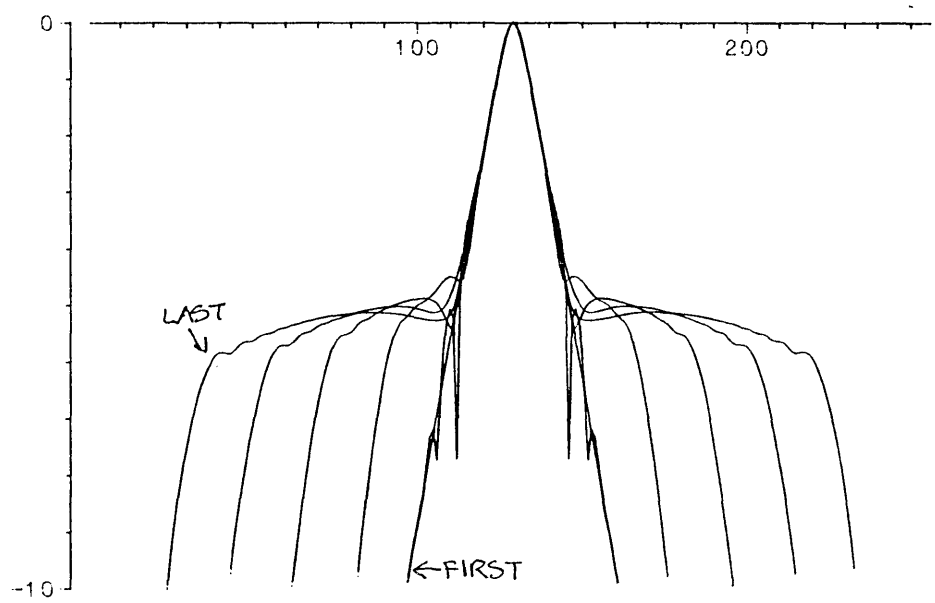

FIGURE 5.2b. GTI propagation test, z step = 5 μm.

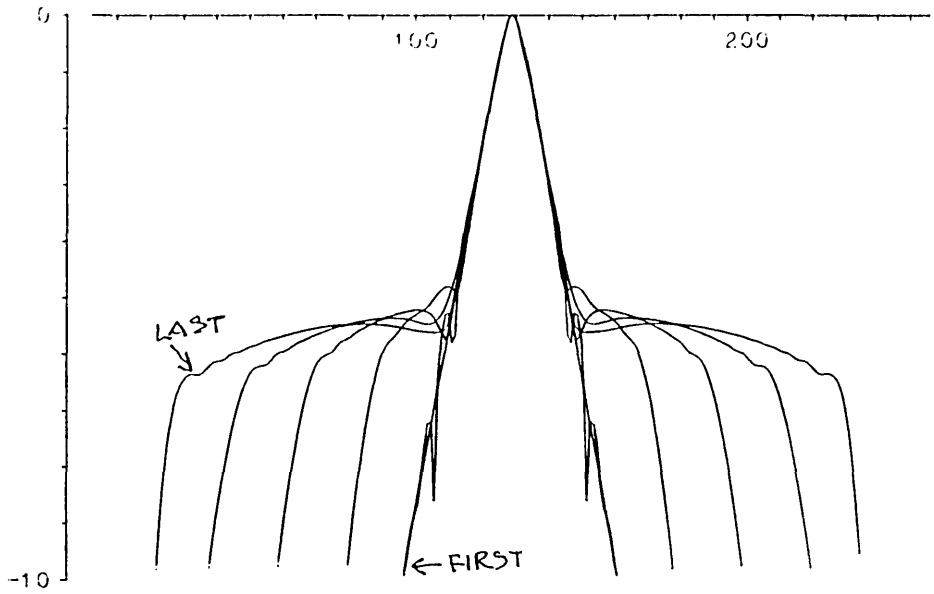

FIGURE 5.2c. GTI propagation test, z step = 2.5 μm.

5.7 Conclusions

The GTI transform warranted investigation because it was a novel method. There are limits to the applicability of coupled mode theory and the BPM. It may be that the GTI transform method is applicable in regions of parameter space where one or other of the former are not. Although the GTI was perceived to be inferior to the BPM in the present case, other workers should be given the opportunity to try the BPM in their own circumstances and to decide its worth for themselves.

The most serious disadvantage of the GTI for diffraction work is that the paraxial approximation cannot be avoided. The paraxial approximation is only valid when there are no high spatial frequencies propagating in the waveguide. As integrated optics waveguides are weakly guiding, high spatial frequencies, if present, are soon lost. However, if it is necessary to model the propagation of a field distribution which is not a mode of the structure, the paraxial approximation will not work accurately because high spatial frequencies will be present. The GTI in its present form will only be able to model instances where the field profile is close to being a mode of the structure. In the case of the BPM, the paraxial approximation gives cost benefit, so it is not used.

The results of the GTI work initially caused some disappointment, but only because it had been hoped that the BPM would be replaced by a faster and equally accurate algorithm. But whereas the BPM's accuracy has been honed over many years by many different workers, the GTI transform has only just been discovered. More investigations are required to optimise it for integrated optics; however, comparisons between the BPM and GTI results presented in this chapter indicate that the observed lack of accuracy of the GTI was not due to the paraxial approximation.

CHAPTER 6

EXPERIMENTS WITH A $LiNbO_3$ DIRECTIONAL COUPLER.

6.1 Introduction 121
6.1.1 Introduction to chapter 121
6.1.2 Background to experimental work 121

6.2 Fabrication of directional coupler 123
6.2.1 Preparation 123
6.2.2 Photolithography 124
6.2.3 Results 127

6.3 Experiments 132
6.3.1 Experimental set-up 132
6.3.2 Laser details 133
6.3.3 Alignment of directional coupler 133
6.3.4 Results 135

6.4 Conclusions 135

Chapter 6 Experiments with a $LiNbO_3$ directional coupler.

6.1 Introduction

6.1.1 Introduction to chapter

This chapter concerns the experimental side of the project. Later in this section, the motivation behind the experiments is discussed. The fabrication of the directional coupler is described in section 2. Section 3 presents calculations pertaining to the experiments, details of equipment and procedures used and the results. The results are discussed and conclusions drawn in section 4.

6.1.2 Background to experimental work

The work presented in this thesis was always intended to be predominantly theoretical, but it was recognised from the outset that there was a potential for novel experiments. The CASE collaborating company, Barr and Stroud (now part of the Pilkington group) was the sole supplier of optical quality $LiNbO_3$ in Britain and had facilities for making $LiNbO_3$ waveguides. Imperial College Physics Department's Laser Optics Group had lasers capable of producing short pulses at or near the power densities necessary to produce optical switching in $LiNbO_3$. The group also had streak cameras capable of directly observing the pulse shapes without autocorrelation. It seemed then that a collaboration between the two would give access to new results.

$LiNbO_3$ was not the ideal material with which to embark on all-optical switching experiments because its nonlinearity is not high enough to give switching without risking damage to the material. Even if optical switching was demonstrated, $LiNbO_3$ could not be used to develop

commercial devices because very high power lasers would be needed to cause nonlinearity; a commercial optical switch would need to use a semiconductor laser.

At the time the research programme started, the value of n_2 for $LiNbO_3$ was not known, and had only been estimated empirically. While it was well known that exposure of $LiNbO_3$ to moderate intensities of visible green light would result in reversible photorefractive damage, there was less information about thresholds for reversible and non-reversible damage in the near infra-red. The experiments of Lattes et al (1983) had, however, demonstrated that some nonlinear modulation could be achieved in $LiNbO_3$ despite giving a value for n_2 that was about ten times lower than a previous empirical estimate.

In conclusion, despite the fact that the calculated switching powers in chapters 2 and 4 were so much higher than the damage threshold, it was thought that at least a small amount of nonlinearity could be achieved with the equipment available. Even if the crystal was damaged, it was possible that reversible photorefractive damage would be noticed at lower power levels than catastrophic permanent damage and so the latter would be avoided.

6.2 Fabrication of $LiNbO_3$ directional coupler

6.2.1 Preparation

Cylindrical single crystals of $LiNbO_3$ up to 4" in diameter are grown at Barr and Stroud's Strathleven site. From these, chips approximately 1 cm by 3 cm by 2 mm thick are prepared. One face is polished to optical flatness. The other face is ground rough, to enable the chip to be held in the polisher with wax. Grinding the back face causes problems later - see 6.2.3.

$LiNbO_3$ is called x-, y- or z-cut depending on the crystal axis to which the polished face is perpendicular. Titanium diffuses fastest along the z axis and since the refractive index change is proportional to the Ti concentration, this makes the z-cut waveguide profile deeper and more round than x- or y-cut crystal. It is normal to use y-cut crystal in integrated optics as more electro-optic interaction can be achieved. However, the present experiment did not use the electro-optic effect, but did involve coupling the waveguides to focused laser beams, and for this reason z-cut crystal was used for the substrate.

Single mode optical waveguides are typically a few microns wide by a few millimetres long. Any dirt on the substrate before fabrication is likely to ruin the waveguides, because they are so long in relation to their width and they only have to be broken once to be rendered useless. Work on optical waveguides starts with a cleaning process, and must be carried out in a "clean room".

The crystal can be cleaned by scrubbing it with a detergent-soaked sponge, warming it in a variety of solvents and subjecting it to ultrasound while in a solvent bath. Some dirt may remain on the surface even

after this process. The chance of producing a crystal that is clean can be increased by producing a large batch of devices simultaneously.

6.2.2 Photolithography

The object of the photolithography is to transfer a technical drawing of the directional coupler to a micron-sized pattern of increased refractive index on the $LiNbO_3$ substrate. In outline, the process is as follows;

- make the drawing of the device,
- reduce the drawing onto photographic film,
- reduce the film image onto a glass mask,
- coat the $LiNbO_3$ substrate with photo-resist,
- contact-print the mask onto the substrate,
- develop the substrate,
- coat the substrate with titanium,
- remove the unwanted titanium,
- diffuse the Ti into the substrate.

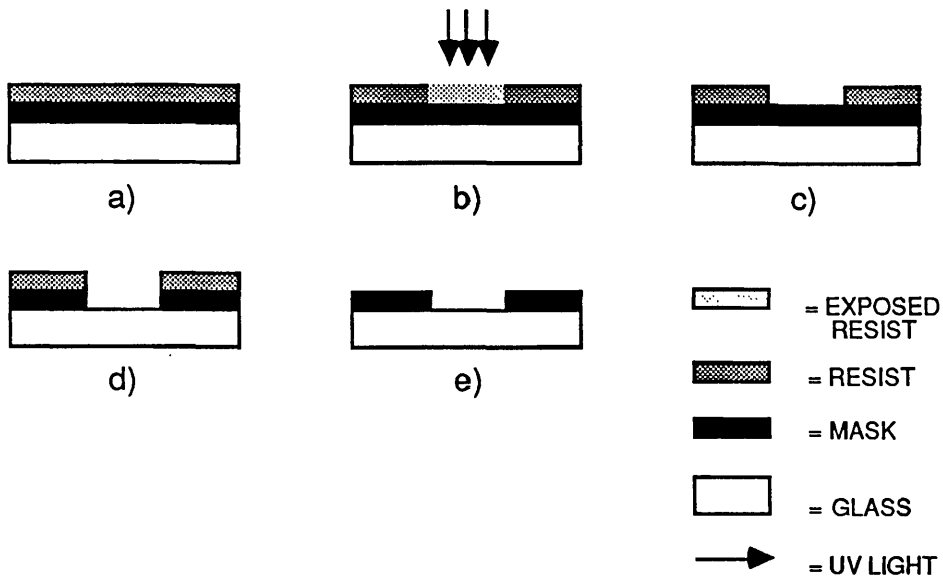

FIGURE 6.1a-e. Steps in making photolithographic mask.

The drawing and initial photography are done using standard techniques of draughtsmanship and photography.

In order to make a glass mask, the film is printed onto a 5 cm square glass slide, coated with a film of masking material and a film of photoresist (see figure 6.1a). During this process, the areas where waveguides are required are exposed to ultraviolet light (figure 6.1b). When the mask is developed, those areas of resist are removed (figure 6.1c). The slide is etched, removing masking material from the areas that are not protected by the resist (figure 6.1d). Finally, the remaining resist is removed with a solvent (figure 6.1e).

Masking materials must be opaque to the UV wavelengths used in the exposure. When only one exposure is necessary, a chromium mask may be used. However if two or more exposures are required (eg while making a waveguide device with electrodes) the masks for subsequent exposures must be transparent to visible light in order to permit their alignment with existing structures on the substrate. In these situations ferric oxide masks are used.

A drop or two of the resist is applied to the surface of the $LiNbO_3$ substrate using a syringe and then the substrate is spun. The thickness of the resulting film depends in a quantifiable way on the dilution of the resist, spin rpm and spin time, but is largely independent of the amount of resist placed on the surface initially. A spin at 4000 rpm for 30 seconds gives the required thickness in this case. Once the resist has been applied, the substrate is heated to 100° c for about 30 minutes to drive off residual solvent. The substrate is then ready for exposure (figure 6.2a).

The precise alignment of the mask and the substrate is

achieved using an instrument called a mask aligner. This enables the experimenter to manipulate the substrate and mask using fine verniers while looking through a microscope. During alignment the mask and the substrate are almost in contact. When the alignment is satisfactory, they are brought into direct contact by evacuating the air between them. Then the microscope is replaced by the UV source and the exposure is made. Again, the UV light exposes the resist in the areas where waveguides are required, and is prevented from exposing other parts of the resist by the mask (figure 6.2b). The chip is developed, removing the exposed resist from the areas where titanium is required (figure 6.2c).

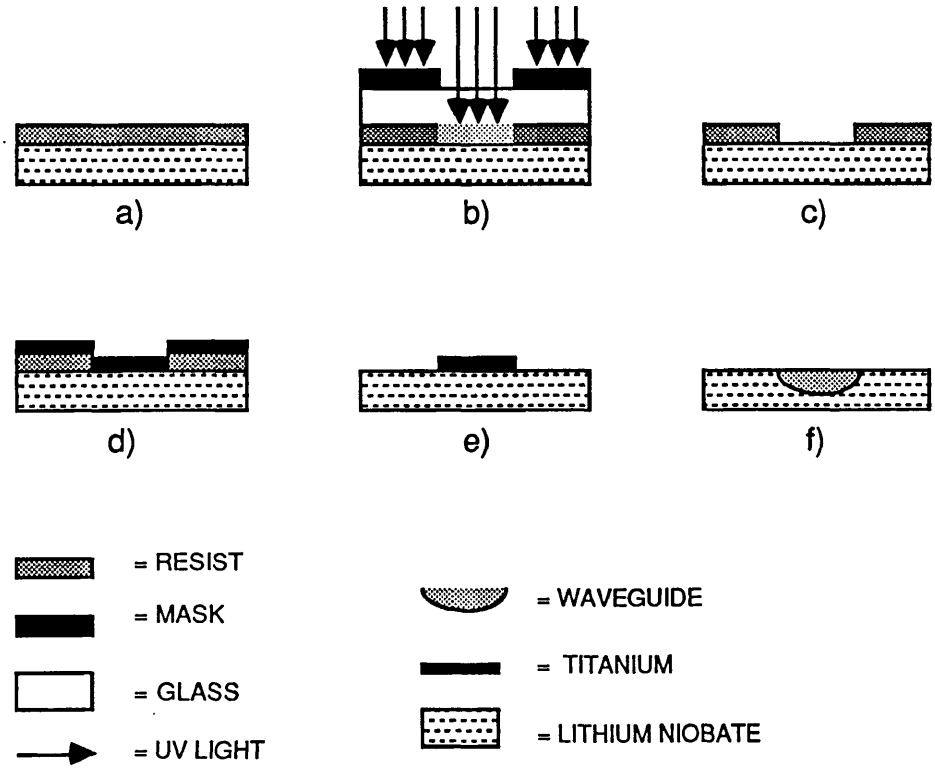

FIGURE 6.2a-f. Steps in exposure of $LiNbO_3$ substrate.

The titanium film is applied by electron beam evaporation (figure 6.2d). The thickness of the titanium is controlled

by a quartz crystal oscillator which is coated with Ti at the same time as the substrate. As Ti is deposited on the oscillator, it becomes heavier and its vibration frequency decreases. The mass deposited can be calculated from the change in frequency. The thickness of the layer on the substrate is the same as that on the oscillator, and is obtained from the oscillator's surface area and the mass deposited. This thickness and the diffusion parameters govern the waveguide profile. The unwanted Ti is on top of the photoresist and so can be removed by soaking in the solvent for the resist (figure 6.2e).

The final stage is the diffusion, which is done by placing the substrate in a furnace, typically at 1000° C for 8 hours (figure 6.2f). Increasing the time makes the waveguide profile deeper for z-cut crystal and wider for x and y cut. This is a convenient way of altering the wavelength at which the guide will be single mode; for instance a mask which would produce a 1.3μm waveguide could be used to produce a 1.06μm waveguide by diffusing the waveguide for slightly less time than normal.

To finish the device, the input and output edges are polished and possibly anti-reflection coated for the appropriate wavelength.

6.2.3 Results

The resulting waveguides are quite robust and dirt-proof. The waveguides are actually under the surface of the substrate and only constitute an area of changed refractive index. Consequently it is impossible to view them with the naked eye or a microscope. The difference in refractive index in the region of the waveguides does render them visible with phase sensitive microscopy, but the ordinary transmission technique cannot be used because the back surface of the substrate was ground and acts as a

phase scrambler. Hence reflection or Nomarski phase sensitive microscopy is required. Photographs of the device using this method are shown in figures 6.4a - 6.4c, all of which have a total magnification of x580. Figures 6.4a-c show the input region, the interaction region and the output region, respectively. A schematic diagram of the device is shown in figure 6.3.

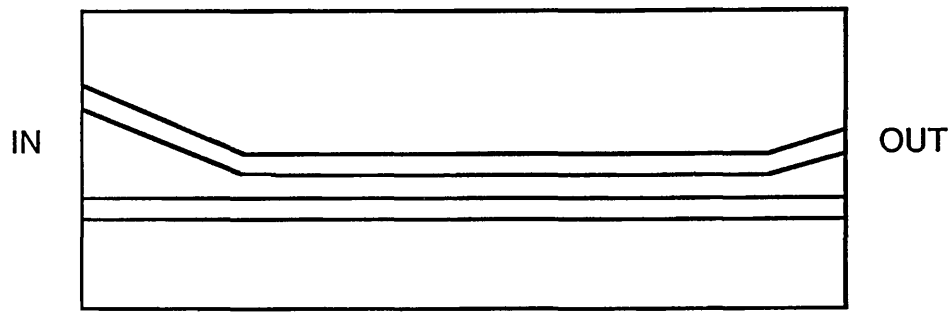

FIGURE 6.3. Schematic of the $LiNbO_3$ directional coupler used in the experiments.

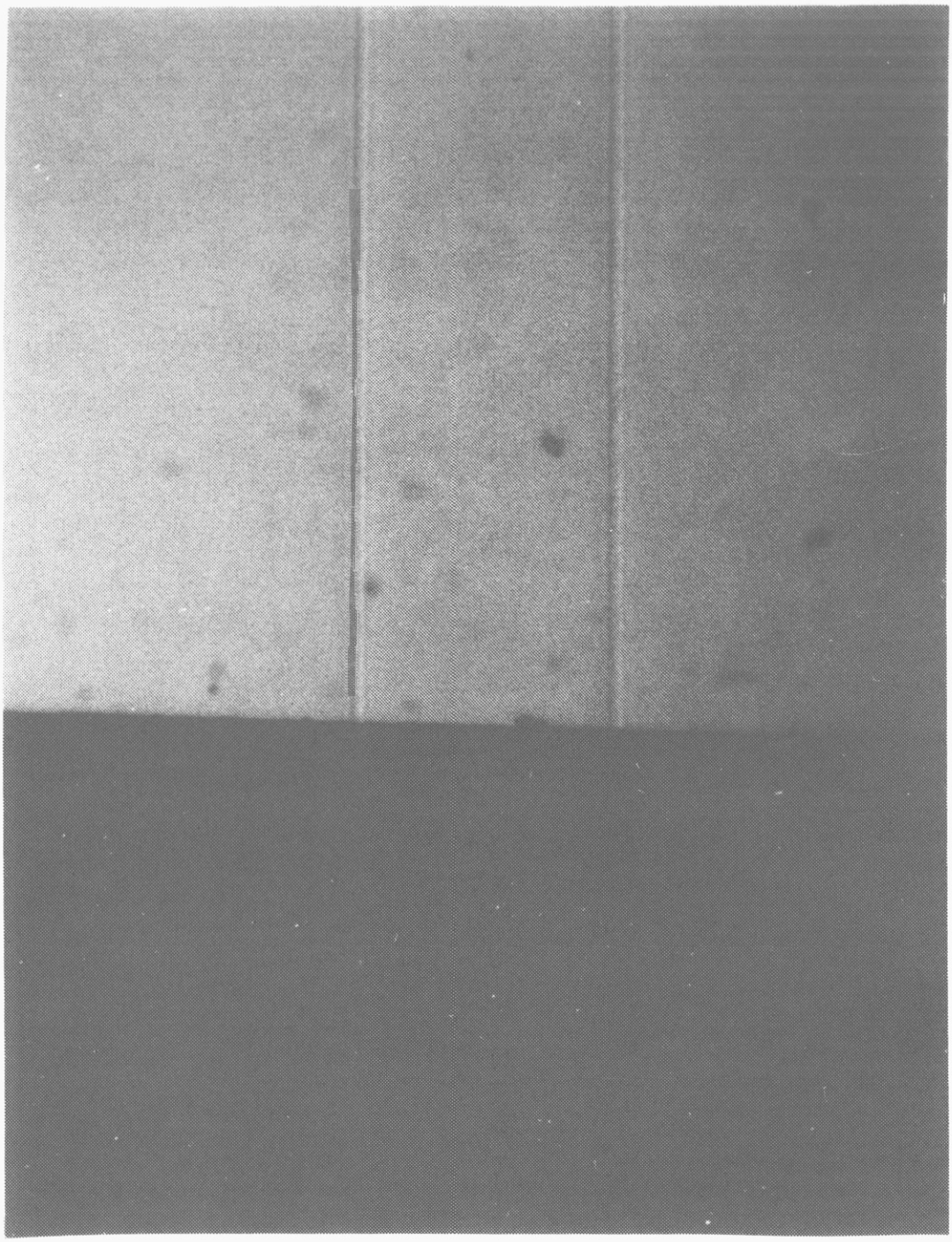

FIGURE 6.4a. Input region of the $LiNbO_3$ directional coupler used in the experiments.

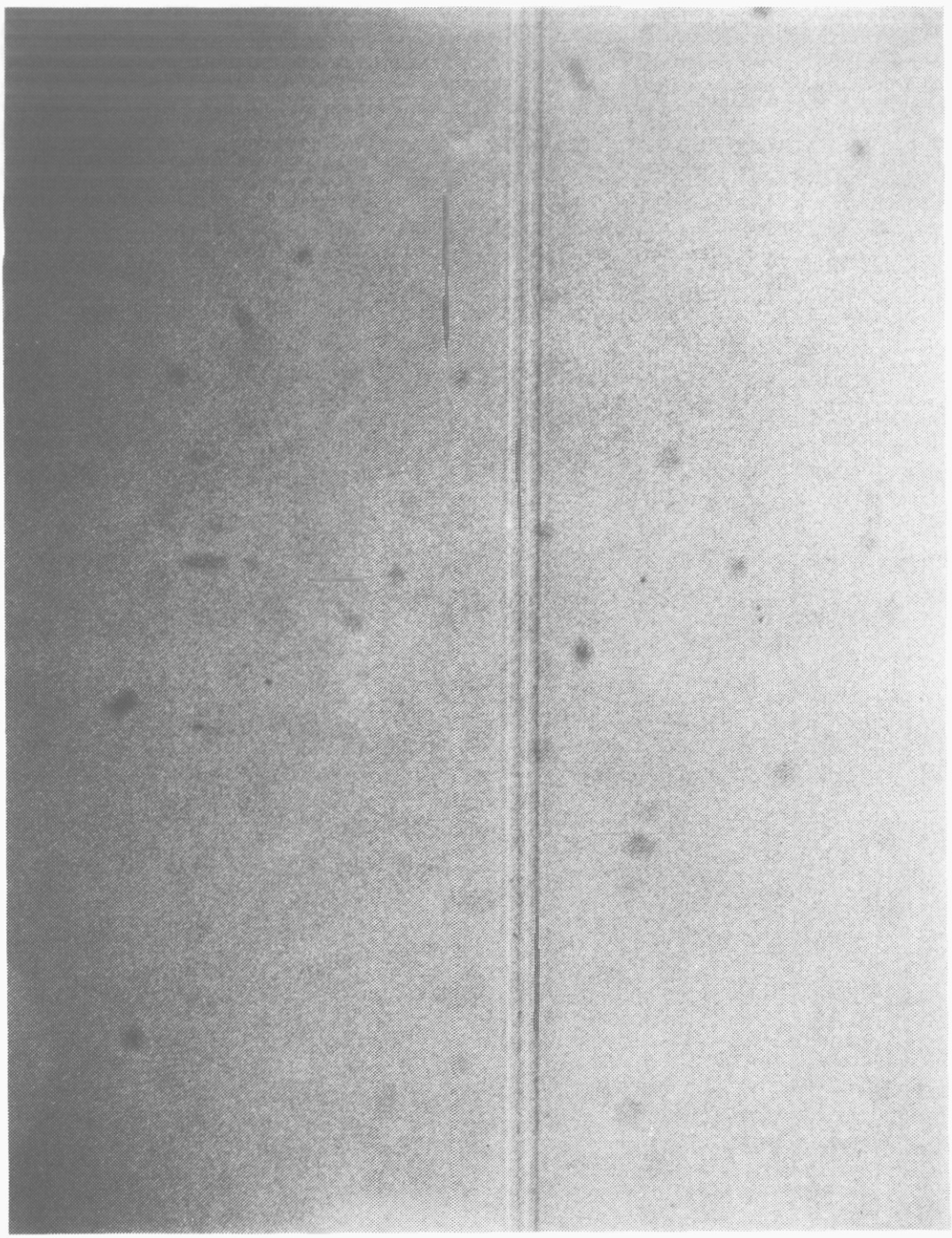

FIGURE 6.4b. Interaction region of the directional coupler.

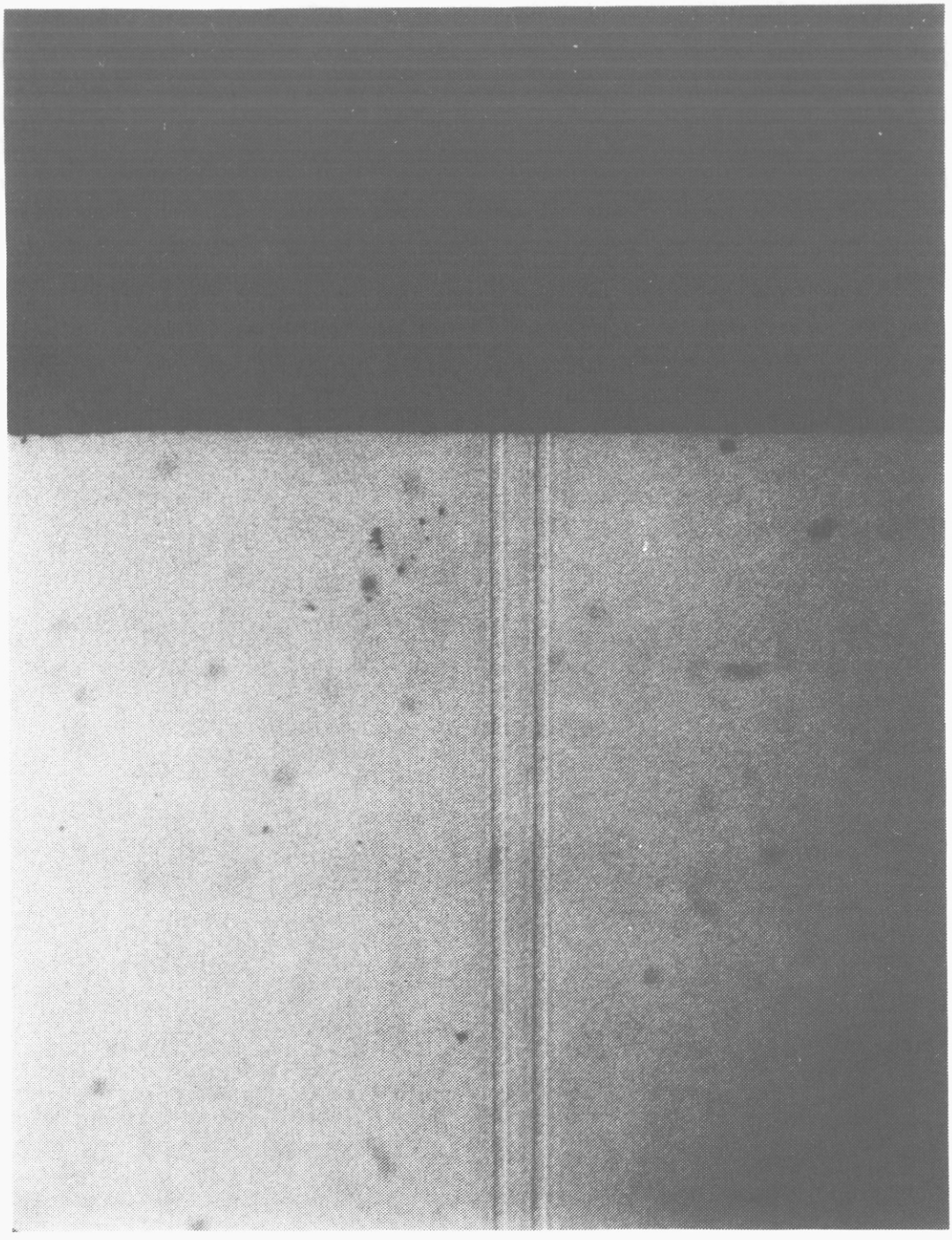

FIGURE 6.4c. Output region of the directional coupler

6.3 the experiments

The experimental set up is shown in figure 6.5. The YAG and HeNe lasers were aligned so that their beams were coincident. The directional coupler was aligned with visible light from the HeNe laser. The YAG beam was attenuated using two polarisers, one of which could be rotated. The chip was held on a goniometer of the sort normally used for X-ray crystallography to allow several degrees of freedom of movement. The input and output beams were focused using microscope objectives which were mounted on xyz stages. The output beams from the two channels of the directional coupler were split by reflecting one of them from a mirror and sending it round a delay path of known length. The outputs were then recombined into the streak camera, where they formed two pulses whose width in time could be determined by comparison with the delay between the pulses.

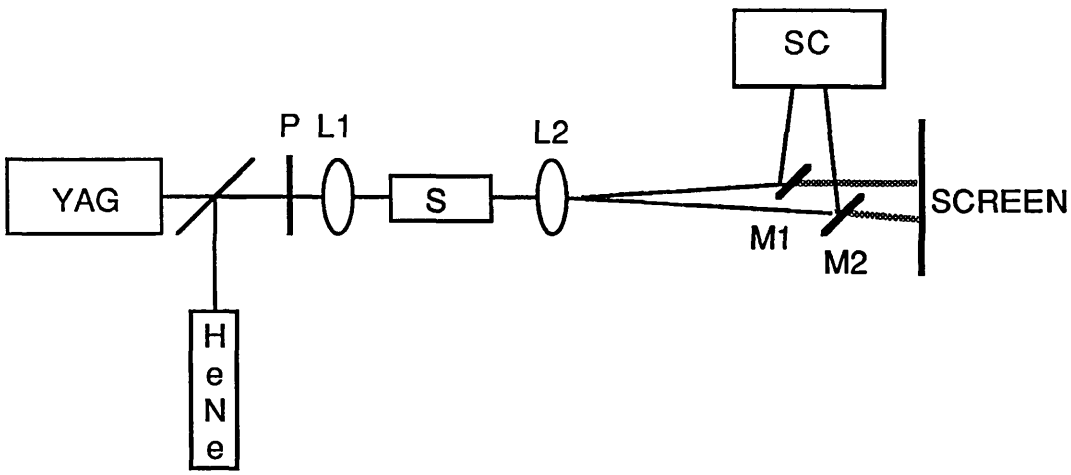

P - crossed polarisers
L1 - input lens
L2 - output lens
S - substrate
SC - streak camera
M1, M2 - 100% mirrors

FIGURE 6.5. Experimental set-up.

6.3.2 Laser details

The laser was a mode-locked and Q-switched Nd: YAG operating at 1.06μm and capable of producing 2W average power. The mode-locked pulses were 100ps long repeated every 10ns, and could be reduced to 5ps long by turning on the Q-switch, without much loss of power. The waveguide inputs were nominally 3μm x 3μm, resulting in power densities of 22MW/cm^2 or 440MW/cm^2 when Q-switched. The latter figure is within the right order of magnitude to cause catastrophic damage according to Normandin et al (1979).

6.3.3 Alignment of directional coupler

The HeNe pilot beam was aligned along the YAG beam and then the YAG laser was turned off temporarily. A viewing screen was put in the distance beyond the outputs instead of the mirrors to guide the outputs into the streak camera. The lenses and goniometer were arranged so that the beam went straight through the lenses and over the top of the goniometer. The substrate was mounted on the goniometer so that the input lens roughly focused the beam onto the its input face. The height of the lens was adjusted relative to the chip until horizontal bars were seen in the top half of the screen (see figure 6.6a). These bars are interference fringes caused by reflection from the surface of the substrate.

The output lens was focused until the edge of the substrate appeared sharp and the interference pattern was sharp. The substrate was moved across the beam in a transverse horizontal direction until a rising sun pattern was seen. One rising sun pattern is the result of diffraction from one waveguide (figure 6.6b). In the case of a directional coupler, a double rising sun is seen (figure 6.6c). However, when the coupler is badly aligned,

the rising sun is distorted (figure 6.6d). The input lens and substrate were moved iteratively until the rising sun pattern was symmetric (like figure 6.6c). The input lens was then moved vertically so that the input beam was going into the substrate. The vertical position and focus of the input beam were adjusted for maximum output.

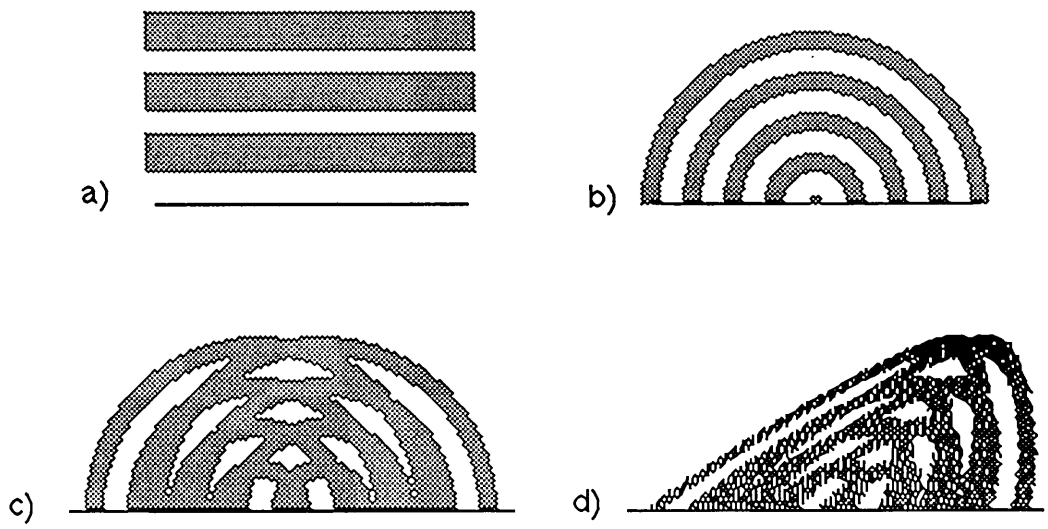

FIGURE 6.6a-d. Far-field diffraction "rising sun" patterns.

It was then possible to check that the laser input was going into just one of the input ports of the device and that the device was not back to front. The input lens was moved sideways across the input side of the substrate. With the lens focused onto the space between the two inputs the output intensity dropped substantially. If it does not, then either the device is back to front, the

device is dirty or the input lens has too low a magnification and is focusing the input onto both waveguides. Once the set-up was optimised in the visible, only the input lens focus needed alteration for the YAG input.

6.3.4 Results

Once the directional coupler was aligned with visible red light, two outputs were observed, of roughly equal intensity, indicating that the interaction region of the device was about a half-integral number of coupling lengths long. The actual number of coupling lengths in the device was not known. It is possible to count the coupling lengths in a directional coupler by examining it with a microscope while laser light is passing through it; one can observe the scattered light from the waveguides. This was not attempted due to the difficulty of aligning the substrate in both a laser and a moving microscope platfrom and also due to the danger of using focusing optics in laser light.

With the YAG laser turned on (attenuated and without the Q switch) and the HeNe turned off, the alignment was repeated, using a hand-held viewer to observe the far-field diffraction patterns. Again, two approximately equal outputs were seen.

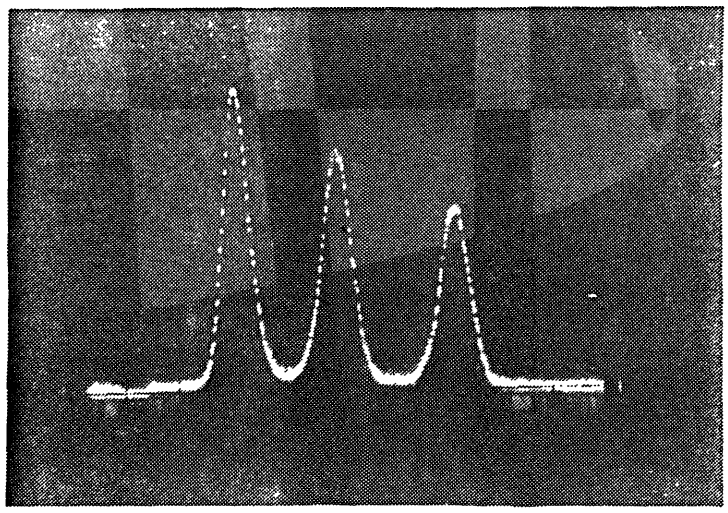

FIGURE 6.7. Laser input (left) and the two outputs (right) at 200mW. Pulses approx 100ps long.

Mirrors were inserted in front of the screen, to redirect the outputs to the input slit of the streak camera (see M1 and M2 in fig 6.5). As the two output beams were very close together, it was difficult to get them both into the input slit of the camera, and impossible to ensure that both beams were coupled into the camera equally well. For this reason the relative heights of the two outputs as seen on the streak camera did not indicate their relative brightness. Only a change in the relative height would have been meaningful. Figure 6.7 shows a typical streak

CHAPTER 7

IDEAS FOR FURTHER WORK AND CONCLUSIONS

7.1 Computational work 137

7.2 Experimental work 138

7.3 Materials 138

7.4 Conclusions 138

Chapter 7 Ideas for further work and conlcusions.

7.1 Computational work

The BPM has been used to construct a model of an all-optical directional coupler. The computational program was just a beginning to the work that could be done with the BPM in nonlinear integrated optics. In particular, more work could be done on the $LiNbO_3$ directional coupler.

The present model takes no account of the anisotropy of the medium, but this can be quite easily coped with using the BPM, as reported by Fleck et al (1983).

Any realistic study of the device will have to include a model of short pulse propagation in the NLDC. To do this, the pulse must be Fourier transformed and each frequency treated separately. Again this has been reported in (Feit and Fleck 1979) for optical fibre.

However, the obvious improvement to the model would be to model in three dimensions. This would require access to a supercomputer, for instance the University of London's Cray or Amdahl, a DAP or other parallel processor.

The GTI transform would benefit from further study and refinement, and more work on this may be undertaken.

It would be easy to alter the AODC model to investigate the operation of the device in another material, for instance one with negative n_2 such as InSb, and it would also be easy to investigate other devices. Indeed, the research programme has been carried on by Lauder (1986) to model other integrated optics devices.

7.2 Experimental work

While the experiments did not appear promising, the prospect of coupling the laser to the waveguide using a fibre rather than by end-fire coupling holds some promise. This would eliminate the movement of the beam when the intensity is adjusted, which was the cause of the thermal shock suffered by the experimental device.

7.3 Materials

The really interesting prospect for this work would be the development of materials with high n_2 and short relaxation time. Some candidates are doped glasses, which would need to be made more nonlinear, diacetylene and related organic compounds which are new and have no established fabrication techniques, liquid crystals, which are probably too slow and GaAs and related semiconductors, which also need to be speeded up.

7.4 Conclusions

A computational method based on the BPM has verified Jensen's results. This has been used to predict that seeing nonlinearity in $LiNbO_3$ directional couplers is unlikely. However, the model could be used to investigate the feasibility of other materials, including those with negative n_2.

A new transform for split-step methods has been introduced and evaluated. Further evaluation is necessary but initial results are encouraging.

In view of the low nonlinear n_2 coefficient of $LiNbO_3$ coupled with its low damage threshold, one must have reservations about the likely application of this material

to all-optical directional couplers for commercial use. However, when the right material is discovered and developed, all-optical directional couplers will be useful for all-optical processing.

APPENDIX A

PROGRAMMING DETAILS

A.1 Introduction 141

A.2 Hardware 141

A.3 Choice of language 142

A.4 BPM program variables 144

A.5 BPM program modules 146

A.6 Program function 148

A.7 Graphics 148

Appendix A Programming details

A.1. Introduction

This appendix is intended to supply detailed information on the programs used at a level that was not considered relevant to the main text. Section 2 lists the equipment used. Section 3 discusses the pros and cons of different languages for computational physics and explains the choice of Pascal. Sections 4, 5 and 6 document the BPM programs, describing data, subprograms and the overall function respectively. Finally, section 7 explains how the graphics, and in particular, the 3-dimensional plots of the results, were generated. Source code for the BPM and GTI (where different from the BPM) programs can be found inside the back cover.

A.2 Hardware

Program development was started on an Apple IIe micro. This proved suitable until serious number-crunching was attempted, at which point it became necessary to move onto the Imperial College mainframe, which consists of a CDC Cyber 855 and 174.

The results from the computations were plotted using a Hewlett-Packard 7550A plotter connected between the mainframe and the terminal used to request pictures.

A.3 Choice of language

Algol 68, Fortran 77 and Pascal were all available on the IC mainframe. Software engineering principles indicated that a strongly-typed language supporting modular design would help the programmer to write quickly and de-bug easily. This narrowed the choice to Algol 68 and Pascal. Pascal was chosen, despite its drawbacks, as it is easier for non-users to understand than Algol 68, which would have presented a communications barrier to some colleagues.

The most serious disadvantage of standard Pascal for number-crunching is the difficulty with complex numbers. Pascal allows "record types" to be declared in addition to the usual real, integer and character types found in other languages, and so a complex number can be declared as a record of two real types (and so one can implement complex numbers in cartesian or polar form according to convenience). However, operators such as +, -, * and / are not defined for record types. Also, in standard Pascal, it is not possible to get round this using a function, eg

```
c3 := complexsum (c1, c2)
```

because a function is not allowed to return a record type. And so it is necessary to use a procedure which alters one of its parameters;

```
complexsum (c1, c2, cresult).
```

This makes any reasonable amount of complex arithmetic awkward to write and more difficult to understand once written. Algol 68 and Fortran both allow complex arithmetic to use the normal operators and Algol 68 also allows users to extend or completely redefine the function of operators. Extended Pascals, for example the Vax implementation, allow functions to return structured

types, alleviating the problem somewhat.

Additional inconveniences of standard Pascal are, one cannot assign an expression to a constant when it is declared, eg

```
CONST six = 3 * 2
```

would not work, and one cannot read in an integer and dimension an array with it - the size of arrays must be fixed at compile time. Finally, there is no NAG library for Pascal as there is for Algol 68 and Fortran, but this was no real drawback as no NAG routines were required and in any case it is possible to import Fortran routines into Pascal.

Despite the drawbacks for computational work, Pascal allowed comprehensible and reliable programs to be developed quickly, and was the best choice under the circumstances. The original BPM programs were developed in UCSD Pascal on the Apple IIe and ported with little difficulty to the mainframe.

A.4 BPM Program variables

The most important parameters governing program operation are listed below.

Computational mesh:

number of points in array,
Δx,
Δz,
array containing values of x for every mesh point,
main array containing values of complex field.

Apodisation:

number of points of array apodised,
width of sech profile used,
array containing values of apodisation profile,

Waveguide profile:

substrate and peak refractive index,
Epstein's a, v^2, w and $2\Delta n^2$,
number of mesh points separating waveguides in coupler,
array containing refractive index profile.

Diffraction:

vacuum wavelength of light,
k for vacuum and medium,
array containing phase changes for diffraction step.

Nonlinearity:

nonlinear refractive index of medium,
maximum intensity of beam,
vacuum speed of light and permittivity of free space.

The results were stored in files which were declared as files of arrays. Pascal allows an array to be written to a file of this type explicitly, eg

```
write (filename, arrayname)
```

rather than element by element in a loop. Similarly, an array can be read from the file with a single read command.

A.5 BPM Program modules

External libraries of mathematics functions and complex arithmetic procedures were linked into the code at compile time. Apart from these and the procedures used to initialise program arrays, the functions and procedures used are listed below.

FUNCTION energy; computes a measure of the energy in the main array to check conservation and the operation of the apodiser.

PROCEDURE sendata; sends complex field to data file and other diagnostics to text files.

PROCEDURE transf; fast Fourier transform speeded up by performing its constant array initialisations during program initialisation.

PROCEDURE diffstep; performs a Fourier transform, multiplies program array by constant phase factors for diffraction and then performs reverse transform. Can do either full or half Δz step.

PROCEDURE ristep; apodises main program array, calculates the new refractive index if nonlinear operation is being used and then multiplies program array by phase factor for refractive index change corresponding to full Δz step.

PROCEDURE propagate. If a diffraction step is reperesented by D and a refractive index step by R then since the BPM is a split-step method, a propagation step ought to involve

D/2, R, D/2

However, if this propagation step were repeated, there would be two adjacent half diffraction steps where one

full one was required, and a corresponding waste of calculations, including two extra FFTs. On the other hand, if the whole propagation was done as

D/2, R, D, R, D.....D, R, D/2

there would be no convenient time to take snapshots of the propagation. As a compromise, the propagation step is

D/2, R, D, R, D, R, D, R, D, R, D, R, D/2.

so that results are written to the data files every six Δz steps.

A.6 Program function

The main program requests values for the number of propagation steps and, for nonlinear propagation, the maximum intensity of the beam. It then initialises all the variables which have to be calculated from other constants and initialises the program arrays. In the case of a directional coupler, the initial condition is a mode of a single waveguide in one of the guides and nothing in the other. The directional coupler refractive index profile is set up by superimposing two single waveguides a number of mesh points apart. The data files are opened and the initial value of the field is sent to the data files.

The main program step does a propagation step, sends a report of progress and energy measure to the screen and sends the results to the data file.

A.7 Graphics

Results were plotted locally using a plotter which intercepts messages going from the mainframe to the terminal. Two simple plotting programs were written, both of which used a locally-written library of commands to control the plotter. The two-dimensional program plots selected curves from a data file in combinations of linear or log and real space or Fourier transform. The three-dimensional program scales the picture to the largest output value in the data file and shifts each successive curve along by an integer number of array points. It does not perform any perspective distortions or rotations.

REFERENCES

E Abraham and SD Smith, J Phys E Sci Instrum 15 33-39 (1982a).

E Abraham and S D Smith, Optical bistability and related devices, Reports on Progress in Physics 45 815-885 (1982).

M Abramowitz and I A Stegan, Handbook of mathematical functions, New York: Dover 1965.

M J Adams, An Introduction to Optical Waveguides, Wiley (1981).

I Andonovic, PhD Thesis, University of Glasgow (1983).

A Ashkin, G D Boyd, J M Dziedzic, R G Smith, A A Ballman and K Nassau, Applied Physics Letters, 9 72 (1966).

H Avramopoulos and G H C New, to be published.

R Baets and P E Lagasse, Loss calculation and design of arbitrarily curved integrated-optic waveguides, J Opt Soc Am 73 177-182 (1983).

D W Berreman, A lens or light guide using convectively distorted thermal gradient in gases, Bell Syst Tech J 43 1469-1475 (1964).

J E Bjorkholm, P W Smith, W J Tomlinson and A E Kaplan, Optical bistability based on self-focusing, Optics Letters 6 345-347 (1981).

M Born and E Wolf, "Principles of Optics" (Oxford: Pergamon 1965).

E O Brigham, The Fast Fourier Transform, Prentice-Hall (1974).

G M Carter, Y J Chen and S K Tripathy, Intensity dependent index of refraction in multilayers of polydiacetylene, Applied Physics Letters 43 891-893 (1983).

T Y Chang, Fast self-induced refractive index changes in optical media: a survey, Optical Engineering 2 220-232 (1981).

J W Cooley and J W Tukey, Math Comput 19 297 (1965).

M A Duguay and J W Hansen, Compression of pulses from a mode-locked HeNe laser, Applied Physics Letters 14 14-15 (1969).

M D Feit and J A Fleck Jr, Light propagation in graded-index optical fibres, Applied Optics 17 3990-3998 (1978).

M D Feit and J A Fleck Jr, Calculation of dispersion in graded-index multi-mode fibres by a propagating-beam method, Applied Optics 18 2843-2851 (1979).

M D Feit and J A Fleck Jr, Computation of mode properties in optical fibre waveguides by a propagating beam method, Applied Optics 19 1154-1164 (1980).

M D Feit and J A Fleck Jr, Computation of mode eigenfunctions in graded-index optical fibres by the propagating beam method, Applied Optics 19 2240-2246 (1980).

M D Feit and J A Fleck Jr, Mode properties and dispersion for two optical fibre index profiles by the propagating beam method, Applied Optics 19 3140-3149 (1980).

M D Feit, J A Fleck Jr and L McCaughan, Comparison of calculated and measured performance of diffused channel waveguide couplers, J Opt Soc Am 73 1296-1304 (1983).

R Feynman, Feynman Lectures on Physics.

R A Fisher and W K Bischel, Numerical studies of the interplay between self-phase modulation and dispersion for intense plane-wave laser pulses. Journal of Applied Physics 46 4921-4934 (1975).

J A Fleck Jr, J R Morris and M D Feit, time-dependent propagation of high energy laser beams through the atmosphere, Applied Physics 10 129-160 (1976).

J A Fleck Jr and M D Feit, Beam propagation in uniaxial anisotropic media, J Opt Soc Am 73 920-926 (1983).

P M W French, G F Chen and W Sibbett, Tunable group velocity dispersion interferometer for intracavity and extracavity applications, Optics Communications 57 263-268 (1986).

P M W French, A S L Gomes, A S Gouveia-Neto and J R Taylor, Temporal compression of ND: YAG pulses using chirp compensation, Optical and Quantum Electronics 18 171-174 (1986).

M Fukuma, J Noda and H Iwasaki, Optical properties in titanium-diffused $LiNbO_3$ strip waveguides. Journal of Applied Physics 40 3693-3698 (1978).

H M Gibbs, S L McCall and T N C Venkatesan, Physical Review Letters 36 1135 (1976).

F Gires and P Tournois, Interferometre utilisable pour la compression d'impulsions lumineuses modulees en frequence, C R Acad Sc Paris t258 6112-6115 (1964).

A M Glass, The photorefractive effect, Optical Engineering 17 470-479 (1978).

A M Glass, I P Kaminow, A A Ballman and D H Olson, Absorption loss and photorefractive-index changes in Ti:$LiNbO_3$ crystals and waveguides, Applied Optics 19 276-281 (1980).

D Gloge and W H Steier, Pulse shuttling in a half-mile optical lens guide, Bell Syst Tech J. 47 767-782 (1968).

A S L Gomes, A S Gouveia-Neto, J R Taylor, H Avramopoulos and G H C New, Optical pulse narrowing by the spectral windowing of self-phase modulated picosecond pulses, Optics Communications 59 399-404 (1986).

G Goubau and F Schwering, On the guided propagation of electromagnetic wave beams, IRE Trans Antenna + Propagation AP-9 5 248-256 (1961).

H A Haus and C G Fonstad Jr, Three-waveguide couplers for improved sampling and filtering, IEEE Journal of Quantum Electronics, QE-17 12 2321-2325 (1981).

H A Haus and L Molter-Orr, Coupled multiple waveguide systems, IEEE Journal of Quantum Electronics QE-19 5 (1983).

H A Haus and N A Whitaker Jr, All-optical logic in optical waveguides, Phil Trans R Soc Lond A 313, 311-319 (1984).

H A Haus, W P Huang, S Kawakami and N Whitaker, IEEE J Lightwave Tech LT-5 16 (1987).

E Hecht and A Zajac, Optics, Addison-Wesley (1974).

R W Hellwarth, Third order optical susceptibility of liquids and solids, Progress in Quantum Electronics 4 11-67 (1978).

B Hermansson, D Yevick and L Thylen, A propagating beam method analysis of nonlinear effects in optical waveguides, Optical and Quantum Electronics 16 525-534 (1984).

J Heppner and J Kuhl, Intracavity chirp compensation in a colliding pulse mode-locked laser using thin-film interferometers, Applied Physics Letters 47 453-455 (1985).

R G Hunsperger, "Integrated Optics: Theory and Technology", (Springer-Verlag 1982).

S M Jensen, The non-linear coherent coupler, a new optical logic device, presented at the Conference on Integrated and Guided-Wave Optics, Incline Village, CA, 1980.

*
S M Jensen, The nonlinear coherent coupler, IEEE Trans Microwave Theory and Techniques MTT 30 10 Oct 82.

K C Kao and G A Hockham, Dielectric-fiber surface waveguides for optical frequencies, Proc IEE (London) 113 1151-1158 (1966).

N S Kapany, "Optical fibres - principles and applications" Academic Press, New York, 1967.

A E Kaplan, Hysteresis reflection and refraction by a nonlinear boundary - a new class of effects in non linear optics, JETP Letters 24 114-119 (1976).

F P Kapron et al, Radiation loss in glass optical waveguide, Applied Physics Letters 17 423-425 (1970).

A E Karbowiak, Guided wave propagation in submillimetric region, Proc IRE 41 10 1706-1711 (1958).

* S M Jensen, An optical logic element and its use in optical logic circuits, presented at the Rank Prize Funds conference, London (1980a).

A E Karbowiak, New type of waveguide for light and infrared waves, Electronics Letters 1 47-48 (1965).

A E Karbowiak, Microwaves 37 (1966).

J Kuhl and J Heppner, Compression of femtosecond optical pulses with dielectric multiple interferometers, IEEE Transactions on Quantum Electronics QE-22 182-185 (1986).

A Lattes, H A Haus, F J Leonberger and E P Ippen, An ultrafast all-optical gate, IEEE Journal of Quantum Electronics, QE-19 11 (1983).

M A Lauder and G H C New, private communication, (1986).

P Li Kam Wa, J E Sitch, N J Mason, J S Roberts and P N Robson, All optical multiple-quantum-well waveguide switch, Electronics Letters 21 1 26-27 (1985).

D J Love, G H C New and M A Lauder, Beam propagation analysis of a nonlinear dual-channel directional coupler, Optics Communications 59 3 177-182 (1986).

E A J Marcatili, dielectric rectangular waveguide and directional coupler for integrated optics, Bell Systems Technical Journal 48 2071 (1969).

E A J Marcatili, IEEE Journal of Quantum Electronics QE-22 988 (1986).

D Marcuse and S E Miller, Analysis of a tubular gas lens, Bell Syst Tech J. 43 1759-1782 (1964).

D Marcuse, Theory of Dielectric Optical Waveguides, New York, Academic (1974).

L M Milne-Thomson, Jacobian elliptic function tables, Dover Publications Inc, New York NY (1956).

J W Mink, Experimental investigations with an iris beam waveguide, IEEE Trans Microwave Theory Tech. MTT-17 No 1 48-49 (1969).

L F Mollenauer, Solitons in optical fibres and the soliton laser, Phil Trans R Soc Lond A 315 437-450 (1985).

A Neyer, Electro-optic x-switch using single-Mode Ti:LiNbo3 channel waveguides, Electronics Letters, 19 14 553-554 (1983).

R Normandin, V C Y So, G A Teh and G I Stegeman, Optical damage thresholds of thin-film and in-diffused waveguides, Applied Physics Letters 34 200-202 (1979).

T Okoshi, "Optical Fibres" Academic Press 1982.

Optel atmospheric communications products are distributed by Laser Lines Ltd, Beaumont Close, Banbury, Oxon, OX16 7TQ.

M Paillette, Ann Phys 4 671 (1969).

A E Siegman, Lasers Physics, Systems and Techniques, ed W J Firth and R G Harrison, Scottish Universities Summer School in Physics (1982).

P W Smith, I P Kaminow, P J Maloney and L W Stulz, Self-contained integrated bistable optical devices, Applied Physics Letters 34 62-65 (1979).

P W Smith, J P Hermann, W J Tomlinson and P J Maloney, Optical bistability at a nonlinear interface, Applied Physics Letters 34 846-848 (1979).

A W Snyder, Coupled-mode theory for optical fibres, Journal of the Optical Society of America 62 11 (1972).

R R A Syms, Asymmetric switch response of three-arm directional couplers in Ti:$LiNbO_3$, Optics Communications 64 248-252 (1987).

R R A Syms and R G Peall, Explanation of asymmetric switch response of three-arm directional couplers in Ti:$LiNbO_3$ using strong coupling theory, accepted for publication in Optics Communications (1988).

I Thomazeu, J Etchepare, G Grillon and A Migus, Electronic nonlinear optical susceptibilities of silicate glasses, Optics Letters 10 223-225 (1985).

L Thylen, The beam propagation method: an analysis of its applicability, Optical and Quantum Electronics 15 433-439 (1983).

J Van Roey, J van der Donk and P E Lagasse, Beam propagation method: analysis and assessment, J Opt Soc Am 71 803-810 (1981).

A Yariv, Coupled-mode theory for guided-wave optics, IEEE Journal of Quantum Electronics QE-9 (1973).

BEAM PROPAGATION ANALYSIS OF A NONLINEAR DUAL-CHANNEL DIRECTIONAL COUPLER

D.J. LOVE [1], G.H.C. NEW and M.A. LAUDER

Laser Optics Group, Physics Department, Imperial College, Prince Consort Road, London SW7 2BZ, UK

Received 17 April 1986

The dynamics of a nonlinear dual-channel directional coupler are studied numerically using a two-dimensional beam propagation method. The results are in good agreement with those of Jensen, which were based on the analytical solution of a pair of coupled-mode equations.

1. Introduction

The dual-channel directional coupler is an established component in integrated optics research. As shown schematically in fig. 1, it consists of a pair of optical waveguides which run in sufficiently close proximity, for a distance D, that coherent coupling takes place between them. If a signal is fed into guide 1, a simplified coupled-mode theory indicates that the field in guide 2 varies with propagation distance as $\sin^2(\pi z/2L)$, where L is a characteristic coupling length. Thus, at $z = L$, all the energy is in guide 2 whilst at $z = 2L$ the initial situation is restored. At first sight it would appear that the overall performance of the device, determined by the ratio D/L, would be fixed for a given coupler geometry. Fortunately, the coupling characteristics are sensitively dependent upon the refractive index difference between the guides, and in a non-centrosymmetric nonlinear material, such as $LiNbO_3$, this can be controlled through the Pockels' effect. In practice, this is effected by positioning a pair of electrodes asymmetrically with respect to the two channels (see fig. 1), which makes L a function of the applied voltage V. The coupling characteristics can therefore be controlled by an external electrical signal, allowing optical switches and modulators to be constructed.

An important goal for the future is the development of all-optical logic systems in which light is controlled by light, rather than by electricity. With this in mind, Jensen [1] has earlier studied the properties of a nonlinear coherent coupler. This is a dual-channel device in which the coupling characteristics are a function of the intensity of the waves in the guides due to the nonlinear, intensity dependent, refractive index. Hensen's results were based on a pair of coupled-mode

[1] Now at the Department of Electrical and Electronic Engineering, Kings College, The Strand, London WC2, UK.

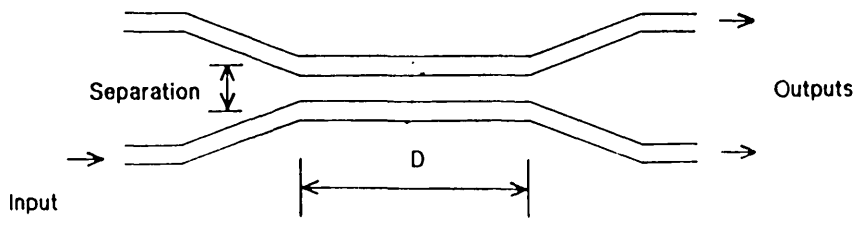

Fig. 1. Dual channel coupler with coupling controlled by the Pockels' effect.

0 030-4018/86/$03.50

equations in which the nonlinear terms were included; these equations can be solved analytically and the results are reviewed in section 2 below. In the present paper we solve the problem numerically, using the beam propagation method (BPM) [2–4], with a single transverse dimension. Our results are in good agreement with those of Jensen.

2. Coupled-mode approach

Jensen's coupled-mode equations governing the variation of the field amplitudes (A_1 and A_2), in the two identical guides 1 and 2 are [1]

$$-i\partial A_1/\partial z = [Q_K + Q_{Na}|A_1|^2 + Q_{Nb}|A_2|^2]A_1 + Q_C A_2, \quad (1)$$

and a similar equation with the indices 1 and 2 exchanged. Of the four coefficients in eq. (1), Q_K represents the change in propagation constant of the mode in a guide caused by the adjacent guide, Q_{Na} and Q_{Nb} control nonlinear modifications to Q_K, which are proportional to the mode intensities in guides 1 and 2 respectively, and Q_C controls the coupling of energy between the two guides. Note that, if the nonlinear coefficients are set to zero, the equations reduce to the standard form to be found in any textbook analysis of linear dual-channel devices [5].

If, as we have assumed, the two guides are identical then Q_C can be taken as real without any loss of generality. This allows a solution of eq. (1), and the analogous equation for A_2, to be written in terms of Jacobi elliptic functions. In the special case where all the power is initially launched into one guide, say guide 1, the solution reduces to the particularly simple form

$$P_1(Z)\,(=|A_1(Z)|^2) = P_1(0)\,[1 + \mathrm{cn}\,(2Z|m)]/2, \quad (2)$$

where $Z = Q_C z$, and $m = P_1^2(0)/P_c^2$ is a measure of the

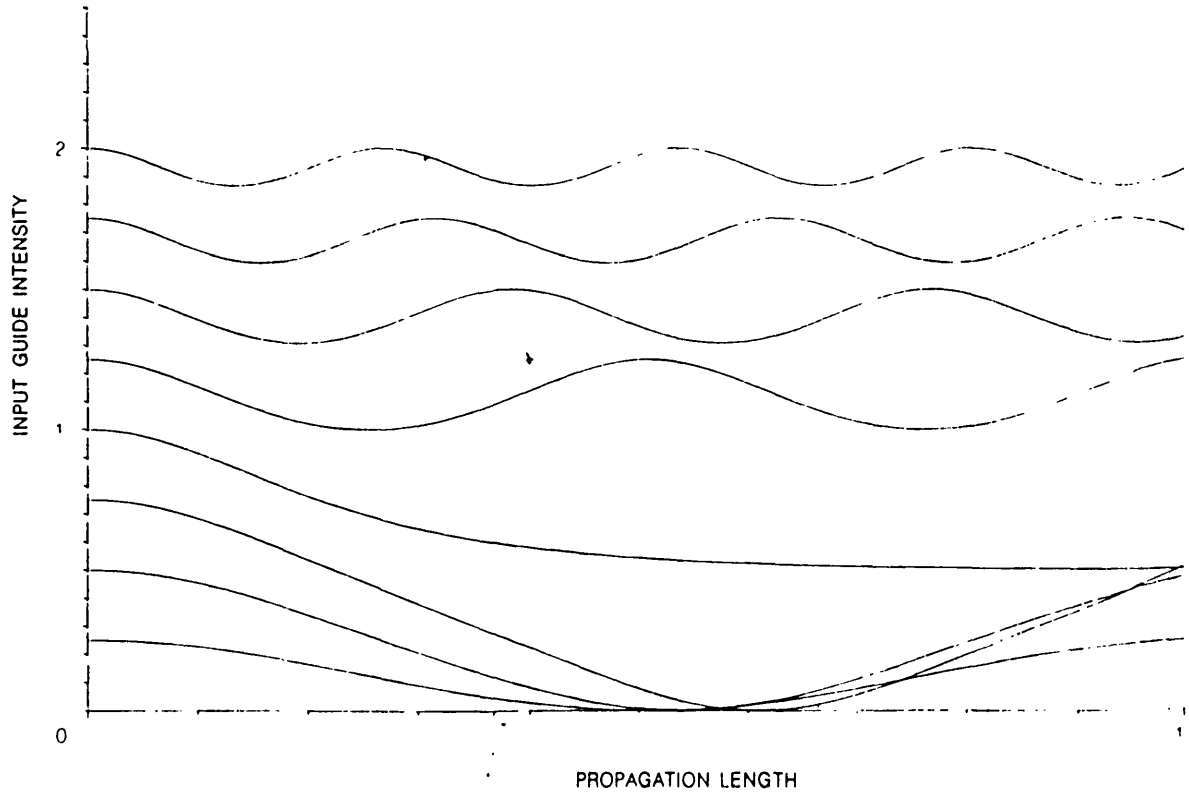

Fig. 2. Analytical solution of the peak intensity in one guide against the input intensity (from Jensen [1]).

input power in terms of a critical power defined by

$$P_c = 4Q_C/(Q_{Na} - Q_{Nb}). \quad (3)$$

Solutions of eq. (2) are plotted in fig. 2 which is identical to fig. 2 of Jensen [1]. In the limit of very small intensities, that is $m \ll 1$, cn $(2Z\,|m) \to \cos(2Z)$ and eq. (2) reduces to the well known solution for a linear coherent coupler, having coupling length $L = \pi/2Q_C$. As the input power in guide 1 is raised, the coupling increases, going to infinity at $m = 1$, in which case a stationary state is achieved where the power is eventually divided equally between the two guides. Further increase of m leads again to periodic energy exchange but the amount of energy transferred to guide 2 becomes progressively smaller as m gets larger.

3. Beam propagation method

The accuracy and conditions under which the beam propagation method is valid has been studied in previous papers [2–4]. The BPM is a split operator technique which successively models the diffraction and focusing of the propagating beam. The focusing effect is modelled in x space by imposing a phase front on the beam. The diffraction is modelled in k space thus requiring the use of a Fourier transform. This sequence of operations is equivalent to replacing the fibre with a series of lenses. Each lens accounts for the focusing whilst the free space propagation between lenses accounts for the diffraction. Each step in the solution thus requires four operations. An x space phase modification, a fast Fourier transform (FFT), a k space phase modification and a reverse FFT. The large amount of computing involved in the FFT's is counteracted by the large steps which can be taken with this method compared to the solution of the Helmholtz equation by difference techniques.

4. The nonlinear coherent coupler

This technique is applied to the nonlinear coherent coupler solved analytically by Jensen [1]. The coupler consists of two optical waveguides placed in close proximity such that they periodically exchange power.

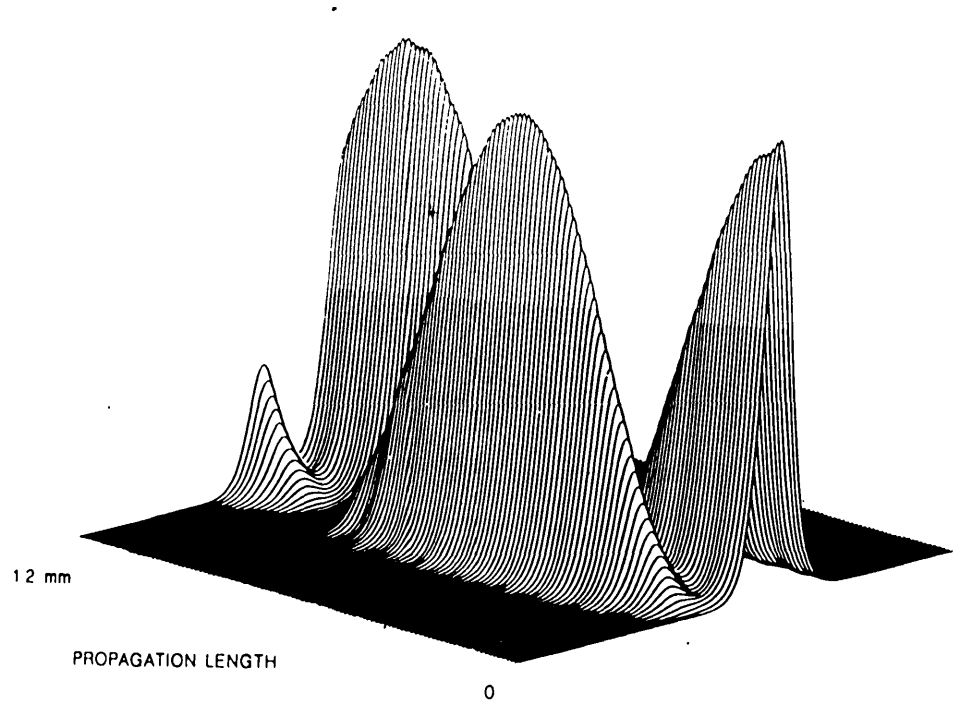

Fig. 3. The coupling between the guides with a very weak input intensity.

In our model each guide has an Epstein layer refractive index profile [6], given by

$$n^2(x) = n_s^2 + (n_p^2 - n_s^2)\,\mathrm{sech}^2\,(x/a), \tag{4}$$

where n_s is the refractive index of the substrate (that is at large $|x|$), n_p is the peak refractive index in the guide and a is a parameter governing the width of the guide. This type of profile is used and, for a single guide, it has an exact analytical solution [6] where the electric field envelope is given by

$$E(x) \propto \mathrm{sech}^w\,(x/a), \tag{5}$$

where

$$w = \{[1 + 4a^2k_0^2(n_p^2 - n_s^2)]^{1/2} - 1\}/2, \tag{6}$$

and k_0 is the free-space propagation constant ($k_0 = 2\pi/\lambda_0$). The coupling with the second guide depends upon the transverse coherence of the beam. This coherence is upset by any nonlinearity in the refractive index causing the periodic power exchange to be modified. The refractive index profile for the two-guide nonlinear system is given by a "sum" of two individual profiles and a nonlinear part, so that

$$n(x) = \{n_s^2 + (n_p^2 - n_s^2)\,[\mathrm{sech}^2\,((x - x_1)/a) + \mathrm{sech}^2\,((x - x_2)/a)]\}^{1/2} + n_2\,|E(x)|^2, \tag{7}$$

where x_1 and x_2 are the positions of the peaks of the two profiles, assumed identical in height, and n_2 is the nonlinear refractive index. For the nonlinearity to have any effect n_2 must be large enough such that $\Delta n \sim \lambda_0/L$, where $\Delta n = n_2\,|E_{\mathrm{peak}}|^2$. This is calculated from the criterion that the total phase difference induced by the nonlinearity between the peak and the wings of the profile, over the coupling length L, must be of the order of 2π.

5. Results

Fig. 3 shows the development of the wave launched into guide 1 as it propagates along the coupler. The intensity is very weak so that the nonlinear part of the refractive index is negligible. In this case the energy is periodically fully exchanged between the two guides. The total propagation distance shown is 12 mm with

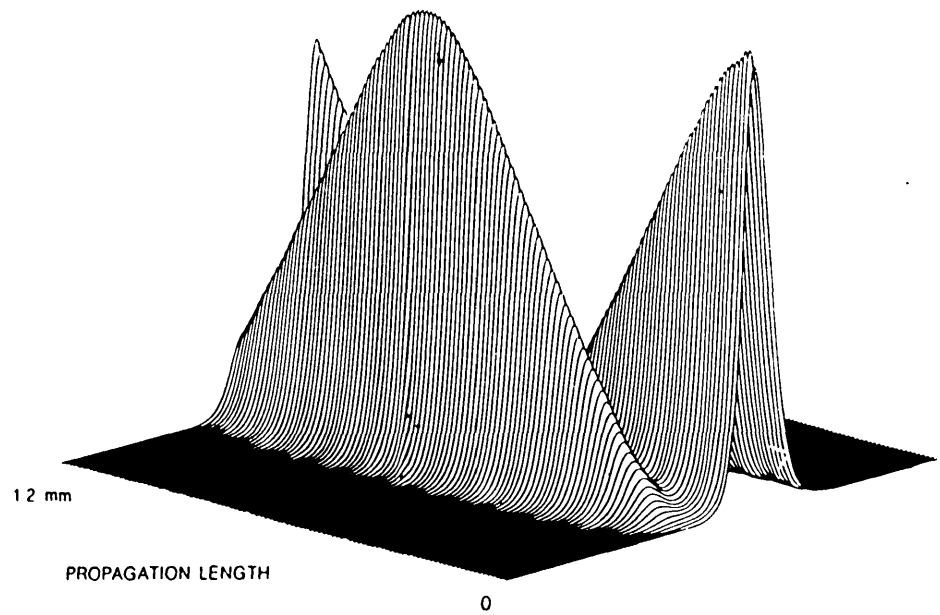

Fig. 4. The intensity is increased to make the nonlinear refractive index important, but the coupling still takes place.

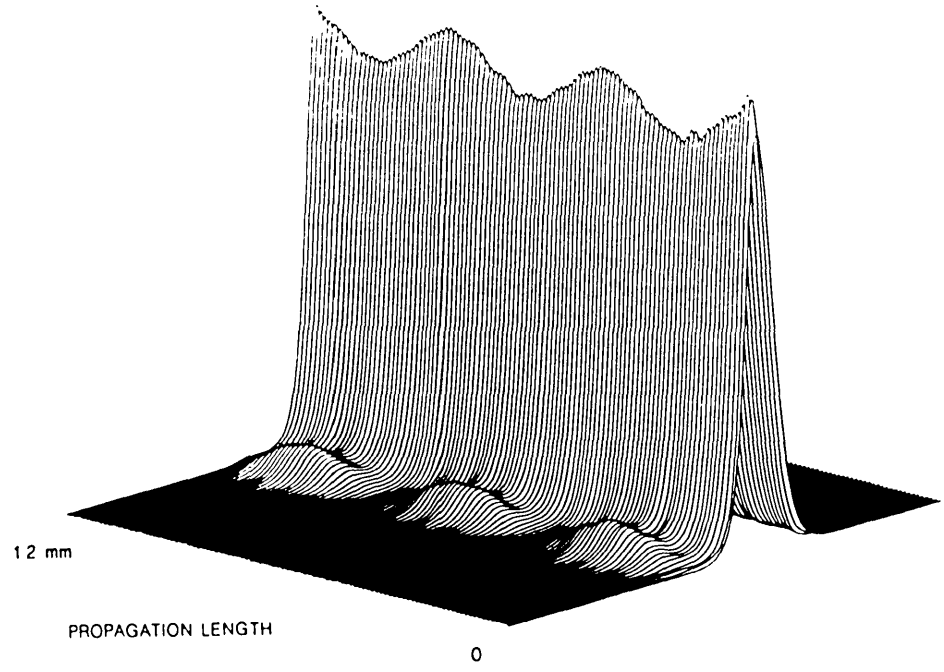

Fig. 5. Doubling the intensity of that in fig. 4 increases the nonlinearity so that the coupling is destroyed.

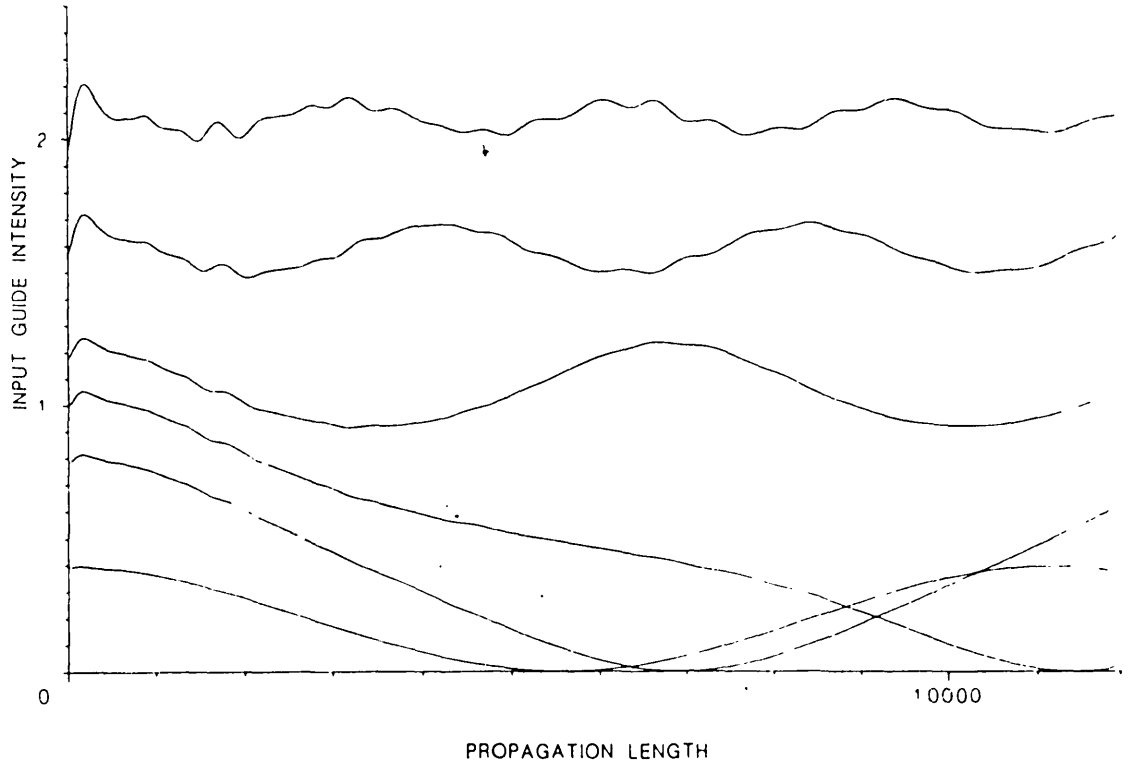

Fig. 6. The numerical values of the peak intensity in the input guide against normalised input intensity. Compare with the analytical results in fig. 2.

the actual numerical step length being 10 μm. This propagation distance corresponds to just over one full exchange cycle. The guides are 11.76 μm apart, with the total width shown being 67.84 μm, and the a parameter, which sets the size of the guides, is 3 μm. Fig. 4 shows the same propagation but with the intensity increased enough to make the nonlinear refractive index important, $\Delta nL/\lambda_0 \sim 2$. The exchange of energy is still present, and full, but the period over which this occurs has increased slightly. Fig. 5 shows the nonlinear regime, where $\Delta nL/\lambda_0 \sim 4$. The intensity is only twice that of the previous example, but the behaviour is now completely altered. The nonlinearity causes a mismatch in the phase across the wavefront which is enough to stop full excitation of the other guide. Thus if a coupler was made half an exchange cycle long, pulses launched into a guide below the critical intensity would be emitted from the opposite guide, whilst those above would be emitted out of the same guide. Fig. 6 is a numerical equivalent of fig. 2, showing the peak intensity in guide 1 against the propagation distance for a range of values. This agrees very well with the results of Jensen, showing the decreasing period and amplitude as the relative intensity increases. The high frequency oscillations, which increase in magnitude for increasing nonlinearity, are due to the mismatch between the guide and the field mode. As the intensity, and so the nonlinearity, is increased the field modifies the guide causing it to deviate from the ideal profile.

6. Conclusions

This shows remarkable agreement between a theoretical coupled mode approach and a numerical beam propagation method with one transverse dimension. The advantage of the numerical technique is that it is not necessary to start with exact modes. Even with the Epstein profile the nonlinearity perturbs the profile enough to cause shock oscillations when the wave is launched into the guide (fig. 6). This numerical method is to be used to model an experiment to be carried out using a $LiNbO_3$ coupler where the index and beam profiles are not matched.

Acknowledgement

Two of us (DJL and MAL) are pleased to acknowledge the financial support of the SERC; DJL was supported under an SERC CASE studentship with Barr and Stroud.

References

[1] S.M. Jensen, IEEE MIT 30 (1982) 1568.
[2] M.D. Feit and J.A. Fleck Jr., Appl. Optics 17 (1978) 3990.
[3] J. Van Roey, J. van der Donk and P.E. Lagasse, J. Opt. Soc. Am. 71 (1981) 803.
[4] L. Thylén, Opt. and Quantum Electron. 15 (1983) 433.
[5] A.W. Snyder and J.D. Love, Optical waveguide theory (Chapman and Hall, New York, 1983) chapter 29.
[6] P.S. Epstein, Proc. Nat. Acad. Sci. USA 16 (1930) 627.

University of London

Imperial College of Science and Technology
Blackett Laboratory
Optics Section

Theoretical analysis of an all-optical directional coupler

by

Diane Joan Love

Thesis submitted in partial fulfillment of the requirements for the PhD degree of the University of London, and the Diploma of Imperial College of Science and Technology.

1988

```
PROGRAM COUPLER (INPUT/, OUTPUT, D256, P256) ;

(* ECH41 PLOTS FOR CHAPTER FOUR - NONLINEAR COUPLER *)


(*$I'COMPLEX' *)
(*$I'MATH' *)

CONST

  N        = 256 ;          (* POINTS IN MESH *)
  NHP      = 129 ;
  NH       = 128 ;
  PROPLEN  = 6 ;            (* NUMBER OF DZ IN PROPAGATION STEP *)
  AF       = 3E-6 ;         (* EPSTEIN A FOR FIELD *)
  AR       = 3E-6 ;         (* EPSTEIN A FOR RI PROFILE *)
  LAMBDA   = 1.06E-6;       (* WAVELENGTH IN METRES *)
  OFFSET   = 10 ;           (* POINTS BETWEEN CENTRES OF MESH AND FIELD *)
  CUTWIDTH = 30 ;           (* WIDTH OF CUTOFF ARRAY *)
  CUTPARAM = 20 ;           (* WIDTH PRAMETER FOR CUTOFF SECH PROFILE *)
  N1       = 2.002 ;        (* REFRACTIVE INDEX MAXIMUM *)
  N2       = 2.0 ;          (* REFRACTIVE INDEX MINIMUM *)
  DELTAX   = 0.49E-6 ;      (* MESH SIZE IN X DIRECTION *)
  DELTAZ   = 5E-6 ;         (* STEP SIZE IN Z DIRECTION *)
  NTWO     = 3E-13 ;        (* METRES SQUARED / WATTS *)
  EPSNOT   = 8.854E-12 ;    (* EPSILON NOUGHT *)
  CLIGHT   = 2.997924590E8 ; (* SPEED OF LIGHT, METRES PER SECOND *)


TYPE

  CARRAY   = ARRAY[1..N] OF COMPLEX;
  CHARRAY  = ARRAY[1..NH] OF COMPLEX;
  CURVE    = ARRAY[1..N] OF REAL;
  CUTARRAY = ARRAY[1..CUTWIDTH] OF REAL ;


VAR

  NREPEAT    : INTEGER ;      (* NUMBER OF PROGRAM STEPS *)
  K          : INTEGER ;      (* MAIN LOOP COUNTER       *)

  VSQRD      : REAL ;         (* EPSTEIN COEFFICIENTS    *)
  W          : REAL ;
  TWODNSQRD  : REAL ;

  KAPPA      : REAL ;         (* MISCELLANEOUS *)
  KAPPAMED   : REAL ;
  LENGTH     : REAL ;
  DISTGONE   : REAL ;

  EPSNOTC    : REAL ;         (* NONLINEAR VARIABLES *)
  IMAX       : REAL ;
  EMAX       : REAL ;

  CZERO      : COMPLEX ;      (* (0 + 0I) *)

  CFIELD     : CARRAY ;       (* MAIN PROGRAM ARRAY FOR FIELD *)
  KPHASE     : CARRAY ;       (* K SPACE PHASE CHANGE ARRAY FOR FULL STEP *)
  HALFKPHASE : CARRAY ;       (* K SPACE PHASE CHANGE ARRAY FOR HALF STEP *)

  WP, WM     : CHARRAY ;      (* ARRAYS OF COMPLEX FOR TRANSF             *)

  X          : CURVE ;        (* VALUES OF MESH IN REAL SPACE  *)
  INDEX      : CURVE ;        (* REFRACTIVE INDEX DISTRIBUTION *)

  CUTOFF     : CUTARRAY ;     (* ARRAY OF VALUES FOR CUTOFF    *)

  D256, P256 : FILE OF CURVE ;  (* OUTPUT FILES FOR INTENSITY AND PHASE *)


FUNCTION ENERGY (C : CARRAY) : REAL;

  VAR
    K : INTEGER ;
    E : REAL ;

  BEGIN (* ENERGY *)

    E := 0;
    FOR K := 1 TO N DO
      E := E + SQR (CABS (C[K])) ;
      ENERGY := E

  END ; (* ENERGY *)


PROCEDURE SHRINK (VAR C : COMPLEX ;
                      X : REAL) ;

  BEGIN (* SHRINK *)

        C.RE := C.RE * X;
        C.IM := C.IM * X;

  END ; (* SHRINK *)

PROCEDURE SENDATA (CF : CARRAY) ;

(* SENDS FIELD CF TO D256, PHASE TO P256 *)

  VAR
    K          : INTEGER ;
    FIELD      : CURVE ;
    PHASEFRONT : CURVE ;

  BEGIN  (* SENDATA *)
```

```
    FOR K := 1 TO N DO

    BEGIN
      FIELD[K] := SQR (CABS (CF[K]));
      IF (CF[K].RE <> 0)
        AND (CF[K].IM <> 0)
      THEN PHASEFRONT[K] := ARCTAN2 (CF[K].IM, CF[K].RE)
      ELSE PHASEFRONT[K] := 0
    END ;

    WRITE (D256, FIELD);
    WRITE (P256, PHASEFRONT)

  END ; (* SENDATA *)


PROCEDURE SETXANDFIELD (VAR X    : CURVE ;
                        VAR CF   : CARRAY ;
                            EMAX : REAL) ;

(* INITIALISES THE ARRAYS FOR X AND FIELD *)

  VAR
    TEMP  : REAL;
    K     : INTEGER ;

  BEGIN (* SETXANDFIELD *)

    (* SET X *)
    FOR K := 1 TO N DO
      X[K] := (K-NHP) * DELTAX ;

    (* SET FIELD *)
    FOR K := 1 TO N DO
    BEGIN
      CF[K].IM := 0;
      IF K <= N - OFFSET
      THEN
        BEGIN
          TEMP := COSH (X[K + OFFSET]/AF);
          CF[K].RE := 1/(POWER(TEMP,W));
          CF[K].RE := CF[K].RE * EMAX ;
        END
      ELSE
        CF[K].RE := 0 ;
    END; (* FOR *)

  END ; (* SETXANDFIELD *)


PROCEDURE SETCUTOFF (VAR CUTOFF : CUTARRAY) ;

  VAR
    K    : INTEGER ;
    TEMP : REAL ;

  BEGIN (* SETCUTOFF *)

    FOR K := 1 TO CUTWIDTH DO
    BEGIN
      TEMP := 1/SQR (COSH ((K-CUTWIDTH)/CUTPARAM));
      CUTOFF[K] := TEMP;
      WRITELN (CUTOFF[K])
    END;

  END ; (* SETCUTOFF *)


PROCEDURE SETTRANSF (VAR WP : CHARRAY ;
                     VAR WM : CHARRAY) ;

(* SETS ARRAYS FOR TRANSF *)

  VAR
    K     : INTEGER ;
    CTEMP : COMPLEX ;

  BEGIN (* SETTRANSF *)

    FOR K := 1 TO NH DO
    BEGIN
      CMPLX (0, (K-1)*PI/NH, CTEMP);
      CEXP (CTEMP, WP[K] );
      CMPLX (0, -(K-1)*PI/NH, CTEMP);
      CEXP (CTEMP, WM[K])
    END;

  END ; (* SETTRANSF *)


PROCEDURE SETKSPACE (    X   : CURVE ;
                     VAR KP  : CARRAY ;
                     VAR HKP : CARRAY) ;

(* SETS K-SPACE PHASE CHANGE ARRAYS *)

  VAR
    K      : INTEGER ;
    KM     : INTEGER ;
    KX     : REAL ;
    KXSQRD : REAL ;
    TERM   : REAL ;
    CTEMP  : COMPLEX ;

  BEGIN (* SETKSPACE *)

    FOR K := 1 TO N DO
    BEGIN
```

```
      KM := K - NHP ;
      KX := 2 * PI * KM / LENGTH ;
      KXSQRD := SQR (KX);
      TERM := KXSQRD / (SQRT (-(KXSQRD) + SQR (KAPPAMED)) + KAPPAMED) ;
      CMPLX (0, DELTAZ * TERM, CTEMP);
      CEXP (CTEMP, KP[K]);
      CMPLX (0, DELTAZ * TERM / 2, CTEMP);
      CEXP (CTEMP, HKP[K]);
    END ; (* FOR *)

  END ; (* SETKPHASE *)


PROCEDURE SETREFIND (    X     : CURVE ;
                     VAR INDEX : CURVE) ;

(* SETS REFRACTIVE INDEX DISTRIBUTION FOR COUPLER *)

  VAR
    K         :    INTEGER ;
    INDEXSQRD : REAL ;

  BEGIN (* SETREFIND *)

    FOR K := 1 TO N DO
    BEGIN
      INDEXSQRD := SQR (N2);
      IF K <= N - OFFSET
      THEN INDEXSQRD := INDEXSQRD + TWODNSQRD
                        * SQR (1 / COSH (X[K+OFFSET] / AR)) ;
      IF K >= OFFSET + 1
      THEN INDEXSQRD := INDEXSQRD + TWODNSQRD
                        * SQR (1 / COSH (X[K-OFFSET] / AR)) ;
      INDEX[K] := SQRT (INDEXSQRD)
    END ; (* FOR *)

  END;    (* SETREFIND *)


PROCEDURE TRANSF (VAR T1 : CARRAY; TRANSTYPE : INTEGER);
VAR     A, B                : COMPLEX;
        J, L, IH, IQ, IP, JK, NH, NHX, K      : INTEGER;
        SW : BOOLEAN;                R, RTEMP : REAL;
        TEMPAR, T2 : CARRAY;        W : CHARRAY;

        PROCEDURE CARRAYMEND (C : CARRAY; VAR RESULT : CARRAY );
        VAR KM : INTEGER;
        BEGIN
                FOR KM := 1 TO NH DO
                BEGIN
                        RESULT[KM+NH] := C[KM];
                        RESULT[KM] := C[KM+NH];
                END
        END;

        PROCEDURE CARRAYMENDIV (C : CARRAY; VAR RESULT : CARRAY );
        VAR KM : INTEGER;
        BEGIN
                FOR KM := 1 TO NH DO
                BEGIN
                        RESULT[KM+NH].RE := C[KM].RE/R;
                        RESULT[KM+NH].IM := C[KM].IM/R;
                        RESULT[KM].RE := C[KM+NH].RE/R;
                        RESULT[KM].IM := C[KM+NH].IM/R;
                END
        END;

BEGIN
        NHX := N DIV 2; NH := NHX;
        IF TRANSTYPE = 1
        THEN W := WP
        ELSE W := WM;
        R := SQRT (N);
        CARRAYMEND (T1, TEMPAR);
        T1 := TEMPAR;
        SW := TRUE; IH := NH;
        WHILE IH > 0 DO
        BEGIN
                FOR J := 1 TO NH DO
                BEGIN
                        L := J + NH; JK := IH*((J-1) DIV IH);
                        IP := J + JK; IQ := IP + IH;
                        IF SW THEN
                        BEGIN
                                A := T1[IP];
                                CMUL (T1[IQ], W[JK + 1], B);
                                CADD (A, B, T2[J]);
                                CSUB (A, B, T2[L]);
                        END ELSE
                        BEGIN
                                A := T2[IP];
                                CMUL (T2[IQ], W[JK + 1], B);
                                CADD (A, B, T1[J]);
                                CSUB (A, B, T1[L]);
                        END;
                END (*FOR*);
                IH := IH DIV 2;
                SW := NOT SW;
        END (*WHILE*);
        IF NOT SW THEN T1 := T2;
        CARRAYMENDIV (T1, TEMPAR);
        T1 := TEMPAR
END (*TRANSF*);


PROCEDURE DIFFSTEP (VAR C  : CARRAY ;
                        KP : CARRAY) ;
```

```
(* DOES DIFFRACTION STEP FOR KP *)

  VAR
    K       : INTEGER ;
    CRESULT : COMPLEX ;

  BEGIN  (* DIFFSTEP *)

    TRANSF (C, 1);
    FOR K := 1 TO N DO
    BEGIN
      CMUL (C[K], KP[K], CRESULT);
      C[K] := CRESULT
    END ; (* FOR *);
    TRANSF (C, -1);

  END ; (* DIFFSTEP *)


PROCEDURE RISTEP (VAR C      : CARRAY ;
                      INDEX  : CURVE ;
                      EMAX   : REAL) ;

(* LINEAR REFRACTIVE INDEX STEP, SAME LENGTH AS DELTAZ *)

  VAR
    K        : INTEGER ;
    NEWINDEX : REAL ;
    PHASE    : REAL ;
    CTEMP    : COMPLEX ;
    CRESULT  : COMPLEX ;
    CPHASE   : COMPLEX ;

  BEGIN  (* RISTEP *)

    (* APODISE *)

    FOR K := 1 TO CUTWIDTH DO
    BEGIN
      SHRINK (C[K], CUTOFF[K]);
      SHRINK (C[N+1-K], CUTOFF[K]);
    END;

    (* DO REFRACTIVE INDEX STEP *)

    FOR K := 1 TO N DO
    BEGIN

      (* CALCULATE NEW REFRACTIVE INDEX *)
      NEWINDEX := INDEX[K] + (NTWO * EPSNOTC * SQR (CABS (CFIELD[K]))) ;

      (* CALCULATE PHASE CHANGE FROM REFRACTIVE INDEX *)
      PHASE := -KAPPAMED * DELTAZ * ((NEWINDEX/N2-1));
      CMPLX (0, PHASE, CTEMP);
      CEXP (CTEMP, CPHASE);

      (* APPLY PHASE CHANGE TO FIELD *)
      CMUL (C[K], CPHASE, CRESULT);
      C[K] := CRESULT
    END;  (* FOR *)

  END; (* RISTEP *)


PROCEDURE PROPAGATE (VAR C : CARRAY );

(* SPLIT - STEP ALGORITHM SIX STEPS LONG *)

  CONST
    NUMSTEPS = 5 ; (* SO THAT PROPAGATION STEP SAME AS OTHER METHODS *)

 VAR
   K : INTEGER;

  BEGIN (* PROPAGATE *)

    DIFFSTEP (C, HALFKPHASE);
    FOR K := 1 TO NUMSTEPS DO
    BEGIN
      RISTEP (C, INDEX, EMAX) ;
      DIFFSTEP (C, KPHASE) ;
    END;
    RISTEP (C, INDEX, EMAX) ;
    DIFFSTEP (C, HALFKPHASE) ;

  END; (* PROPAGATE *)

BEGIN (* MAIN *)

  (* READ IN NUMBER OF STEPS AND NONLINEARITY FROM KEYBOARD *)

  WRITELN ('ENTER NUMBER OF STEPS ') ;
  READLN; READ (NREPEAT) ;
  WRITELN ('ENTER MAX INTENSITY W/M SQRD ') ;
   READLN ; READ (IMAX) ;

  (* SET VARIABLES *)

  CMPLX (0, 0, CZERO) ;
  TWODNSQRD := (SQR(N1) - SQR (N2));
  KAPPA := 2 * PI  / LAMBDA;
  KAPPAMED := KAPPA * N2;
  VSQRD := TWODNSQRD * SQR (KAPPA) * SQR (AF);
  W := (SQRT (1 + 4 * VSQRD) -1)/2;
  LENGTH := DELTAX * N;
  EPSNOTC := EPSNOT * CLIGHT ;
  EMAX := SQRT (IMAX/EPSNOTC) ;
```

```
  (* SET ALL ARRAYS *)

  SETXANDFIELD (X, CFIELD, EMAX) ;
  SETREFIND (X, INDEX) ;
  SETKSPACE (X, KPHASE, HALFKPHASE) ;
  SETTRANSF (WP, WM) ;
  SETCUTOFF (CUTOFF) ;

  (* SEND INITIAL VALUES TO DATAFILES ; W TO SCREEN *)

  REWRITE (D256) ; REWRITE (P256) ;
  SENDATA (CFIELD) ;
  WRITELN ('W = ', W) ;

  (* PROPAGATION *)

  DISTGONE := 0 ;

  FOR K := 2 TO NREPEAT DO
  BEGIN
    PROPAGATE (CFIELD);
    DISTGONE := DISTGONE + (DELTAZ * PROPLEN) ;
    WRITELN (K:2, ' ENERGY MEASURE = ', ENERGY (CFIELD));
    SENDATA (CFIELD) ;
  END (* FOR *)

END. (* MAIN *)
```

```
PROGRAM GTI (INPUT/, OUTPUT, D256, P256);

(* EPSTEIN VERSION 1.1; SINGLE GUIDE, LINEAR, NON-SPLIT OPERATOR ALGORITHM

(* VERSION FOR GTI CHAPTER *)

(*$I'COMPLEX' *)
(*$I'MATH' *)

  CONST

    N          = 256 ;        (* NUMBER OF POINTS IN ARRAY *)
    NP         = 257 ;
    NH         = 128 ;
    NHP        = 129 ;
    PROPLEN    = 6 ;          (* NUMBER OF DELTAZ'S IN PROPAGATION STEP *)
    LAMBDA     = 1.06E-6;     (* WAVELENGTH IN MICRONS *)
    N1         = 2.002 ;      (* PEAK REFRACTIVE INDEX *)
    N2         = 2.0 ;        (* SUBSTRATE REFRACTIVE INDEX *)
    A          = 3.0E-6 ;     (* EPSTEIN'S A COEFFICIENT *)
    CUTWIDTH   = 30 ;         (* NUMBER OF POINTS AFFECTED BY CUTOFF *)
    CUTPARAM   = 20 ;         (* WIDTH PARAMETER FOR CUTOFF ARRAY *)

  TYPE

    CARRAY  = ARRAY[1..N] OF COMPLEX;
    CHARRAY = ARRAY[1..NH] OF COMPLEX;
    CPARRAY = ARRAY[1..NP] OF COMPLEX ;
    CURVE   = ARRAY[1..N] OF REAL;
    CUTARRAY = ARRAY[1..CUTWIDTH] OF REAL ;

  VAR

    NREPEAT : INTEGER ;          (* MAIN LOOP MAXIMUM *)
    COUNT   : INTEGER ;          (* MAIN LOOP COUNTER *)

    VSQRD      : REAL ;
    W          : REAL ;          (* EPSTEIN PROFILE PARAMETERS *)
    TWODNSQRD  : REAL ;

    KAPPA      : REAL ;
    KAPPAMED   : REAL ;
    LENGTH     : REAL ;
    DISTGONE   : REAL ;

    DELTAZ     : REAL ;        (* PROPAGATION PARAMETERS *)
    DELTAX     : REAL ;
    RGTI       : REAL ;
    THETA      : REAL ;

    TGTI       : REAL ;         (* MISC GTI VARIABLES *)
    EMINITH    : COMPLEX ;

    CTEMP      : COMPLEX ;
    CZERO      : COMPLEX;

    CFIELD     : CARRAY ;       (* MAIN ARRAY CONTAINING FIELD DISTRIBUTION *
    COUT       : CARRAY ;
    CMEM       : CPARRAY ;

    X          : CURVE ;        (* VALUES OF X COORDINATES OF MESH *)
    INDEX      : CURVE ;        (* REFRACTIVE INDEX PROFILE *)

    CUTOFF     : CUTARRAY ;     (* ARRAY CONTAINING CUTOFF NUMBERS *)

    D256, P256 : FILE OF CURVE; (* OUTPUT DATA FILES FOR INTENSITY & PHASE *)

    APODISING  : BOOLEAN ;      (* INDICATES WHETHER USING CUTOFF ROUTINE *)

    SYMBOL     : INTEGER ;          (* USED FOR INPUT FROM KEYBOARD *)

PROCEDURE CFACT (    C      : COMPLEX ;
                     R      : REAL ;
                 VAR RESULT : COMPLEX) ;

  BEGIN (* CFACT *)

    RESULT.RE := R * C.RE ;
    RESULT.IM := R * C.IM ;

  END ; (* CFACT *)

PROCEDURE SWAP (VAR EFIELD : CARRAY ;
                    EOUT   : CARRAY) ;

(* READS ARRAY EOUT BACKWARDS INTO EFIELD *)

VAR K : INTEGER ;

BEGIN

  FOR K := 1 TO N DO
    EFIELD[K] := EOUT[N-K+1] ;

END ; (* SWAP *)


PROCEDURE GUESSBEGIN (    EFIELD : CARRAY ;
                      VAR EMEM   : CPARRAY) ;

(* GUESSES ENDS OF ARRRAY WHEN THEY SLIP OFF MESH *)
```

```
PROCEDURE GTI (    EFIELD : CARRAY ;
               VAR EOUT   : CARRAY ;
               VAR EMEM   : CPARRAY) ;

VAR
  K : INTEGER ;
  LHS, RHS, CTEMP  : COMPLEX ;

BEGIN
  GUESSBEGIN (EFIELD, EMEM) ;
  FOR K := 1 TO N DO
  BEGIN
    CFACT (EFIELD[K], -RGTI, LHS) ;
    CFACT (EMEM[K], TGTI, RHS) ;
    CADD (LHS, RHS, EOUT[K]) ;
    CFACT (EFIELD[K], TGTI, RHS) ;
    CFACT (EMEM[K], RGTI, LHS) ;
    CADD (LHS, RHS, CTEMP) ;
    CMUL (CTEMP, EMINITH, EMEM[K+1]) ;
  END ; (* FOR *)
END ; (* GTI *)


  PROCEDURE PROPAGATE (VAR CFIELD : CARRAY );

  (* GTI ALGORITHM *)

    VAR
      EOUT : CARRAY ;
      EMEM : CPARRAY ;
      COUNT : INTEGER ;

    BEGIN (* PROPAGATE *)

        GTI (CFIELD, EOUT, EMEM) ;
        SWAP (CFIELD, EOUT) ;
        GTI (CFIELD, EOUT, EMEM) ;
        SWAP (CFIELD, EOUT) ;

        RISTEP (CFIELD, INDEX, APODISING) ;

    END; (* PROPAGATE *)



  BEGIN (* MAIN *)

  (* READ IN PROGRAM PARAMETERS FROM KEYBOARD *)

  WRITELN ('DELTAX, DELTAZ (METRES), R, THETA ?') ;
  READLN ;
  READ (DELTAX, DELTAZ, RGTI, THETA) ;
  WRITELN ('NREPEAT, APODISING 0/1 ') ;
  READLN ;
  READ (NREPEAT, SYMBOL) ;
  APODISING := (SYMBOL = 1) ;

  (* SET "CONSTANT" VARIABLES *)

  LENGTH := DELTAX * N ;
  CMPLX (0, 0, CZERO) ;
  TWODNSQRD := (SQR(N1) - SQR (N2));
  KAPPA := 2 * PI  / LAMBDA;
  KAPPAMED := KAPPA * N2;
  VSQRD := TWODNSQRD * SQR (KAPPA) * SQR (A);
  W := (SQRT (1 + 4*VSQRD) -1) / 2 ;
  WRITELN ('W = ', W) ;

  (* SET GTI CONSTANTS *)

  TGTI := SQRT (1 - SQR (RGTI)) ;
  CMPLX (0, -THETA, CTEMP) ;
  CEXP (CTEMP, EMINITH) ;

  (* INITIALISE PROGRAM ARRAYS *)

  SETXANDFIELD (X, CFIELD, W) ;
  SETREFIND (X, INDEX) ;
  IF APODISING
  THEN SETCUTOFF (CUTOFF) ;

  (* SEND INITIAL ARRAYS TO DATA FILES; OUTPUT VALUE OF W TO SCREEN *)

  REWRITE (D256); REWRITE (P256);
  SENDATA (CFIELD) ;
  WRITELN ('W = ', W);

  (* PROPAGATION PART *)

  DISTGONE := 0 ;

  FOR COUNT := 1 TO NREPEAT DO
  BEGIN
    PROPAGATE (CFIELD);
    DISTGONE := DISTGONE + DELTAZ ;
    WRITELN (COUNT, ' DISTANCE: ', DISTGONE, ' ENERGY: ', ENERGY (CFIELD))
    SENDATA (CFIELD) ;
  END (* FOR *)

END. (* MAIN *)
```